

# Research & Development

## 2017



This issue is dedicated to Trans-Trio-Sciences international co-operation between Gent, Gödöllő and Baia Mare. The professional discussion about the published topics were organized in the frame of Synergy 2017 international Conference, Gödöllő, Hungary. Special thanks go to Hungarian Academy of Sciences, Committee on Mechanical Structures, Subcommittee on Tribology for the organization, too.

# **Mechanical Engineering Letters, Szent István University**

Technical-Scientific Journal of the Mechanical Engineering Faculty,  
Szent István University, Gödöllő, Hungary

Editor-in-Chief:  
Dr. István SZABÓ

Editor:  
Dr. Gábor KALÁCSKA

## Executive Editorial Board:

Dr. István BARÓTFI	Dr. István HUSTI
Dr. János BEKE	Dr. Sándor MOLNÁR
Dr. István FARKAS	Dr. Péter SZENDRŐ
Dr. László FENYVESI	Dr. Zoltán VARGA

## International Advisory Board:

Dr. Patrick DE BAETS (B)  
Dr. Radu COTETIU (Ro)  
Dr. Manuel GÁMEZ (Es)  
Dr. Klaus GOTTSCHALK (D)  
Dr. Yuri F. LACHUGA (Ru)  
Dr. Elmar SCHLICH (D)  
Dr. Nicolae UNGUREANU (Ro)

Cover design:  
Dr. László ZSIDAI

HU ISSN 2060-3789

All Rights Reserved. No part of this publication may be reproduced, stored in a retrieval system or transmitted in any form or by any means, electronic, mechanical, photocopying, recording, scanning or otherwise without the written permission of Faculty.

Páter K. u. 1., Gödöllő, H-2103 Hungary  
dekan@gek.szie.hu, www.gek.szie.hu,

Volume 15 (2017)

This volume contains the selected articles of Trans- Trio Sciences workshop held in the frame of Synergy International Conference, 2017, Gödöllő, Hungary



Synergy 2017, Session : Materials and Industrial Technologies

- materials and testing
- tribology
- industrial technologies

# Contents

Hasan Muhandes, Gábor Kalácska, Nawar Kadi, Mikael Skrifvars Thermoplastic biocomposite based on cellulose fibers	7
Tétény Baross, László Jánosi, Gábor Veres Analytical and numerical model of the temperature distribution of diffusion welding specimens on a Gleeble 3800 thermomechanical simulator	16
Ádám Sarankó, Róbert Keresztes, Gábor Kalácska, Jacob Sukumaran Evaluation of cutting force of PA6 and POM C	27
Zoltán Szakál, Tamás Pataki, Attila Kári-Horváth, Mátyás Andó, Rajini Nagarajan Shear strength of overlap bonds of plasma treated PA6 and PEEK	35
Hayder Al-Maliki, Zoltán Károly, Szilvia Klébert Surface morphology and chemical composition of PP and PETP treated by atmospheric plasma	47
Miklós Odrobina, Zoltán Szakál, Gábor Kalácska, Róbert Keresztes, Otto Eberst, Sever Pop The effect of sizes of the cast Polyamide 6 rods upon impact strength	56
Kannaki Pondicherry, Timothy Galle, Jacob Sukumaran, Dieter Fauconnier, Stijn Hertelé, Patrick De Baets Finite-element model development of single asperity scratch: a step-by-step approach	62
Róbert Zsolt Keresztes, Miklós Odrobina, Gábor Kalácska, Fledrich Gellért Development of polymer gear test rig for loadbearing examination	72
Alessandro Ruggiero, Nicolae Ungureanu, Radu Cotetiu Some recent tribological results from eco-friendly vegetal lubricants	81
Jacob Sukumaran, Adam Kalacska, Kannaki Pondicherry, Patrick De Baets Wear mechanisms prevalent in agricultural tines	87
Roland Biczó, Mátyás Andó, Róbert Keresztes, Gábor Kalácska Pin-on-disc tribology test of dry sliding frictional hybrid woven composite material samples cut with abrasive water jet machining	94
Ádám Kalácska, Jacob Sukumaran, Patrick De Baets Comparison of lab-scale erosion testing machines	100

Klára Bartha, Jacob Sukumaran, Dieter Fauconnier, Jozef Vleugels, Shuigen Huang, Patrick De Baets Wear Mechanism Classification by Image Processing	109
Karthikeyan Subramanian, Rajini Nagarajan, Jacob Sukumaran, Patrick De Baets, Gábor Kalácska Tribological characteristics of tailor made PTFE coated basalt/ vinyl ester composites for large scale system	117
Karthikeyan Subramanian, Rajini Nagarajan, Jacob Sukumaran, Patrick De Baets, Gábor Kalácska Dynamic mechanical and thermogravimetric analysis of PTFE blended tailor made textile woven basalt/vinyl ester composite on tribological characteristics	132
Adrian Dan Pop, Nicolae Stelian Ungureanu Analysis of Production and Physical Distribution of baked products at Andana Pan Bakery – Baia Mare, Romania	141
Eszter Sárközi, László Földi Evaluation of PID-P cascade control algorithm used in positioned pneumatic drives	148
Costel Ieremie Breban, Nicolae Stelian Ungureanu Analysis and optimization of gas meters	158
Viktor Erdélyi, László Jánosi Model based optimization in smart livestock farming - an introduction	164
Radu-Iacob Cotețiu, Adriana Cotețiu Synergy of the triad: human, machine and environment in Design of Technologies and Products	173
Tamas Pataki, Attila Kári-Horváth, László Zsidai 3D metal printing technologies and materials	178

## **Thermoplastic biocomposite based on cellulose fibers**

Hasan MUHANDES<sup>1</sup>, Gábor KALÁCSKA<sup>1</sup>, Nawar KADI<sup>2</sup>,  
Mikael SKRIFVARS<sup>2</sup>

<sup>1</sup>Institute for Mechanical Engineering Technology, Szent István University  
Páter K. u. 1., Gödöllő, H-2103, Hungary

<sup>2</sup>Department of textile Technology, University of Borås  
Allégatan 1, 503 32, Borås, Sweden

### **Abstract**

Bio-composites today are a popular choice for applications in composite manufacturing, based on the sustainability benefits.

The use of thermoplastic resins in some of the composite application is clearly of higher potential because of: good impact strength, easier recycling, faster processing conditions (no time for curing is required), possibility of production in longer series, lower cost, absence of toxic solvents and higher fracture toughness and elongation on fracture.

Natural fibers today are a popular choice for applications in composite manufacturing. In fact, a major challenge for natural fiber reinforced composites is to achieve high mechanical performance at competitive prices.

The hybrid yarns give a good distribution of reinforcement and matrix, where the quality of the component distribution in yarn is known to affect the mechanical properties of the composites.

A current trend in bio-composite fabrication is to reduce the number of processes required to produce a component rapidly and cost-effectively

Finally, in order to obtain high performance of thermoplastic bio-composites the process parameters must be identified and optimized.

### **Keywords**

composite, bio-composite, thermoplastic composite, hybrid yarn, natural fiber

### **1. Introduction**

The preservation of our environment requires that we stop developing materials that will, like many plastics, last indefinitely require in order to save our planet and our environment (Marsh, 2003). The development of “green” materials for industrial applications (Figure 1) is one of the most highly researched topics around the globe. Among other structural components, fabric used inside the automotive with multi-functionalities has attracted considerable interest as well. (Mohanty, Misra, & Drzal, 2005) define the bio composites as a composites made from environmentally friendly, biodegradable, and renewable resources.

According to the preparation method, biodegradable polymers are classified into two types: (Polymer Properties Database, 2015)

1. synthesize polymers are prepared from renewable sources
2. synthetic polymers (biodegradable) are prepared from mineral oils.

(La Mantia & Morreale, 2011) mentioned that the environmental impact can be reduced in significant way if we are using Fully biodegradable composites were matrix and reinforcement are made up of biodegradable materials.

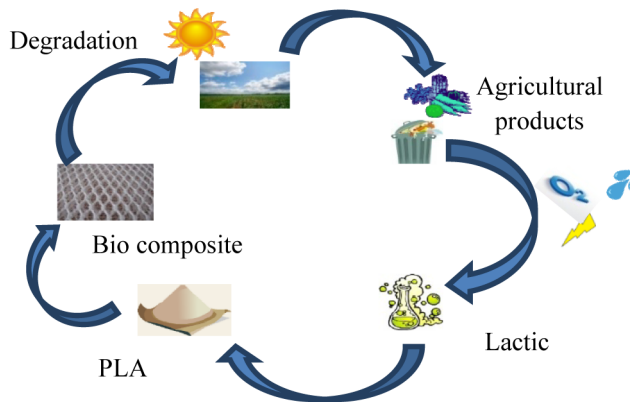


Figure 1. Life cycle of bio-composites materials

(Sawpan, Pickering, & Fernyhough, 2011) reported that the environmental problems of composite are related to the use of polymer from petroleum origin.

(La Mantia & Morreale, 2011) demonstrate that the recycling of composite is very difficult process and very limited, for example when we have two different component in the composite it will be hard to separate and recycle them, and often they use the incineration which are considered as unsatisfactory way.

## 2. Thermoplastic bio-composite

Thermoplastic bio-composites experience a continuing demand for various industrial applications (Sawpan et al., 2011; Thakur et al., 2014). This is due to several specific advantageous characteristics that can be combined in these materials. Thermoplastics, reduced processing times, highly increased storage times, and favorable recycling capabilities (Kim & Park, 2017), by using thermoplastics we can separate the components after using them. and the process will be easier, cleaner and faster (Svensson, Shishoo, & Gilchrist, 1998) . Environmentally friendly, degradable biomaterials, used to create true bio-composites, possess the ability to significantly improve the environmental impact of commonly used composite materials (La Mantia & Morreale, 2011).

This includes both natural fibers, used for the reinforcement component of a composite, as well as matrix materials from renewable resources. The using of thermoplastic matrices is better than using thermosets, because thermoplastics has facilitated recycling by being able to be molten and reshaped for numerous times (Biron, 2013). (Khondker, Ishiaku, Nakai, & Hamada, 2006) demonstrate that thermoplastic materials like PP (polypropylene), PE (polyethylene) and PVC (polyvinyl chloride) are dominate as matrices for natural fibers.

The most important biodegradable polymers is (bio-based) aliphatic polyesters. Some bio-based polyesters that have gained commercial use or that are currently investigated for commercial applications are polylactic acid (PLA), polyglycolic acid (PGA), poly- $\epsilon$ -caprolactone (PCL), polyhydroxy butyrate (PHB), and poly(3-hydroxy valerate).

Among these, PHB and PLA are the most extensively studied biodegradable thermoplastic polyesters. Both have excellent biodegradability and biocompatibility and exhibit relatively high melting point (160 to 180 °C). However, practical applications have often been limited by their brittleness.

(Sawpan, Pickering, & Fernyhough, 2011) show that the (PLA) represent the most common example for a polymer matrix from renewable resources. It has a high mechanical properties and it will degrade to carbon dioxide, water and methane in the environment after several months to 2 years, not like the based-petroleum polymers which need hundreds of years to degrade. And it considered as one of the most important bio-polymer, the advantage of it compare to the petroleum-based polymers and is was presented by (Thakur, Thakur, & Gupta, 2014)

The properties of PLA were demonstrated by (La Mantia & Morreale, 2011) like it is also comparably easy to produce, and with increasing demand, increasingly cheaper in the production.

### **3. Natural fibers as reinforcement**

(Masirek, Kulinski, Chionna, Piorowska, & Pracella, 2007) demonstrated that composites which use natural plant-based fibers have several advantages over synthetic fibers, like high toughness, and good thermal resistance. other advantages were mentioned by (Alagirusamy, Fangueiro, Ogale, & Padaki, 2006), like lower cost, lower weight and density, high stiffness, favorable specific mechanical properties and originate from renewable sources, and all of these are beside the most important properties which are being biodegradable and recyclable

There are several different options of fiber materials that can be used as the reinforcement component in bio-composites, (Summerscales, Dissanayake, Virk, & Hall, 2010) study of using the flax, hemp, jute and kenaf in preparing the composites.

The natural fibers as a reinforce materials for composites start to use in car like door panels, seat backs, headliners, package trays, dashboards, and interior parts (Holbery & Houston, 2006).

(Ku, Wang, Pattarachaiyakoop, & Trada, 2011) reported that having properties like low cost, low density, comparable specific tensile properties, nonabrasive to the equipment, nonirritating to the skin, reduced energy consumption, less health risk, renewability, recyclability and biodegradability, made natural fibers better than synthetic fibers like (glass and carbon) leads to become more useful.

Regenerated cellulose fibers can use for the reinforcement in bio-composites. These result in somewhat less environmentally friendly bio-composites compared to the usage of hemp fibers since the regenerated cellulose fibers are produced industrially. While the raw material, usually wood pulp, is biodegradable and stems from renewable resources, the process of manufacturing regenerated cellulose fibers has a larger environmental impact than that of several natural fibers, like flax or hemp (Shen, Worrell, & K.Patel, 2010).

The most important disadvantages which can form some difficulties in using natural fibers are hydrophilic nature which leads to a high moisture absorption. and during the process of making composites materials, presence of moisture can leads to have voids, these voids have an effect on the mechanical properties of the composite (La Mantia & Morreale, 2011). Another problem could face using of natural fiber based on cellulose is low thermal stability, where thermal degradation take place over 200 °C, and this will leads to form a 'cortex' or in other words leads to constitute an outer layer cause interface issues between natural fiber and resin (Kim & Park, 2017).

#### **4. Hybrid yarns**

Reducing the melt flow distance of the molten matrix can be consider as a solution to improve the processing of the thermoplastic composites. this solution is depending on producing intermediate materials (like hybrid yarns, dry powder coatings or film stackings) and the reinforcement fibers and matrix fibers are mixed together in a solid form before processing them into composites (Alagirusamy, Fangueiro, Ogale, & Padaki, 2006).

(Alagirusamy, Fangueiro, Ogale, & Padaki, 2006) mentioned that a fast and improved impregnation of the reinforcing fibers. and this will happen by uniformly distributing the matrix and reinforcement components in the hybrid yarns which lead to significantly reduce in the flow path of the melting thermoplastic after heat application.

#### **5. Process production of thermoplastic composite**

The processing of composite materials production is involving heating, melting and cooling when thermoplastics are used (Alagirusamy, Fangueiro, Ogale, & Padaki, 2006).

(Alagirusamy, Fanguero, Ogale, & Padaki, 2006) mentioned several techniques which are used to manufacturing thermoplastic composites like injection molding, filament winding, and pultrusion.

And beside of all these methods, they mentioned compression molding is one of the most common manufacturing methods.

(Tatara, 2017) Gave a simple explanation of this method is depending on heating the materials between the mold's parts in a closed cavity under application of pressure.

(Park & Lee, 2012) gave a figure to illustrate how this method works as the following:

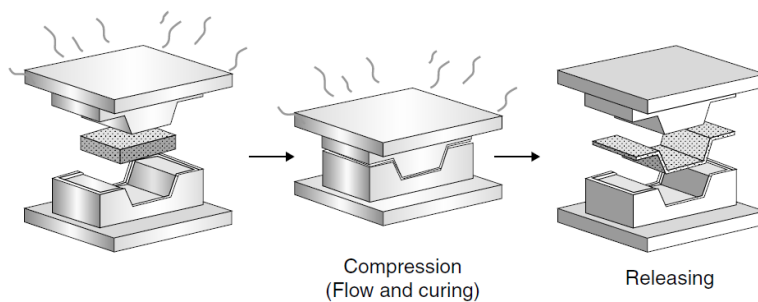


Figure 2. compression molding process

1. preparing the materials and placing them in the heated mold.
2. closing the mold, in this step one of the two mold's pieces will move to the other one and compresses the composite materials, during this step the pressure will be built up slowly and air will be pressed out of the structure.
3. maintained pressure and temperature application, consolidation taking place and the liquefied matrix spreads and impregnates the fibers. the required time for this step is depending on the used materials, he thickness of the lay-up and applied temperature and pressure.
4. removed and left to cool down outside of the mold

(Park & Lee, 2012) mentioned that thermoplastic composites which are produced by compression molding, and nowadays some parts in automobile industry are producing by using this method.

During thermoplastics process the viscosity is a major problem, which leads to make uniform and proper impregnation of the fibers very challenging and time-consuming and can introduce voids into the composite structure (Kim & Park, 2017).

(Kim & Park, 2017) gave a solution for this problem by working with elevated temperature, the elevated temperature leads to decrease the matrix viscosity and thereby improve the flow of the matrix.

but this solution is depending on the used materials, and especially when natural materials are used, the acceptable processing temperatures are

comparably low. And this can make a limits of using higher temperatures to improve the processing (Kim & Park, 2017).

### 6. Some experiments of using biocomposite materials

Some experiments which scientists did them by using bio-composite materials like (Khondker, Ishiaku, Nakai, & Hamada, 2006) when they prepared three samples of bio-composite materials and they processed at 170 °C, jute were used as a reinforcement and PLA as Matrix material, and he evaluated tensile and 3 point bending properties. the three samples had a variations in fiber contents (fiber volume fraction ( $V_f$ )) as  $V_{f1}$  (38%),  $V_{f2}$  (27.5%) and  $V_{f3}$  (22.5%).

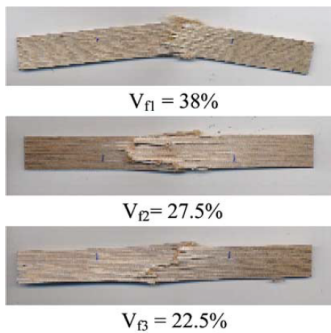


Figure 3. Tensile tested jute/PLA composite specimens processed at 170 °C.

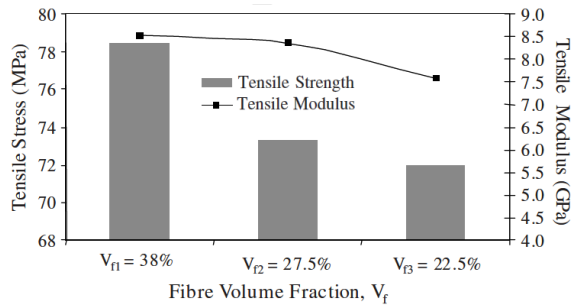


Fig. 4. Tensile properties of jute/PLA composites processed at 170 °C

Figure 4 shows the tensile stresses and moduli, and from this figure we can say that by increasing fiber content the samples exhibited superior tensile properties, and this improvement were in both strength and modulus was fairly consistent with respect to the increase in the reinforcing fiber content.

Another experiment had been done also by (Khondker, Ishiaku, Nakai, & Hamada, 2006) in order to study the effect of molding temperatures and pressures. studying the temperatures effect were by comparing the bending properties of samples at 170 , 175 °C and the matrix content  $V_m$  were 62 and 77.5%. While for studying the effect of pressure, they used to values 2.3 and 2.7 MPa with stable temperature which equal to 175, and the results were as the following figures.From

This result support what we mentioned earlier, at this optimized processing condition, matrix resins were adequately fused and the presence of voids between the fibres and the matrices was minimum.

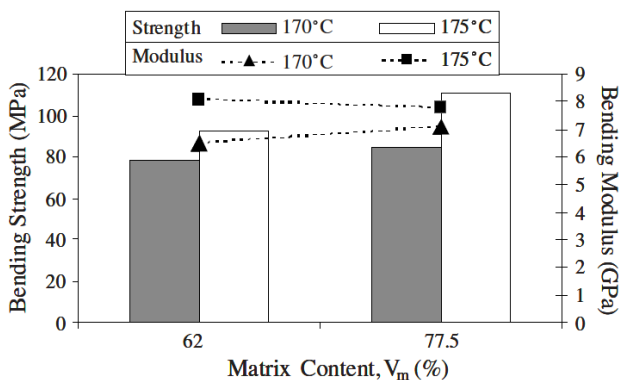


Figure 5. Effect of molding temperature on bending properties of jute/PLA composites.

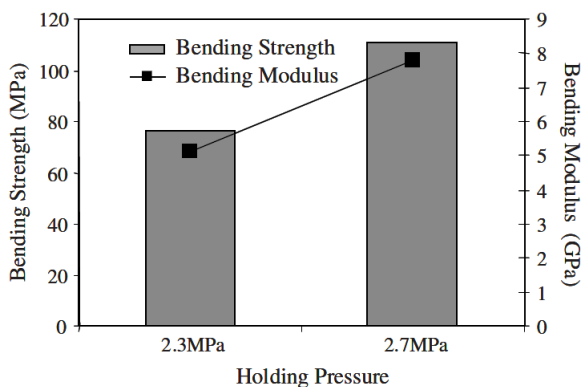


Figure 6. Effect of molding pressure on bending properties of jute/PLA composites molded at 175 °C

## Conclusion

The demand of bio-composite are significantly increase due to several specific advantageous characteristics that can be combined in these materials especially for the environmental raison.

Simultaneously, both thermoplastic matrices and natural, mostly plant-based fibers entail a new set of challenges concerning the production and usage of their composites, which can complicate their spread of applications.

We note that the natural fibers today are a popular choice for applications in composite manufacturing. Based on the sustainability benefits, bio fibers such as plant fibers are replacing synthetic fibers in composites. These fibers can be produced in the form Hybrid yarn.

Where the manufactures of thermoplastic composites based on Hybrid yarns give significant improvements in the mechanicals and thermo-mechanical properties compering with traditional yarns. These improvements do to the good impregnation of thermoplastic polymer.

The process parameters of bio-composites must be identified and optimized using the finites elements method in order to obtain high performance and reduced amount of process cycle times, by determining the most efficient processing conditions through simulations.

## Reference

- [1] *Polymer Properties Database*. (2015). Retrieved September 06, 2017, from <http://polymerdatabase.com/polymer%20classes/Biodegradable%20Polyester%20type.html>
- [2] Alagirusamy, R., Fanguero, R., Ogale, V., & Padaki, N. (2006). Hybrid Yarns and Textile Preforming for Thermoplastic Composites. *Textile Preforming for Thermoplastic Composites, Textile Progress*, 38(4), 1-71.
- [3] Biron, M. (2013). Outline of the Actual Situation of Plastics Compared to Conventional Materials. In *Thermoplastics and Thermoplastic Composites 2nd ed* (pp. 1-29). Oxford, UK: William Andrew Publishing.
- [4] Holbery, J., & Houston, D. (2006). Natural-Fiber-Reinforced Polymer Composites in Automotive Applications. *Journal of The Minerals, Metals & Materials Society*, 58(11), 80-86.
- [5] Khondker, O., Ishiaku, U., Nakai, A., & Hamada, H. (2006). A novel processing technique for thermoplastic manufacturing of unidirectional composites reinforced with jute yarns. *Composites Part a-Applied Science and Manufacturing*, 37(12), 2274-2284.
- [6] Kim, S. H., & Park, C. H. (2017). Direct impregnation of thermoplastic melt into flax textilereinforcement for semi-structural composite parts. *Industrial Crops and Products*, 95, 651–663.
- [7] Ku, H., Wang, H., Pattarachaiyakoop, N., & Trada, M. (2011). A review on the tensile properties of natural fibre reinforced polymer composites. *Composites Part B: Engineering*, 42, 856–873.
- [8] La Mantia, F. P., & Morreale, M. (2011). Green composites: A brief review. *Composites: Part A*, 42, 579–588.
- [9] Marsh, G. (2003). Next step for automotive materials. *Materials Today*, 6(4), 36-43.
- [10] Masirek, R., Kulinski, Z., Chionna, D., Piorowska, E., & Pracella, M. (2007). Composites of Poly(L-lactide) with Hemp Fibers: Morphology and Thermal and Mechanical Properties. *Journal of Applied Polymer Science*, 15, 255–268.
- [11] Mohanty, A. K., Misra, M., & Drzal, L. T. (2005). *Natural Fibers, Biopolymers, and Biocomposites*. Boca Raton, Florida: CRC Press.

- [12] Park, C. H., & Lee, W. I. (2012). Compression molding in polymer matrix composites. In S. G. Advani, & K.-T. Hsiao, *Manufacturing Techniques for Polymer Matrix Composites (PMCs)* (pp. 47-94). Cambridge, UK: Woodhead Publishing Limited.
- [13] Sawpan, M. A., Pickering, K. L., & Fernyhough, A. (2011). Improvement of mechanical performance of industrial hemp fibre reinforced polylactide biocomposites. *Composites Part A: Applied Science and Manufacturing*, 42(3), 310-319.
- [14] Shen, L., Worrell, E., & K.Patel, M. (2010). Environmental impact assessment of man-made cellulose fibres. *Resources, Conservation and Recycling*, 55(2), 260-274.
- [15] Summerscales, J., Dissanayake, N. P., Virk, A. S., & Hall, W. (2010). A Review of Bast Fibres and their Composites. Part 1 – fibres as reinforcements. *Composites: Part A*, 41, 1329–1335.
- [16] Svensson, N., Shishoo, R., & Gilchrist, M. (1998). Manufacturing of Thermoplastic Composites from Commingled Yarns-A Review. *Journal of Thermoplastic Composite Materials*, 11(1), 22-56.
- [17] Tataru, R. A. (2017). Compression Molding. In M. Kutz, *Applied Plastics Engineering Handbook* (pp. 291-320). Oxford, UK: William Andrew Publishing.
- [18] Thakur, V. K., Thakur, M. K., & Gupta, R. K. (2014). Review- Raw Natural Fiber–Based Polymer Composites. *International Journal of Polymer Analysis and Characterization*, 19(3), 256-271.

# **Analytical and numerical model of the temperature distribution of diffusion welding specimens on a Gleeble 3800 thermomechanical simulator**

Tétény BAROSS<sup>1</sup>, László JÁNOSI<sup>2</sup>, Gábor VERES<sup>1</sup>

<sup>1</sup>WIGNER RCP, RMKI, PO Box 91, H-1521 Budapest, Hungary,

<sup>2</sup>Institute for Mechanical Engineering Technology,  
Szent István University, Páter K. u. 1., Gödöllő, H-2100, Hungary,

## **Abstract**

Welding by diffusion bonding methods as a candidate solution for Plasma Facing Components in fusion reactors involved significant investigations over the last decades. The diffusion bonding methods apply two phenomena in one time: the elevated temperature under recrystallization and pressure perpendicular to the welded surfaces. Gleeble 3800 thermomechanical simulator is able to demonstrate this welding method expensively. This paper intends to give an overview of the 1D analytical and numerical calculations on thermal distribution of specimens during a diffusion bonding test in a Gleeble machine. These calculations are able to give a good conception about impact of different jaws at fixing of specimens, about the essential temperature measuring methods for a proper control of Gleeble direct resistance Joule heating. Adequate geometry of samples for diffusion welding shall be defined also by preliminary thermal calculations. These calculations shall be used to set up a larger test program on Gleeble 3800 laboratory at UNIDUNA.

## **Keywords**

Diffusion welding, thermal distribution, Gleeble 3800 thermomechanical simulator

## **1. Introduction**

The actuality of the topic comes from the ITER (International Thermonuclear Experimental Reactor) fusion tokamak and the fusion power plant planned to be built on the basis of ITER technological experiences. Among others one of the challenging task is to find proper materials and technology for production the Plasma Facing Components.

The plasma-facing components (PFCs) cover the large vacuum vessel, which area is about 850 m<sup>2</sup> including the “Divertor” components bellow the torus and the blanket that protects the wall elements. The so-called Normal Heat Flux and the Enhanced Heat Flux ITER blanket modules – covering the wall – contain

several HIP joints between 316L(N)-IG SS plates, CuCrZr parts, 316L(N)-IG SS pipes and Be tiles. [Lorenzotto, 2016] According to the heat flux test protocols by ITER office for Enhanced Heat Flux modules is a 7500 cycles at  $2 \text{ MW/m}^2$  and 1500 cycles at  $2,5 \text{ MW/m}^2$  have to be followed. Further ultrasonic tests have to be carried out at CuCrZr/Be joints [Banetta, 2015]. Since under these conditions the welded joints are able to conduct this amount of heat, the investigation of diffusion welding at these components and the known quality of diffusion joints are essential.

The following chapters summarize the temperature distribution during diffusion welding simulation on a Gleeble thermomechanical simulator. However numerical simulation program called GLENIS exists already for 3D temperature distribution for Gleeble specimens [Spittle, 1997] [Brown, 1997]. The authors of this article decided to develop for better understanding new calculations for temperature distribution that shall be a good basis for diffusion welding calculations at Gleeble simulator.

## **2. Overview on diffusion welding and simulation on Gleeble thermomechanical simulator**

A Gleeble 3800 thermomechanical simulator (Dynamic Systems Inc.) is a physical simulator of material behavior, able to combine heating and mechanical loading in different scenarios. This is allowed the system to simulate diffusion bonding process. The author of the article has the possibility to test later on the diffusion welding in a Gleeble labor at University of Dunaújváros in Hungary.

The HIP hot isostatic pressing a type of diffusion bonding applies two phenomena in one time: the elevated temperature under recrystallization and isostatic pressure, however in labor environment the isostatic pressure is changed to uniaxial pressure of flat components perpendicular to the contact surface. Following these, a bonding seam arises between the two surfaces.

Mating surfaces are planarized under pressure. Bond takes place by deformation and diffusion processes at the bond interfaces, where 50-80% of the melting temperature  $T_m$  and specific pressure – molecular activity increases and supports the diffusion processes during a certain time. Due the long process time at high temperature and continuous contact of bonding surface by pressure the surface roughness and voids will disappear. However the welding is not ready with full contact surfaces, further time is required for diffusion and grain growing between the two materials.

## **3. Calculation of thermal distributions in a Gleeble specimen**

The Gleeble Thermomechanical thermal simulator is able to test diffusion welding process [Piyush, S. 2013]. System is a general-purpose servo-hydraulic thermomechanical, it applies direct resistance heating up to  $10,000^\circ\text{C/second}$

and apply maximum static pressure 20 t [Uniduna, 2016] under mid  $-10^5$  Torr range. Not a high vacuum, because the chamber has rubber O-ring, but this vacuum is required to control surface oxidation during the diffusion welding process. The required stress during diffusion welding is within the Gleeble's capacity. Figure 1 shows the Gleeble labor at UNIDUNA. Figure 2 shows the simulation of welding heat affected zone.



Figure 1. Gleeble 3800 Termomechanical Simulator, Gleeble labor at Dunaújvárosi Egyetem [Uniduna, 2016]

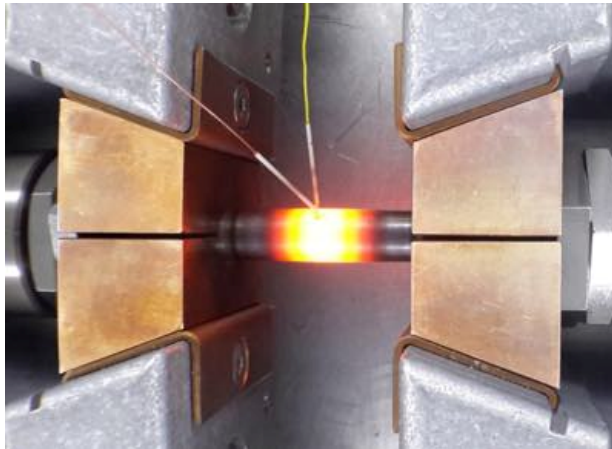


Figure 2. Example for direct resistance heating for welding simulation [www.Gleeble.com]

The specimens are heated by direct Joule heating with 50 Hz alternating current passed through the specimens by grips at the ends. The current is

regulated by a thermocouple welded to the specimen at the middle point. However Gleeble use AC potential difference to drive current one can approximate the applied potential difference between grips by DC – with the root-mean-squared value. [Brown, 1997]

The potential difference through grips and specimens initiate a complex 3D calculation, we choose a 1D calculation for first approximation.

### 3.1 Temperature distribution in specimens, steady-state, analytical calculation

Since the diffusion welding endure 1-2 hours, and the steady-state temperature distribution arise under minutes or seconds, one need to calculate first the steady-state thermal distribution for diffusion welding.

On Figure 3. the simplified view of diffusion welding of two specimens can be seen gripped by two/two copper jaw on both sides. Similar to Figure 2. According to the Gleeble Users Training book (2010) in this case the temperature at gripping – boundary condition – is close to the cooling water temperature thanks to the good thermal conduction.

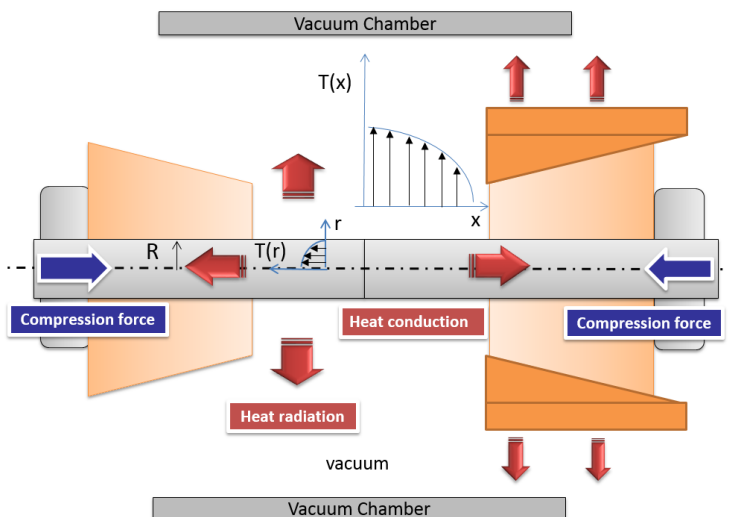


Figure 3. Simplified view of a diffusion welding layout in Gleeble instrument

For simplification we take the following boundary conditions and assumptions during analytical calculation of the steady-state temperature distribution:

- The specimen has a circular cross-section,
- The copper jaw with good thermal conduction ensures approximately a constant temperature at the joining of the free span.
- The heat generation is constant, just the function of material resistance.

- Supposing during this calculation that thermal conductivity does not depend on temperature. However it is required to take into account for a more precise calculation later on.
- The heat radiation between the specimen and the vacuum chamber supposed to be neglectable.
- Under vacuum we do not calculate any convectional heat loss.
- For first thermal calculations we did not assume electrical or contact thermal resistance between the two specimen joining surfaces.

Following standard calculations in 1D, equations 1-2 describe the temperature distribution along x axis. [Gróf, 1999]

I. First ordered boundary condition, at fixed temperature at gripping:

$$t(x) = -\frac{\dot{q}_v}{2\lambda} \cdot x^2 + \frac{\dot{q}_v}{2\lambda} \left(\frac{\delta}{2}\right)^2 + t_\infty \quad (1)$$

III. Third ordered boundary condition, there is heat conduction at gripping:

$$t(x) = -\frac{\dot{q}_v}{2\lambda} \cdot x^2 + \frac{\dot{q}_v \cdot \delta}{2\lambda} \left(\frac{1}{\alpha} + \frac{1}{2\lambda} \cdot \frac{\delta}{2}\right) + t_\infty \quad (2)$$

where

- $\dot{q}_v$ : volumetric heat generation rate (W/m<sup>3</sup>),
- $\lambda$ : thermal conductivity
- $\frac{\delta}{2}$ : half distance of free span
- In I. ordered case  $t = t_\infty$  is constant at  $x = \pm \frac{\delta}{2}$ ,
- In III. ordered case  $t = t_\infty$  is the constant environment temperature
- $\alpha$  is contact conductance between environment and sides at  $x = \pm \frac{\delta}{2}$

The equations in both cases are in this form:

$$f(x) = -C_1 \cdot x^2 + C_2 \quad (3)$$

*Consequences:*

- The characteristic of temperature distribution is the same (see Eq. 3.) in both case. Knowing the thermal conductivity and volumetric heat generation rate, the temperature distribution of the whole free span can be calculated, if one measured temperature and position is known. So the whole temperature distribution can be calculated, especially the maximum temperature can be estimated.

- At constant current - means constant heat generation rate - the maximum temperature depends just on the free span length. In this way choosing a longer lengths for specimens one can save on the required current for Joule heating as well. The length may be limited by size of the Gleeble grip sizes or buckling.
- The heat thermal conductivity is the function of temperature, in general we can take its value for the middle temperature.

### 3.2. Temperature distribution in specimens, steady state, discretized modeling

The temperature distribution in steady state can be approximated also by discretized elements. In discretized elements the material properties can be set easily as the function of temperature or other parameters that may influence the values as thermal conductivity, specific heat, electrical resistance. Even the cross-section of specimen or the element sizes can be modified for a more complex geometry.

Figure 4. represent the simplified model of the discretized calculation. Figure 5 shows the calculation of one electrical resistance on one discretized element.

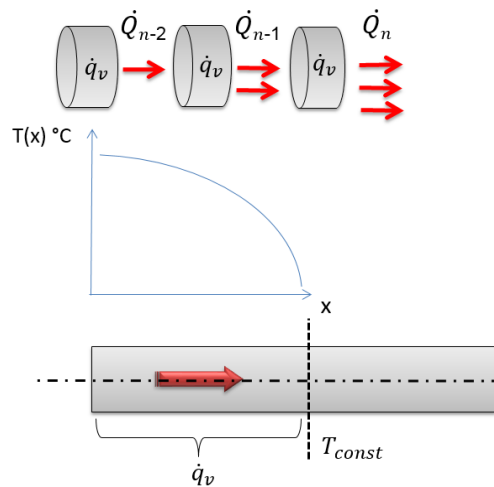


Figure 4. The heat transport in case of a specimen calculated with discrete elements

The heat transport from left to right is increasing element by element. In this way from left to right with a summation the transferred heat is calculable, and the temperature from left to right is determinable knowing the boundary condition at the gripping of specimen.

For first element heat conduction by temperature difference with the adjacent element will be in equilibrium of the heat generated in zero (adjacent) element. See equation (4).

$$\dot{Q}_1 = R_1 \cdot I^2 = \lambda(t) \cdot \frac{F}{l} (t_0 - t_1) \quad (4)$$

The resistance of one element shall be calculated similar to the electrical resistance calculation in a cable. See Figure 5.  $R_k$ :

$$\rho = R_k \cdot \frac{A}{l} \left[ \frac{\Omega \text{mm}^2}{\text{m}} \right]$$

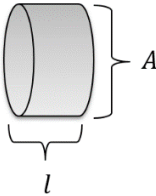
$$R_k = \rho \cdot \frac{l}{A} [\Omega]$$


Figure 5. Electrical resistance calculation of one discrete element

where:

- $\rho$  is the electrical resistivity of the cable  $\left[ \frac{\Omega \text{mm}^2}{\text{m}} \right]$
- $l$  is the specimen element length [m]
- $A$  is the cross-section of the specimen [ $\text{mm}^2$ ]

If we have to estimate the heat transport through  $n$ th element,  $\dot{Q}_n$  – and the temperature distribution knowing the boundary temperature:  $T_{const}$  – assuming heat transport exist just in  $x$  direction.

The  $\dot{Q}_n$  heat transport at constant thermal conductivity:

$$\dot{Q}_n = \lambda_{const} \cdot \frac{F_n}{l} (t_{n-1} - t_n) = \sum_0^{k=n} R_k \cdot I^2 \quad (5)$$

The  $\dot{Q}_n$  heat transport with thermal conductivity as function of temperature of an element is the following:

$$\dot{Q}_n = \lambda(t_{n-1}) \cdot \frac{F_n}{l} (t_{n-1} - t_n) = \sum_0^{k=n} R_k \cdot I^2 \quad (6)$$

where  $\lambda(t_{n-1})$  calculated as the function of  $(t_{n-1})$ .

After rearranging the equation we get the following to the adjacent element's temperature from right to left direction in Figure 4.:

$$t_{n-1} = \frac{l}{F_n \cdot \lambda(t_{n-1})} \sum_0^{k=n} R_k \cdot I^2 + t_n \quad (7)$$

*Consequences, assumptions:*

- The discretized elements of specimen are in series, as visible in Figure 4. A specimen with not suddenly altering cross-section in 1D can be approximated as well.
- The influence of temperature on thermal conductivity was calculable, and give serious different compared to the constant thermal conductivity. As it is visible in results.
- For a more detailed calculation one can take into consideration the specific heat, electrical resistivity and heat radiation during long welding process

#### 4. Results

The calculations detailed in previous chapters were done with Excel program.

*Table1.* Values of thermal distribution estimation in Gleeble specimen

	<b>Notation</b>	<b>Value</b>	<b>Unit</b>
Description	I	800	A
Current through specimen	$\rho$	0,75	$\Omega\text{mm}^2/\text{m}$
Electrical resistivity	$\lambda(t)$	$0,01502 \cdot T + 13,98$	$\text{W}/(\text{mK})$
Thermal conductivity, $f(t)$	L	0,023	m
Free span, length of one specimens	D	10	mm
Diameter	l	0,001	m
Length of one discrete element	qv	77,81	$\text{W}/\text{mm}^3$
Volumetric heat generation rate (calculated)			

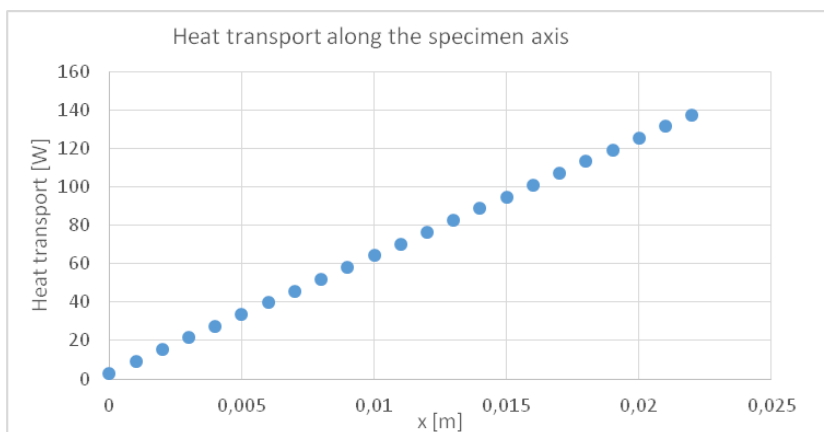


*Figure 6.* Comparison of temperature distribution by analytical and discrete element method

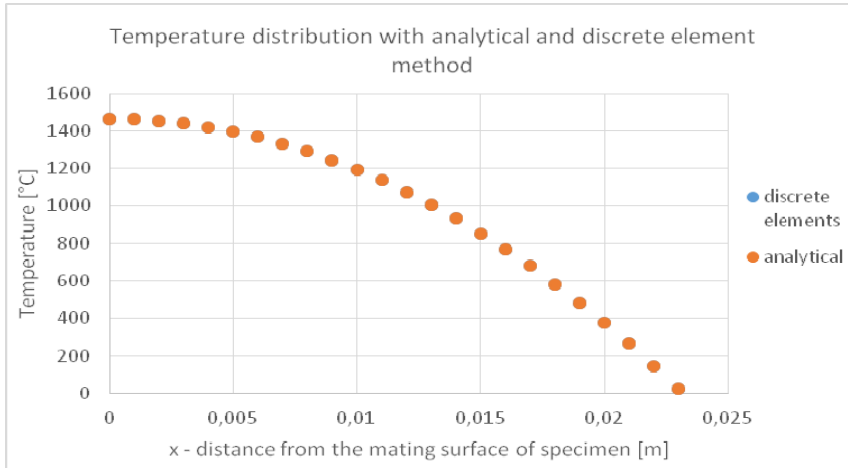


Figure 7. Comparison of temperature distribution by analytical and discrete element method

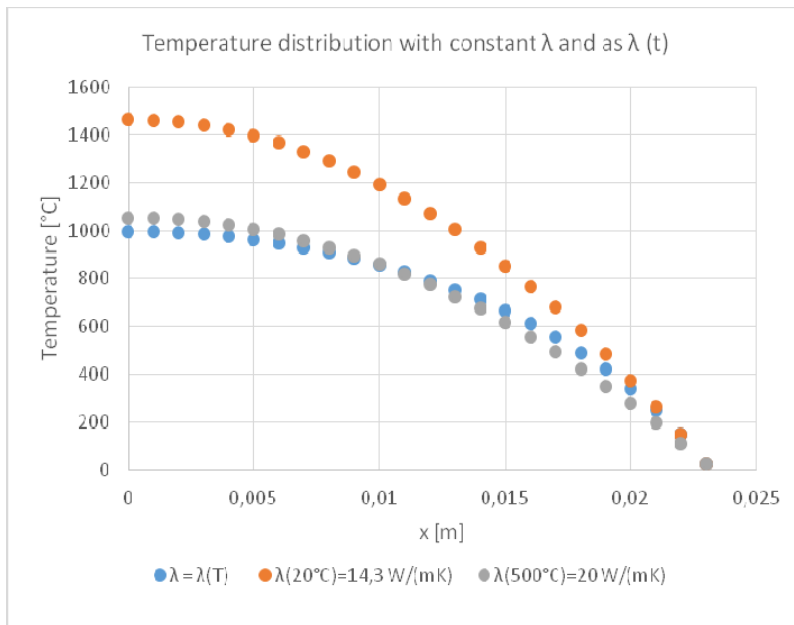


Figure 8. Influence of thermal conductivity on temperature distribution

## Conclusion

This article aims to give the calculation of temperature distribution in a specimen in 1D heated in a Gleeble 3800 Termomechanical Simulator. These calculation aim to define the proper geometry of a diffusion welding specimen between Gleeble grips that may need 1-2 hours welding time. From the above

considerations one can see that analytical and discretized calculations are both able to estimate the temperature distribution in specimens. However discretized modeling help more feasible and more exact calculations.

## Acknowledgement

This calculation was prepared in the frame of SZIE PhD school, in this way many thanks for my supervisors Prof. László Jánosi and the leaders of IPMP (International PhD Mentor Programm) Dr. Gábor Kalácska, furthermore for supervision of Dr. Gábor Veres, who supports the PhD at Wigner RCP institute.

Special thanks to Dr. Péter Bereczki, who demonstrated me the Gleeble 3800 Thermomechanical Simulator at University of Dunaujváros,

## References

- [1] Uniduna, Gleeble labor description, 2016, internet link: [www.uniduna.hu/images/dokumentumok/Gleeble\\_labor.pdf](http://www.uniduna.hu/images/dokumentumok/Gleeble_labor.pdf)
- [2] Gleeble Users Training 2010, Gleeble Systems and Application [www.bleeble.com](http://www.bleeble.com) webpage: <https://www.bleeble.com/products/welding-simulator.html>
- [3] Patrick Lorenzetto, Stefano Banetta, Boris Bellin, Bruno Boireau, Philippe Bucci, Tindaro Cicero, Denis Conchon, Georges Dellopoulos, Stephen Hardaker, Paul Marshall, Patrice Nogué, Marcos Pérez, Leticia Ruiz Gutierrez, Fernando Samaniego, Paul Sherlock, Francesco Zacchia, EU contribution to the procurement of the ITER blanket first wall, Fusion Engineering and Design, Volumes 109–111, Part A, 1 November 2016, Pages 661–665, ISSN 0920-3796, <http://dx.doi.org/10.1016/j.fusengdes.2016.02.024>.
- [4] S. Banetta, B. Bellin, P. Lorenzetto, F. Zacchia, B. Boireau, I. Bobin, P. Boiffard, A. Cottin, P. Nogue, R. Mitteau, R. Eaton, R. Raffray, A. Bürger, J. Du, J. Linke, G. Pintsuk, T. Weber, Manufacturing and testing of a ITER First Wall Semi-Prototype for EUDA pre-qualification, Fusion Engineering and Design, Volumes 98–99, October 2015, Pages 1211–1215, ISSN 0920-3796, <http://dx.doi.org/10.1016/j.fusengdes.2015.01.016>.
- [5] Sabharwall, Piyush & E. Clark, Denis & Glazoff, Michael & Mckellar, M & E. Mizia, Ronald. (2013) Diffusion-Welded Microchannel Heat Exchanger for Industrial Processes. Journal of Thermal Science and Engineering Applications. 5. . 10.1115/1.4007578.
- [6] J.A. Spittle, S.G.R. Brown, J.D. James, R.W. Evans, Numerical Simulation of Temperature Distributions in Gleeble Specimens as a Function of Time, 1997 Proc. 7th Int. Symposium on Physical Simulation of Casting, Hot Rolling and Welding, At Tsukuba, Japan, (Tsokuba National Research Institute for Metals) p 181

- [7] S.G.R. Brown et al 1997, A 3D numerical model of the temperature - time characteristics of specimens tested on a Gleeble thermomechanical simulator, *Modelling Simul. Mater. Sci. Eng.* 5 539, <https://doi.org/10.1088/0965-0393/5/6/001>
- [] S.D. Norris and I. Wilson 1999, Application of 3D numerical modelling for thermal profile optimization on the Gleeble thermomechanical simulator, *Modelling Simul. Mater. Sci. Eng.* 7 297, <https://doi.org/10.1088/0965-0393/7/3/301>
- [8] Gróf Gyula, HŐKÖZLÉS ideiglenes jegyzet, 1999 Budapest
- [9] Tétény Baross, László Jánosi, Gábor Kalácska, Gábor Veres, Diffusion bonding of plasma facing components of fusion reactor (ITER), *Mechanical Engineering Letters*, Szent István University, Volume 12 (2015), page 101-109, HU ISSN 2060-3789

# Evaluation of cutting force of PA6 and POM C

Ádám SARANKÓ<sup>1</sup>, Róbert KERESZTES<sup>1</sup>, Gábor KALÁCSKA<sup>1</sup>,  
Jacob SUKUMARAN<sup>2</sup>

<sup>1</sup>Institute for Mechanical Engineering Technology,

Szent István University, Páter K. u. 1., Gödöllő, H-2100, Hungary,

<sup>2</sup>Department of Electrical energy, metals, mechanical constructions and systems,  
Faculty of Engineering and Architecture, Ghent University, Belgium

## Abstract

In this article, machining tests of polyamide 6 (PA 6) and polyoxymethylene copolymer (POM C) will be introduced. These materials are commonly used in practical engineering. The tests were performed on a NCT CNC lathe machine by changing the machining parameters, while measuring the cutting forces in the feed direction and tangential direction. After examining the results, cutting parameters were determined in optimization for technical practice. The results may serve as a basis for further research in the future.

## Keywords

Plastics materials, polymer cutting, CNC lathe machining, optimization.

## 1. Introduction

Lately, machined plastic parts are increasingly used in mechanical engineering practice. Plastics have a wide range of applications ranging from machine elements to various decorative components. Depending on the manufacturing lot size, plastic products can be made by different methods. Injection molding or extrusion can serve a large lot size, but for a smaller lot size, or in case of high precision requirement, the products are produced by a machining process. One of the most frequently used machining method is turning. Tool catalogues include technical data, which are typically experimentally defined values. However, in economics aspect, total lead-time need to be taken into consideration. The cycle time of manufacturing process can be reduced by increasing feed rate or the depth of cut. Though CNC machining centers are capable of relatively high cutting speeds and high feed rate. The machinability of the processed materials limit the increase of those parameters.

The aim of this research is to optimize the machining parameters for cycle time reduction. It is also important that the chips – which cause many problems in the processing of plastics – peel off in the proper form. After evaluating the achieved results, the appropriate cutting parameters are given. This method of defining the optimal cutting parameters can be applied for different types of plastic.

## 2. Methods

The measurement system was described in a previous article, Machining of engineering polymers.

The tests were run on a type NCT EUROturn-12B CNC machine. The device is located in the school workshop of the Institute of Engineering Technology at Szent István University. The measuring tool is located in a modified DIN69880 standard B7-20x16x30 tool holder. The strain gauges found on the tool and the type Spider 8 measuring amplifier are connected by wires, converting the analogue signals to digital, which are then transmitted to the computer. The chart-like visualization of the digital signals was achieved Catman 3.1 software. The measurement and data collection are both of 50 Hz frequency. For safety reasons, a specimen was sawed across to the middle, making the chips break periodically at each rotation. The measurement results were not affected by this phenomenon (the reasons for this were explained in the previous article).

### *Parameters of the tests*

During experiments, three parameters and two types of turning inserts were applied and measured accordingly. The cutting speed ( $v_c$ ) varied between 500, 300 and 100 m / min, the feedrate ( $f$ ) 0.05; 0.1; 0.2; 0.4 and 0.5 mm / rev, and the depth of cut ( $a$ ) varied between 0.1; 0.2; 0.5; 1; 2 and 5 mm (in case of a cutting depth below 0.1 mm, the cutting forces would have been too small, hence difficult to evaluate due to vibrations from the machine). One of the turning inserts was a type CCGT 09 T3 04 AS IC20, while the other was a CCGX 09 T3 04 AL H10 with a polished surface. For each variation, experiments were performed on both test substances.

### *Materials used in research*

The tested materials were PA 6 and POM C. This measurement method can be used for cutting process of various other polymers and composites, using the aforementioned high cutting speeds.

## 3. Results

To demonstrate the results, 3D charts were used for good illustration. The title of the diagram indicates the force, speed, material and turning insert used while performing the experiment.

The first figure shows the difference between the main cutting force measured, using the polished and the normal surface turning insert, as shown in the title (where the polished insert is „p”, and the normal tool is „s”). In general, using the polished surface tool, the cutting forces in both feed and tangential directions were smaller, especially in the set of larger parameter range.



Figure 1. Main cutting forces by using normal surface (front) and polished inserts (behind) (PA 6,  $v = 500$  m/min)

In the second figure, feed forces is being demonstrated. It can be clearly seen that by increasing the depth of cut and feed rate, the feed force becomes smaller and even become a negative value. This suggests that the tool should not be pushed, but pulled back because the material is crushing into the cutting plane in the machining process.

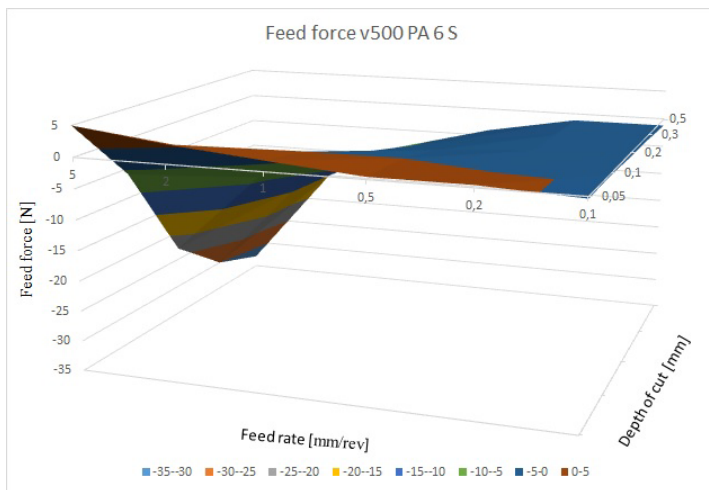


Figure 2. Feeding force with normal insert (PA 6,  $v = 500$  m/min)

At  $v = 500$  m/min, with a cutting depth of 5 and 2 mm and with a feed rate of 0.4 and 0.5 mm / rev, elemental chip formation could be observed, while at other parameters continuous chips were formed.

At  $v=300$  m/min the charts (Fig. 3) show similarities to the previous ones, but the main cutting force was always higher than at  $v=500$  m/min. The feed force was only favorable at 5mm depth and at 0.5 and 0.4mm / rev. The chip formation in case of  $v=300$  m/min is similar to  $v=500$  m/min.

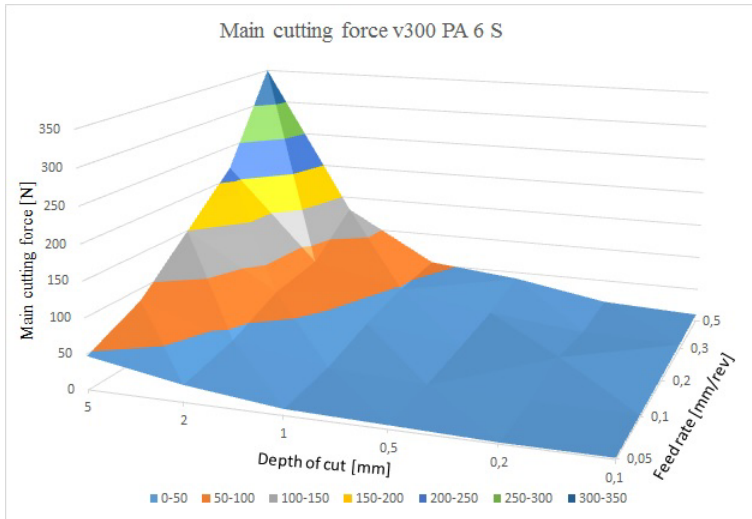


Figure 3. Main cutting force with normal insert (PA 6,  $v= 300$  m/min)

At  $v=100$  m/min, the measured forces show the similar trend. At this speed, continuous chip formation occurred in all cases.

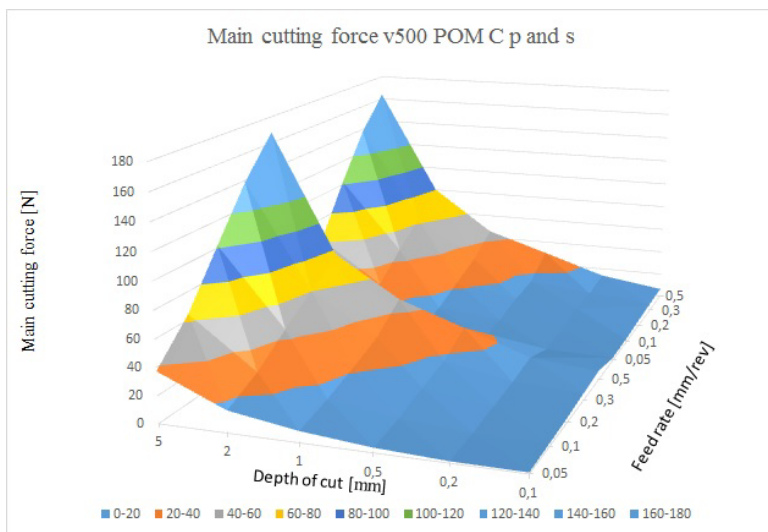


Figure 4. The main cutting forces of POM C by polished (front) and normal insert (behind) ( $v= 500$  m/min)

Fig. 4. shows the 3D diagram of POM C cutting forces measured at  $v=500$  m/min. The chart is similar to the diagrams presented on PA 6. The main cutting force is changing evenly, but the values are considerably lower. No high fluctuations could be observed. It can be stated that there is no significant difference between the inserts used.

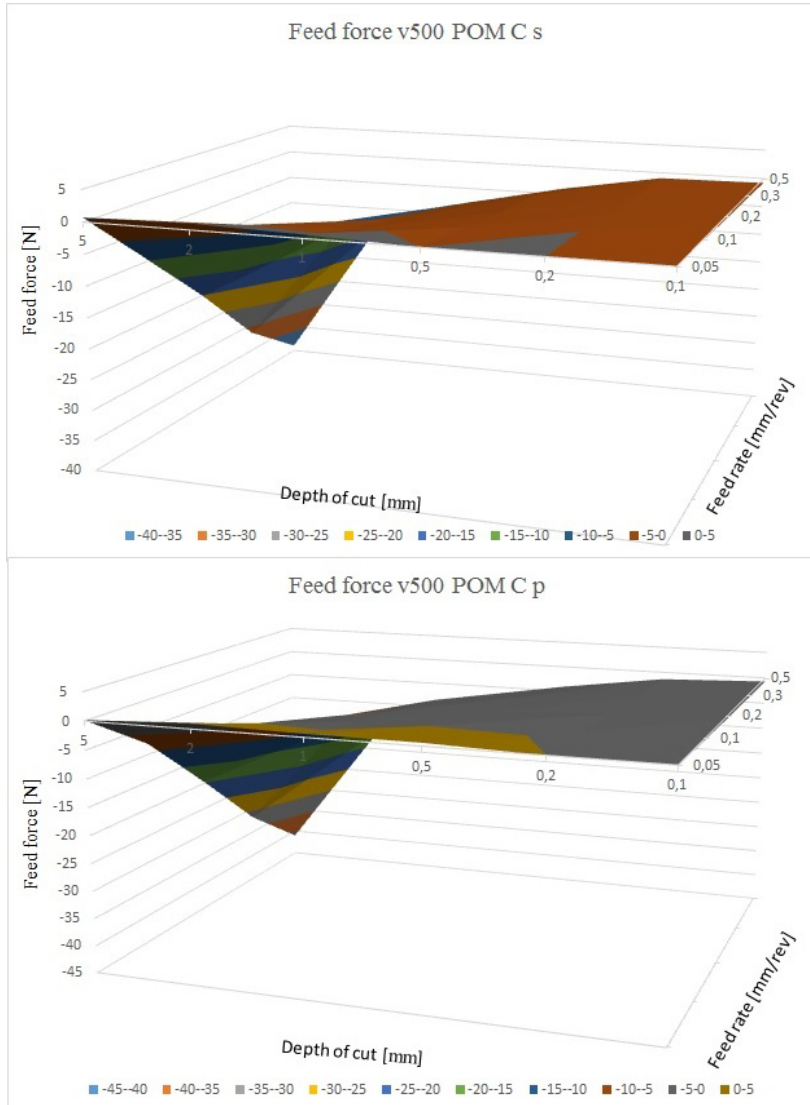


Figure 5. Feed forces when machining POM C by normal and polished inserts ( $v= 500$  m/min)

Fig. 5. shows POM C feed forces at  $v=500$  m/min, polished (front) and normal insert (behind). The shape of the chart in this case is also similar to the

diagrams shown in PA 6, except that the positive forces are smaller, and there is no significant change in the feed force for the inserts.

At 5 mm depth of cut of 0.5 and 0.4 mm / rev, elemental chip formation occurred (Fig. 6). However, at a lower parameter range, segmented and continuous chips were formed, generally easy to break.

At  $v=300$  m/min almost the same main cutting forces were generated as at  $v=500$  m/min. There was similar no significant difference regarding the inserts. The feed force was somewhat higher at this speed than at  $v=500$  m/min. At the highest feed rate and depth of cut values, elongated elemental chips were formed. Measured at other parameters however, continuous chip formation occurred, which is not favourable.



Figure 6. POM C elemental chips

In case of POM C,  $v=100$  m/min has generated the highest main cutting (Fig. 7).

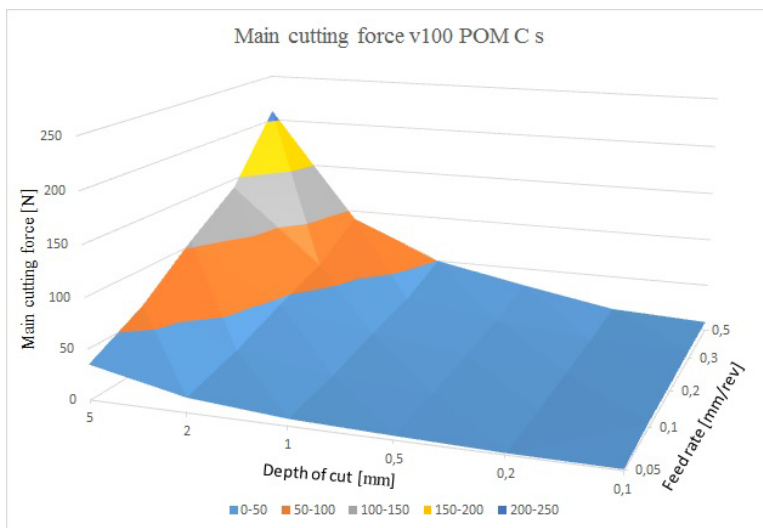


Figure 7. Main cutting force of POM C at  $v= 100$  m/min

There was no difference between the inserts in this case, either. At this speed, continuous chips were formed in all cases.

## Conclusion

From the method suggested in this article, we have conducted experiments in POM C and PA 6. Based on the experimental results obtained, there are some conclusion:

a, For each material, the same machining parameters generate different cutting force value.

b, By increasing the machining parameters, a noticeable sound effect could be observed throughout the machining process, which was probably caused by machine vibrations.

c, While machining PA 6, the chip shape was the most favorable when generated by the upper range of the cutting parameters, since instead of the continuous type, segmented chips were formed. This type of chip breaks easier and thus is safer than the continuous one.

d, Regarding the inserts, the polished surface was more effective as it generated smaller cutting forces and the absolute value of the feed forces were significantly lower, especially in the upper range of parameters, so economically speaking, it is advisable to purchase inserts with a polished surface.

e, While machining PA 6, the negative feed force is an innegligible phenomenon, since in conventional machines, sliding structures may have backlash that impact in the machining accuracy and the sudden change of direction.

f, It can be stated that POM C has a better machinability than PA 6. In the upper range of experimental parameters, elemental chips have been created, which are the most favorable in terms of safety, and in the case of lower parameters, transitional or easily breaking continuous chips were formed. No significant difference occurred between the two types of inserts while measuring this material.

The proposed method in this article is effective in finding the optimal parameters for polymer machining, as in our experiment for PA 6 and POM C. We may elaborate this method to further research with different materials and different machining condition.

## References

- [1] Angyal B., Dobor Lné., Palásti K. B., Sipos S. (1998): A Forgácsolás és Szerszámai, Műszaki Könyvkiadó, Budapest, (in Hungarian).
- [2] Chabbi, A., Yallese, M. A., Nouioua, M., Meddour, I., Mabrouki, T., Girardin, F. (2017): Modeling and optimization of turning process parameters during the cutting of polymer (POM C) based on RSM, ANN, and DF

- methods, *The International Journal of Advanced Manufacturing Technology*, (in English).
- [3] Davim, J. P., Mata, F. (2006): A comparative evaluation of the turning of reinforced and unreinforced polyamide, *The International Journal of Advanced Manufacturing Technology*, (in English).
- [4] Kalácska G. (2005): *Műszaki Műanyag Féltermékek Forgácsolása*, Quattroplast Kft., Gödöllő, (in Hungarian).
- [5] Kalácska, G. (2007): *Műszaki polimerek és kompozitok a gépészmérnöki gyakorlatban*, 3C-Grafika Kft., Gödöllő, (in Hungarian).
- [6] Kári-Horváth, A., Fledrich G., Kakuk, Gy., Zsidai, L. (2016): *Gépgyártástechnológia*, Szent István Egyetemi Kiadó Nonprofit Kft., Gödöllő, (in Hungarian).
- [7] Nagy P. S. (1997): *Szerszámgépek, gyártórendszerek*, BDMF jegyzet, Budapest, (in Hungarian).
- [8] Sarankó, Á., Keresztes, R., Kalácska, G. (2016): *Machining of engineering polymers*. *International Scientific Conference On Advances In Mechanical Engineering*, (in English).
- [9] [www.dieterle-tools.com](http://www.dieterle-tools.com)

## Shear strength of overlap bonds of plasma treated PA6 and PEEK

Zoltán SZAKÁL<sup>1</sup>, Tamás PATAKI<sup>1</sup>, Attila KÁRI-HORVÁTH<sup>1</sup>,  
Mátyás ANDÓ<sup>3</sup>, Rajini NAGARAJAN<sup>2</sup>

<sup>1</sup>Institute for Mechanical Engineering Technology, Szent István University,  
Páter K. u. 1., Gödöllő, H-2100, Hungary,

<sup>2</sup>Kalasalingam University, Anand Nagar, Krishnankoil-626126,  
Tamil Nadu, India.

<sup>3</sup>Savaria Technical Institute, ELTE, Szombathely

### Abstract

In this study we compared the effect of an atmospheric cold plasma treatment and without treatment of surface adhesive strength of joint. In this job we compared the Polyether ether ketone (PEEK) and Polyamide 6 (PA6) adhesive properties of materials. These two polymers greatly differ in their chemical composition and as a consequence in their surface properties, too. During our work, we examined the features of the bonding of the polymers, which are qualified as engineering material. In the course of the research we apply acrylic base and cyanoakrylate adhesives. In this work we used the DPD plasma treated of polymers of surface. The specimen of plasma treated increase the energy of surface. For qualifying the glued bonding we used specimens with lapped bonding made according to standard DIN EN 1465 and by breaking then we used tensile-test machine according to standard ISO 527-1. We make a proposal based on the results, onto the bandage forming coming close to the strength of the base material relating to the examined polymers.

### Keywords

DBD treated surface, PA6, PEEK, adhesion bonding, adhesive, gluing, polymer,

### 1. Introduction

Currently not only the development of polymer composites is going on, but the market of the bonding materials was transformed in the past 5-10 years totally. New and newer adhesives appear with additional surface treatment materials, which help the adhesion of cements and the increase of their strength. The development and adoption as well as testing of sticking technologies of machine parts made of engineering plastics comes into the foreground rather continually. One of the main motivators of this is the industry, where the forming quick high-strength and elastic component contacts have got crucial importance. Here during production (sticking body and casing elements) and repairing (broken

plastics, the bonding of windscreens) structural adhesives are used equally [2,3]. The advantage of adhesion bonding: the constructional margin is growing, homogenous stress distribution, does not harm the structural materials, different structural materials can be bonded, may reduce the number of the machine elements, more aesthetic appearance.

We planned an overall experiment series, with the use of the most used engineering polymers and the new adhesion materials, with adhesives applied widespread in the industry in our present research. The adhesive substances are recommendation by Henkel Magyarország Ltd, we chose it from a product line of Loctite.

We carried out according to the ISO 527-1 standard the shear test of lap joint made by the DIN EN 1465 standard with tensile-test machine. In the literature all the polyolefin [1,5,12], all the fluorine [9,10,11] polymer basis articles, which added a footing to our examinations, are attached to the adhesive and mechanics features of plastics [4,6,7,8].

We call those non-metallic substances an adhesive, that the firm surfaces with the surface adhesion (adhesion), and their own solidity join (cohesion). The sticking is an operation when a mediatory substance, the mucilage connects the surfaces of the solids with its help, and the peculiarities of the surfaces to be connected do not change.

The material to be bonded must fulfil two conditions:

- The mucilage has to moisten the polymer. The surface energy of plastic has to be higher or equal with the surface tension of the mucilage.
- The polymer surface must have adhesion friendly characteristics. This means that a chemical and physical interaction has to come into existence between the mucilage and the surface boundary layer.

In this case, the stock is unsuitable for gluing if these conditions do not come true, or the surfaces demand preparative treatment.

In the technical practice there are well-adhesive polymers and there are hard-wearing polymers. In case the surface energy of the polymer is small, it can not be glued.

Increasing the surface energy of the polymer component:

- burning,
- etching,
- roughening,
- activation.

can be used.

When activating the surface of the polymers, a free chemical connection must be established. One of the methods of creating free surface chemical bonds is DBD plasma treatment. Recently, atmospheric-pressure plasma has been of rising interest from viewpoints of both academic research and industrial applications, and is widely used for surface modification of polymeric materials instead of low-pressure plasma, because it does not need vacuum system as it is operated under atmospheric pressure. In addition atmospheric pressure plasma is characterized by high concentration of activated species generated by plasma, short mean-free path of electrons and high concentration of working gases.

## 2. Experimental methods

The Table 1 shows the tested materials and to them owing (the Loctite made a choice based on Technical Data Sheet (TDS) recommendation) adhesive systems. We examined selected materials on the experiment series with themselves and sticking with a general construction steel.

The test methods were performed on natural polymers, this were the basis of the test. The DBD plasma treatment was performed by modifying the surface energies of the polymers. On the treated specimens, the adhesive bonding shown in Table 1 was again performed.

Table 1. Gluing experiment plan

Material mates	Adhesive
PEEK - PEEK	Superglue: Loctite 406 (Cyanoacrylate)
	Structural adhesive: Loctite 330 (acrylic)
	Structural adhesive: Loctite 9466 (epoxi)
PEEK – S235 steel	Superglue: Loctite 406 (Cyanoacrylate)
	Structural adhesive: Loctite 330 (acrylic)
	Structural adhesive: Loctite 9466 (epoxi)
PA6E – PA6E	Superglue: Loctite 406 (Cyanoacrylate)
	Structural adhesive: Loctite 9466 (epoxi)
	Structural adhesive: Multibond 330 (acrylic)
PA6E – S235 steel	Superglue: Loctite 406 (Cyanoacrylate)
	Structural adhesive: Loctite 9466 (epoxi)
	Structural adhesive: Multibond 330 (acrylic)

### 2.1 Adhesive test

The tensile test was carried out the ISO 527-1 standard, the overlap joints made according to the DIN EN 1465 standard with a lap-shear test. The requirements for bonding of the specimens:

- 5 repeated bonding at the same time with a given materials.
- Overlapping has to be  $12.5 \pm 0.1$  mm.
- The same normal force (5 N) applied during curing.
- Stick-free bonding-jig to prepare the bond.

The experiments were carried out according to the glue producer's (Henkel Loctite, Hungary) recommendations (Technical Data Sheet – TDS – of Loctite):

- Rough cleaning with water.
- Degreasing of the surfaces with Loctite SF 7063.
- Creating the bonds in the jig.

The specimens prepared adequately on a tensile test machine, according to DIN EN 1465 standard (as mentioned). Although the standard mentions more solutions onto the forming of the specimens, the simple overlap joining was

selected. The adhesive test was done within 24 hours after the plasma treatment, To ensure a full effect of DBD plasma.

Where the best results of plasma surface modification were performed immediately after treatment, then the surface starts recovering to the reference state after 24 hours [6,1]. The overlap area of the polymer plates (immediately after plasma treatment) coated with a primary activator (for the glues that have been recommended to use them with primary activator) before adding the adhesives. The glue amounts are 0.035 ml of Loctite 406 and 0.1 ml for the other structural adhesives after the adhesives adding, the plates set up with each other in the apparatus. The test has been repeated 5 times for each polymer and different pairs polymer/polymer and polymer/steel. The tensile test was managed by a (Zwick Roell Z100) tensile machine as shown in Figure 5, with 1.3 m/min pulling speed and 100kN maximum tensile load. The shear strength is equal to the maximum failure force dividing the bonded area.

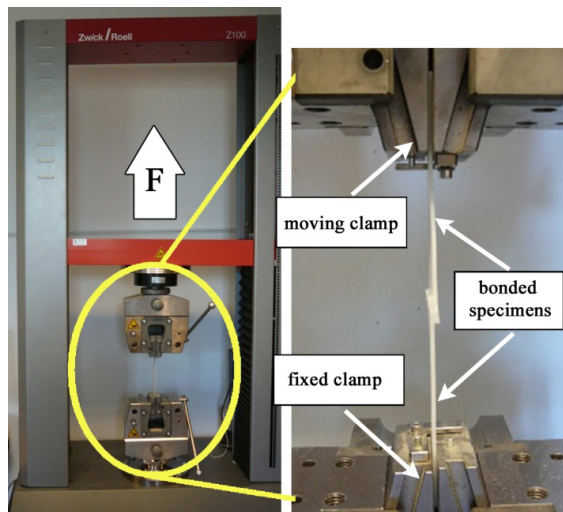


Figure 1. Zwick Roell Z100 tensile-test machine

The specimens used for the gluing were made by sawing from a 2mm thick plate in an identical size. The dimensions of the specimens are shown figure 1.

We fit the specimens with 12,7mm long overlap to each other, for the forming of the bandage. We chose the lap based on standard DIN EN 1465. The requirements made on the gluing of the specimens:

- simultaneously the gluing of 5 specimens,
- overlap size are  $12,5 \pm 0,1$  mm,
- having identical compressive force,
- the specimens should not stick to the apparatus.

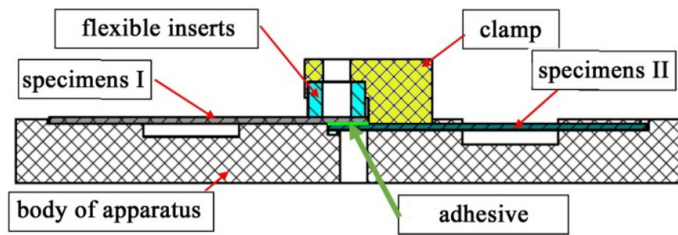


Figure 3. The apparatus used for the gluing

We bonded the specimens (what useful for tensile stress test) in the apparatus which can be seen on the Figure 3. We bonded two pieces of specimens can be seen on the Figure it together. We degreased the specimens with Loctite 7200 detergents before the bonding. We used Loctite 406 and Loctite 3035 adhesive gluing specimens.

The process of bonding technology:

- We cleaning the surface of specimen (Loctite 7063)
- We treated the plastic surfaces with the primer implement first.
- We the necessary adhesive placed on the specimens.
- Finish we laying on one another on the specimens.

We made the bonding according to Loctite Technical Data Sheet (TDS) regulations. The TDS grants the preparation method of gluing surface, the time of adhesive of application and his solidification time.

### 2.3 Dielectric Barrier Discharge (DBD) source

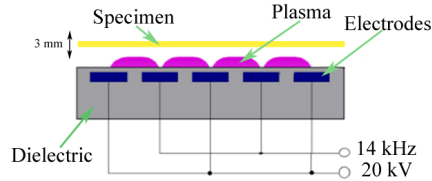
The most popular cold atmospheric plasma sources are based on DBD [16, 17].

A dielectric barrier at one or both electrodes can suppress and, in combination with high frequency power, prevent streamers. There are a large number of different designs, constructions, electrode shapes, and dielectric barriers used in DBD sources for different applications.

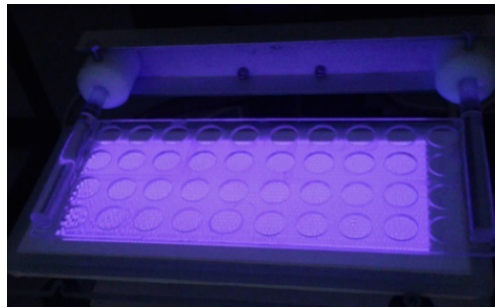
About DBD plasma treatment H. Al-Malaki -G. Kalacska wrote more. They investigated the relationship between surface treatment of polymers and surface energy [15, 18].

The atmospheric pressure ambient air plasma was generated by DCSBD plasma source. The principle of DCSBD plasma is based on a coplanar DBD where comb shape electrodes are embedded in a dielectric. The diffuse plasma is generated in thin 0.3 mm thick flat layer on alumina ceramic which designates the DCSBD to be used especially for treatment of flat surfaces. The DCSBD electrode system was powered by AC HV source of frequency approx. 14 kHz and voltage approx. 20 kV peak-to-peak and the total power in plasma during the experiments was 400 W. The area of generated plasma of DCSBD is 170 cm<sup>2</sup>, thus the surface energy density and volume energy density at power of 400 W are approximately 2 W cm<sup>2</sup> and 80 W cm<sup>3</sup>, respectively. The DCSBD plasma is described in detail [14]. The plasma treatment was performed in dynamic

treatment mode and the distance between the treated polymer surface and DCSBD ceramic was 0.3 mm. The treatment has been done under air atmosphere conditions ( $T = 23^{\circ}\text{C}$ ,  $H = 50\%$ ), the apparatus shown in Figure 4. The treatment time for each specimen was 1 min.



a;



b;

Figure 4. The plasma method  
a; Draw the plasma process,  
b; surface of plasma device

## 2.4 The tested materials

### Adhesives

The Loctite adhesives what were used are reactionary adhesives. Their application happens in a fluent state, and they are consolidated by a reaction between the surfaces. Loctite gave the adhesives for our experiment series. Technical data of the selected adhesives Table 2. contains.

**Loctite 406:** This superglue is designed for bonding of plastics and elastomeric materials where very fast fixturing is required. His benefit, is that is resists up to  $120^{\circ}$  temperature and has got low viscosity The Loctite 770 polyolefin primer increases the gluing solidity in case of the polymers which can be stucked difficultly. His fixing time is 2-10mp. It is colourless, transparent material.

**Loctite 330:** General purpose acrylic based adhesive. Adhesive gluing for bonding plastic with good impact resistance. Two-component scrubber, a mixture of a gel-like base and a thin fluid activator. Curing time is 3 minutes. In principle, the shear strength of the bonded bond is 30 MPa.

**Loctite 9466:** Structured adhesive for increased bond strengths with increased toughness. Two-component epoxy adhesive, it is a product with 1:1 mixing ratio, that mixes during carrying up to the surface thanks its tabulated from. Suitable for bonding metals, ceramics and most plastics. The recording time is 180 minutes and pot life is 60 minutes. The maximum shear strength of the bonded bond is 32 MPa.

Table 2. Technical data of adhesives

	Loctite 406	Loctite 330	Loctite 9466
Technology	Cyanoacrylate	Acrylic	Epoxy
Chemical Type	Ethyl cyanoacrylate	Urethane methacrylate ester	Epoxy
Components	One part without mixing	One part – requires no mixing	Two component - requires mixing
Cure	Humidity	With activator	Room temperature cure after mixing
Working Time, 25 °C, (before assembly):	3min	3min	7 min
Fixture Time	5-10 sec	30 min	1 h
Full strength	24 h	6 h	24 h
Shear Strength	8-15 N/mm <sup>2</sup>	15-30 N/mm <sup>2</sup>	5-32 N/mm <sup>2</sup>

### **Construction steel (S 235 JR N)**

The one with a general function, not alloyed one of the most widespread kinds of steels, with a low carbon content (0.17%) and tensile strength is at  $R_m = 400-500$  N/mm<sup>2</sup> disposal generally. It is easily workable, because of this its use is wide-ranging. For sticking standpoint it can be put among the easily bonding materials, so for any steels in the commerce it can be used with prescribed adhesive.

### **Polyether ether ketone (PEEK)**

The polyether ether ketone can be classified into a group of high performance (HPM) materials. It is a semi-crystalline, highly heat-resistant technical plastic. PEEK crystallinity is max. 48%, which are influenced by processing conditions. The natural crystalline PEEK has a density of 1.3 g / cm<sup>3</sup>, a tensile strength of 75-130 MPa, a breakage elongation of 5-20%.

PEEK is well adhesive to self and other materials with epoxy, cyanacrylate and silicone-based adhesives. Products of "plastic glue" marketed by adhesive manufacturers can be used.

### **Polyamide 6 (PA6E)**

General purpose technical plastic with good mechanical strength, excellent abrasion resistance and gliding properties. Polyamides are partially crystalline thermoplastic technical plastics and, in terms of both their chemical structure

and their mixed filling, reinforcing and modifying materials, many versions are available. All types of polyamides are hygroscopic, their moisture content affects the processing and the properties of the finished product, the water in the polymer behaves like a plasticizer that has an effect, for example. strength, rigidity, toughness. The PA6E has a tensile strength of 70-110 MPa. PA6E is one of the adhesive plastics, which means that any of the commercially available "plastic adhesives" can be used.

### 3. Discussion

We make known the test results carried out during research with different construction adhesive of those plastic which can be glued hardly and are widely used in practice. During our work we stuck PA6E and PEEK plastic with themselves and with construction S235 IR N steel. In the first part of the work a tensile test was performed according to ISO 527-1. The result of the measurement is shown in Table 3. These results refer to the base material without adhesion. The results were measured on a 12.4 x 25 mm cross-section of specimen.

Table 3. The polymers tensile force

Material	Maximum force [N]
PA6E	2479
PEEK	5184

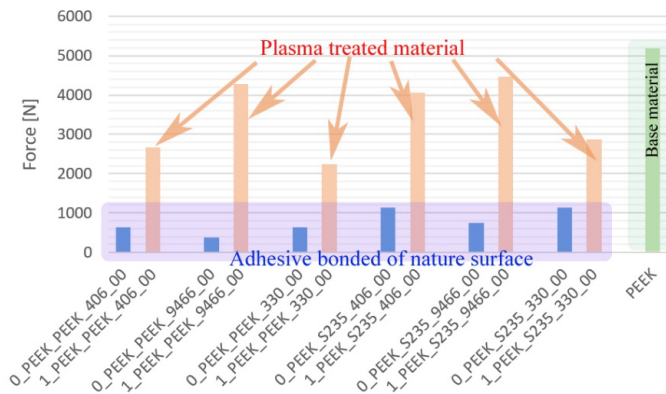


Figure 6. The results of the PEEK and S235JRN mates with different adhesives

PEEK is a brittle high-strength polymer. Small deformation is characterized by high load capacity. During the tensile test, the specimen crashed brittle. PA6E

is a tough technical polymer. Its strength is weaker as PEEK. Depending on the load, it has a large deformation, the protrusion is stretched.

PEEK belongs to the family of high performance engineering plastics. The PEEK is a hard and brittle material, its surface is smooth in nature stat. The surface energy is small in this condition, the adhesive can't connected. In the diagram shown in Figure 6, the blue columns are very small, showing the strength of different adhesives on the untreated surface. The bond strength is very low in this case, only 20% of the base material. This material is difficult to bond with conventional technology. There was no strong connection with any glue either. By treating the surface of PEEK by cold plasma, the bond strength of Loctite 406 and Loctite 9466 has also increased the tensile strength of the adhesive in several cases. Due to the increased surface energy of the treated specimen, all glue types worked well. On the basis of the work this material is best adhesive with the Loctite 9466 adhesive, when the strength of the adhesive is similar to that of the parent material.

Using the Loctite 406 adhesive, the PEEK / PEEK connection is similar to the untreated surface, the glue spread evenly and the adhesive does not penetrate mechanically. In connection with the PEEK / steel connection, the polymer has been broken in the vicinity of the adhesive while the adhesive has been removed from its surface. The glue is fully seeing on the surface of the steel. Loctite 9466 structural glue has created a perfect bond between both polymer / polymer and polymer / steel bonding. The shear strength of the bonded bond exceeded the tensile strength of the parent material.

When bonding with Loctite 330 structural adhesive, the adhesive is separated from one surface. During the polymer / polymer bonding of the test piece on which the glue is attached, the residue is difficult to remove. In the case of a polymer / steel connection, the adhesive on the steel surface was removed from the surface of the polymer.

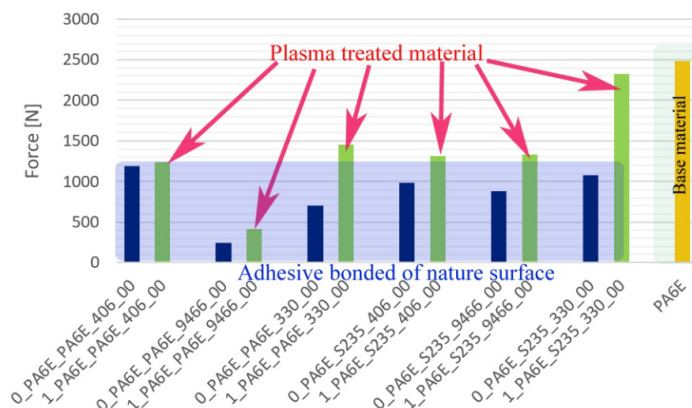


Figure 7. The results of the PA6E and S235JRN mates with different adhesives

In the case of Loctite 406 instant adhesive, the adhesive on the test specimen has a strong bond on the surface, after clipping the polymer / polymer, the adhesive surface is glossy and adherent to the surfaces. Unlike the TDS guidelines, when bonded bonding was established, the adhesive did not harden after hours of bonding. In the case of the polymer / steel connection, the adhesive is replaced by the steel surface. The adhesive completely does not interfere with the PA6E surface mechanical effect.

For PA 6E, the bond strength of Loctite 9466 with the structural glue was better as a result of cold plasma treatment. The adhesive is better attached to the surfaces. PA6E can only be used to remove the adhesive material from the surface of the PA6E.

In bonding with the Loctite 330 adhesive, the surface of the PA6E becomes less adhesive than the adhesive; in the case of the polymer / polymer connection, the adhesive disintegrates from the related surfaces.

## **Conclusion**

During our present research work we made a series of experiment with the most used engineering polymers and the new adhesion adhesives applied widespread in the industry. The material choosing included to the superglues and to the structural glues used generally which house got acrylic base, epoxy basis and case of superglues they are cyanoacrylate types. We have carried out the experiments of those engineering plastics to be rated not or hardly glueable polymers. Present article reports on the results of gluing experiments made on a surface, which were made without special surface treatments. In this paper we also reported on the effect of the DBD plasma surface treatment. Due to the treatment of the surface of the plastics, the bond strength increases in general.

In case of mating polymer and steel beyond choosing the adhesive, the glue must be able developing good adhesion connection with both surfaces, that adhesive should be preferred which is more optimal for the steel. Such case can take place, in the technical practice when it has to be produce glued bonding of polymer-polymer elements, beside the highest strength within reach of the given material. Then it should be consider that between the connection, made by lap it is expedient so put an intermediate rigid steel plate with this method the deformation ability of the bonding can be reduced. The smaller deformation results lower load on the glued bonding, the built in rigid part means a negligible effect so the whole structure.

## **Acknowledgement**



„ Supported BY the ÚNKP-17-4 New National Excellence Program of the Ministry of Human Capacities” and OTKA K 113039.

## References

- [1] A.M. Guedes Pinto, A.G. Magalhães, F. Gomes da Silva, A.P. Monteiro Baptista (2008) Shear strength of adhesively bonded polyolefins with minimal surface preparation International Journal of Adhesion and Adhesives, Volume 28, Issue 8, December 2008, Pages 452-456
- [2] Bernd R. Burchardt, Peter W. Merz (2006). Chapter 6 - Elastic Bonding and Sealing in Industry. Handbook of Adhesives and Sealants, Volume 2, 2006, Pages 355-480, xl-xlii
- [3] J. Daniels (1984). Design implications of adhesive bonding in car body construction. International Journal of Adhesion and Adhesives, Volume 4, Issue 1, January 1984, Pages 5-8
- [4] Ji-Zhao Liang, Qiang Du, Gary Chi-Pong Tsui, Chak-Yin Tang (2016) Tensile properties of graphene nano-platelets reinforced polypropylene composites. Composites Part B: Engineering, Volume 95, 15 June 2016, Pages 166-171
- [5] M. Kalnins, J. Ozolins (2002). Formation of a boundary layer of polyolefins adhesively bonded to steel. International Journal of Adhesion and Adhesives, Volume 22, Issue 3, 2002, Pages 179-185
- [6] M. Zrida, H. Laurent, V. Grolleau, G. Rio, M. Khlif, D. Guines, N. Masmoudi, C. Bradai (2010). High-speed tensile tests on a polypropylene material. Polymer Testing, Volume 29, Issue 6, September 2010, Pages 685-692
- [7] Mohammadreza Eftekhari, Ali Fatemi (2016). Tensile behavior of thermoplastic composites including temperature, moisture, and hygrothermal effects. Polymer Testing, Volume 51, May 2016, Pages 151-164
- [8] P. Poelt, A. Zankel, M. Gahleitner, E. Ingolic, C. Grein (2010). Tensile tests in the environmental scanning electron microscope (ESEM) – Part I: Polypropylene homopolymers. Polymer, Volume 51, Issue 14, 24 June 2010, Pages 3203-3212
- [9] Sina Ebnesajjad (2015). 17 - Surface Treatment of Fluoropolymers for Adhesion. Fluoroplastics (Second Edition), 2015, Pages 564-588
- [10] Sina Ebnesajjad, Arthur H. Landroc (2015). Chapter 12 - Testing of Adhesive Bonds. Adhesives Technology Handbook (Third Edition), 2015, Pages 339-352
- [11] Vacuum (1980). Adhesive bonding of ion-beam-textured metals and fluoropolymers. Vacuum, Volume 30, Issues 8–9, 1980, Page 35
- [12] Yukihiro Kusano, Masato Yoshikawa, Itsuo Tanuma, Kazuo Naito, Masuhiro Kogoma, Satiko Okazaki (1994). Plasma surface treatment of fluoropolymers at atmospheric pressure. Advanced Materials '93, 1994, Pages 657-660
- [13] Zeena Cherian, Richard Lehman (2005). Effects of adhesive type and polystyrene concentration on the shear strength of bonded polystyrene/high-density polyethylene blends. International Journal of Adhesion and Adhesives, Volume 25, Issue 6, December 2005, Pages 502-506

- [14] Cernák M., Cernáková L., Hudec I., Kováčik D., Zahoranová A.: 2009. Diffuse Coplanar Surface Barrier Discharge and its applications for in-line processing of low-added-value materials, *European Physical Journal: Applied Physics*, Vol. 47, pp. 1-6. <http://dx.doi.org/10.1051/epjap/2009131>
- [15] H. Al-Maliki – G. Kalácska (2017); The Effect of Atmospheric DBD Plasma on Surface Energy and Shear Strength of Adhesively Bonded Polymer; *Hungarian Agricultural Engineering*, Volume 31, Pages 52-58, HU ISSN 0864-7410
- [16] U. Kogelschatz (2003): *Plasma Chem. Plasma Proc.* 23, 1.
- [17] R.R. Roth, J. Rahel, X. Dai, D.M. Sherman (2005): *J.Phys D:Appl.Phys.* 38, 555.
- [18] Kalácska G., Zsidai L., Keresztes R., Tóth A., Mohai M., Szépvölgyi J. (2012): Effect of nitrogen plasma immersion ion implantation of polyamide-6 on its sliding properties against steel surface. *Wear*, 290-291, pp 66-73.

# Surface morphology and chemical composition of PP and PETP treated by atmospheric plasma

Hayder AL-MALI<sup>1</sup>, Zoltán KÁROLY<sup>2</sup>, Szilvia KLÉBERT<sup>2</sup>

<sup>1</sup>Institute for Mechanical Engineering Technology,  
Szent István University, Páter K. u. 1., Gödöllő, H-2100, Hungary,

<sup>2</sup>AKI, Research Centre for Natural Sciences, HAS,  
Magyar tudósok krt. 2., Budapest, Hungary

## Abstract

Polypropylene (PP) and Polyethylene terephthalate polyester (PETP) with extruded surface were treated by atmospheric dielectric barrier discharge (DBD) plasma for 1 min in the air. X-ray photoelectron spectroscopy (XPS) was utilizing a XSAM 800 spectrometer to elaborate the surface chemical composition. Theoretical calculations of the surface chemical composition are compared with values for pristine, treated polymer where different states of the surface chemical composition were noted after plasma treatment for both polymers. However, the Oxygen content was enhanced into the surfaces, which indicates wettability improvement. In contrast, The pristine and treated surface morphology was analyzed by scanning electron microscopy SEM. The effect of plasma on the surface morphology has interpreted as increasing in the surface roughness of both polymers and enhancing in the surface cohesion of PETP whereas PP surface cohesion exhibited substantial degradation.

## Keywords

Polymer, Plasma treatment, surface morphology, Chemical composition

## 1. Introduction

Plasma treatment is one form the most common techniques which used to improve polymer hydrophilicity and modify the surface morphology. The adhesion strength of PP has significantly enhanced due to atmospheric plasma treatment under several gas flows. The characteristics of the surface layer were introduced hydrophilic functional groups, where this improvement level was changed with time after treatment (Prat et al., 2000). Luminescence of plasma-treated in helium gas flow for PP enhances the polymer surface hardness (Duran et al., 2001). Treating polymer by cold arc-plasma jet under atmospheric pressure leads to superficial hydrophilicity improvement and decreasing in the water contact angle (Toshifuji et al., 2003). Atmospheric DBD plasma enhances the wettability and the surface roughness of PP, this enhancement increase proportionally with increase the time of plasma exposure (Nishime et al., 2012).

Also, PP roughness increases linearly with the atmospheric DBD plasma exposure time due to the polymer surface degradation and the formation of nodule-like features. (Kostov et al., 2013). The surface modification of different engineering polymers, including PP by atmospheric pressure plasma jet (APPJ), increases the PP surface roughness. However, nodule-like structures were produced as well, but much smaller compared to that one which constituted in the previous study when the polymer was treated by (DBD), researchers attributed that to the higher polymer degradation during the DBD processing. (Kostova et al., 2014). The surface modification of a PET film by atmospheric plasma in combination with different gasses timely improved the hydrophilicity and was followed by hydrophobic recovery after longer times (Gotoh et al., 2012). In parallel, significant changes in surface morphology and reactivity of PET surfaces have been noticed (Esen et al., 2005; Rashed et al., 2009). While operating in air, the processing parameters such as discharge power, processing speed, processing duration, and electrode configurations affect the nature and scale of the surface changes. In general, longer duration (low processing speed and a high number of cycles) and high power induced greater changes in the surface wettability of the PET (Liu et al., 2006). Among the different studied environmental gases, air and oxygen gave the highest hydrophilicity, while argon and nitrogen yielded lower hydrophilicity of the PET surface (Onsuratoom et al., 2010). In this research paper, the effects of atmospheric DBD plasma on the surface chemical composition and morphology of Polypropylene (PP) and Polyethylene terephthalate polyester (PETP) will investigate.

## 2. Methods and materials

### *Materials and preparation*

In this paper, two polymers in commercial version will be elaborated (distributed by Quattroplast Ltd., Hungary

and produced by Ensinger GmbH, Germany) in bulk conditions (unfilled) and extruded surface: the first (polyolefin) is Polypropylene or PP grade Docapren-H (elastic modulus  $E = 1200$  MPa, tensile strength  $\sigma = 32$  MPa, melting temperature  $T_m = 165$  °C), and the second (engineering polymer) is Polyethylene terephthalate polyester or PETP grade DocaPETP (elastic modulus  $E = 3100$  MPa, tensile strength  $\sigma = 79$  MPa, glass transition temperature  $T_g = 81$  °C). Polymer samples were machined into pins with a diameter of 10 mm and thickness of 4 mm. Before testing, the samples were cleaned in an ultrasonic bath with distilled water and 96% ethanol (Reanal, Hungary).

### *Plasma treatment*

The plasma was generated in the air and ambient atmospheric pressure by DCSBD plasma source at AKI, Research Centre for Natural Sciences. Plasma works depending on a coplanar DBD. The electrodes have comb-shape within a dielectric. The diffuse plasma is generated in thin 0.4 mm thick flat layer on

alumina ceramic; the DCSBD was designated to be utilized primarily for flat surfaces treatment (Roplass s.r.o., Brno, Czech Republic), the apparatus is shown in Fig. 1. The DCSBD electrode system was powered by AC High-Voltage source with frequency approx. (10-20) kHz and voltage approx. 20 kV peak-to-peak while the total discharge power in plasma during the experiments is 320 W. The total area of generated plasma is 170 cm<sup>2</sup>. The system is supported with oil recycling (cooling) system to maintain the system at the proper temperature range which keeps the gas temperature around 370 K. The DCSBD plasma is described in detail (Černák et al., 2009). The plasma treatment was performed in dynamic treatment mode, and the distance between the treated polymer surface and DBD plate was 0.5 mm. The treatment has been done under air atmosphere conditions (T= 23°C, H= 50%). The treatment time for each specimen was 1 min determined by preliminary experiments and all the recent experiments were done within 24 hours from the treatment.

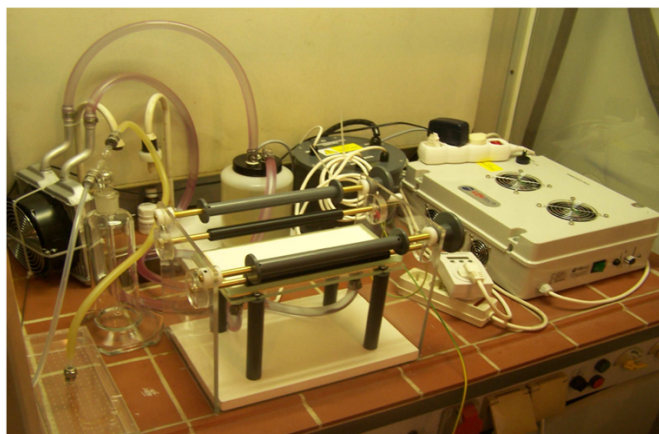


Figure 1. DBD laboratory test equipment used for polymer surfaces

### *Surface chemical composition*

The X-ray photoelectron spectroscopy (XPS) was carried out on a XSAM 800 spectrometer (Kratos, Manchester, UK), as shown in Fig. 2, equipped with a non-monochromatic Mg K $\alpha$ 1,2 radiation source (1253.6 eV) operating under a fixed analyzer transmission mode (chamber pressure < 10<sup>-7</sup> Pa). The pass energy was set at 80 eV for survey spectra (wide scan) and 40 eV for high resolution (detailed) spectra. The wide scan spectra were recorded at 0.5 eV steps in the 50 to 1300 eV energy range while the detailed spectra were recorded at 0.1 eV steps for the respective main elements. As a reference, the C1s line for the hydrocarbon C-Hx component was set to a binding energy of 285.0 eV. The accuracy of binding energy determination was  $\pm$  0.2 eV. The data acquisition and processing were performed with the Kratos Vision 2 software, applying a Shirley type background subtraction and decomposition of the peaks by using a

mixed Gaussian-Lorentzian shape (70/30 ratio) of equal full-width-at-half-maximum (FWHM). The quantitative analysis of the surface composition was based on integrated peak areas calculated by the XPS MultiQuant program (Mohai, 2004) and is expressed in (at.-%). The photo-ionization cross-section data of Evans et al. (1978) and asymmetry parameters of Reilman et al. (1976), were experimentally utilized. The conventional model of the infinitely thick layer was used to estimate the surface chemical compositions.



*Figure 2. X-ray photoelectron spectroscopy (XPS)*



*Figure 3. Scan electron microscopy SEM (Carl Zeiss EVO)*

### *Surface morphology*

The surface morphology of pristine and treated Surfaces was analyzed by scanning electron microscopy SEM (Carl Zeiss EVO, 40 XVP microscope,

Germany) is an electro-optical device as shown in Fig. 3. Which is directed thin electron to scan the surface, the resulting signal going to detect, process and then plot to give an image with information about the surface morphology. SEM resolution is 3.0 nm at 30 kV(SE and W), and 4.5 nm at 30 kV (BSD - XVP® mode) with 0.2 to 30 kV Acceleration Voltage. The magnification capability is 7 to 1,000,000x, the field of view is 6 mm at the Analytical Working Distance; the X-ray Analysis is 8.5 mm AWD and 35° take-off angle.

### 3. Results and discussions

#### Chemical composition

XPS analysis is carried out to monitor the alterations in chemical surfaces composition of PP and PETP. The surface elemental composition (at.-%) is shown in Fig. 4 (PP) and Fig. 5 (PETP), for theoretical calculations, before, and after plasma treatment respectively, these were recorded from the wide-scan XPS spectra. Onto pristine polymer surfaces, oxygen and nitrogen were presented which commonly results from unavoidable polymer surface contamination from the ambient air. The plasma treatment reinforces the surface oxygen content, in contrast, dropping in the carbon content is indicated by the changes of O/C atomic ratios. Furthermore, the activated (treated) surface may contain some atmospheric nitrogen which attributes to the higher reaction. The enhancing of O content suggests the presence of oxygen-containing polar groups into the surface Which introduces reason to the better wettability. The high-resolution XPS analysis of C1s spectra was evaluated to determine the ratio of the various polar groups developed on the surface. The results are in line with previous experiences (Kostova et al., 2014; Bertóti et al., 2015).

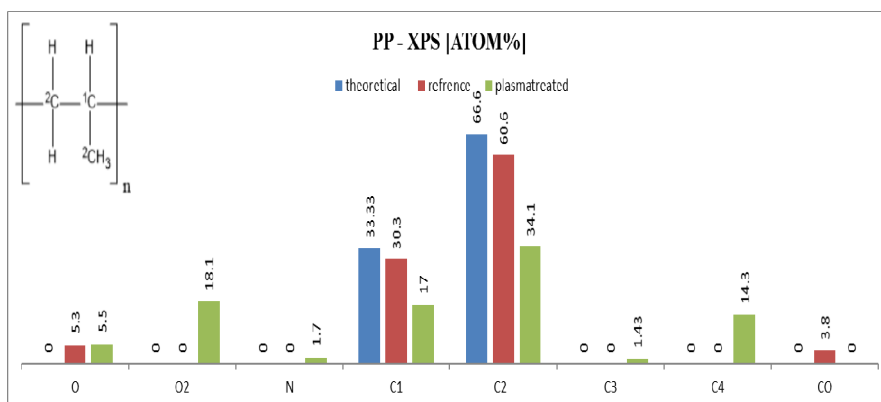


Figure 4. Surface chemical composition for PP, from high-resolution XPS spectra

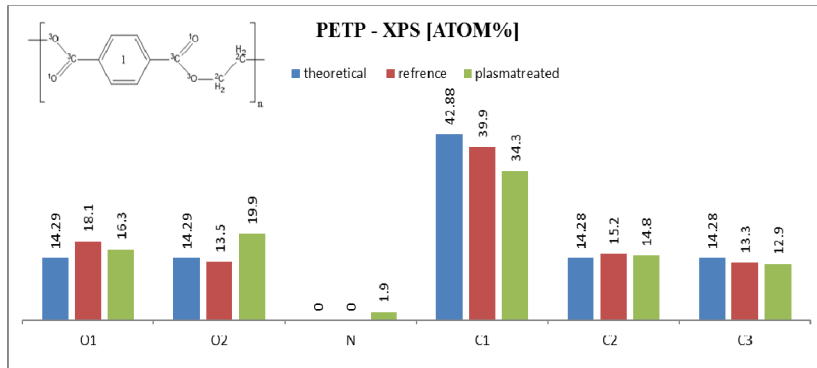


Figure 5. Surface chemical composition for PETP, from high-resolution XPS spectra

### Surface morphology

The morphology of extruded polymer surface was analyzed by scanning electron microscopy SEM. The SEM scans of pristine and treated samples summarized in Fig. 6. For PP and Fig. 7 for PETP. In general, the roughness of extruded surfaces exposes different behaviour upon DBD plasma treatment compared to finished one which is reported in our previous works (Al-Maliki et al., 2017a; Al-Maliki et al., 2017b). The surface roughness illustrates definite increase for the selected polymers, this attributed either to polymer surface degradation or constitution of nodule-link features or both of them. Nodule-links are composing by highly oxidized short polymer fragments, which called in the literature low molecular- weight oxidized materials (LMWOMs) (Kostov et al., 2013).

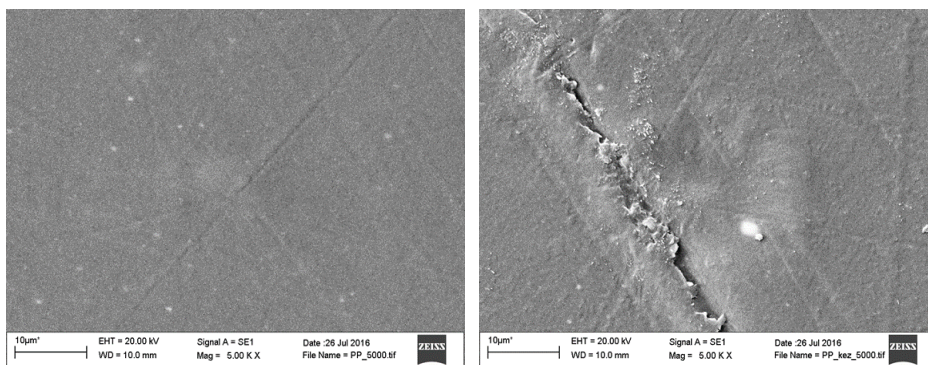


Figure 6. Surface morphology for PP from SEM (magnification 5000X) where to the left side is the pristine surface and to the right side is the treated one

This comparison was carried out to clarify the effect of surface finishing (polishing) on the surface morphology implying tribological behaviour in term of DBD plasma treatment. On the other hand, it is easy to see the decline in PP surface cohesion and appearance of the sharp edge which maybe already was

existed on the pristine surface in small size, and it was enlarged after treatment, or it was generated due to DBD plasma effect. Whereas, the PETP cohesion surface was apparently improved. It can also be seen white nodules which attribute to the high oxidation on the surface.

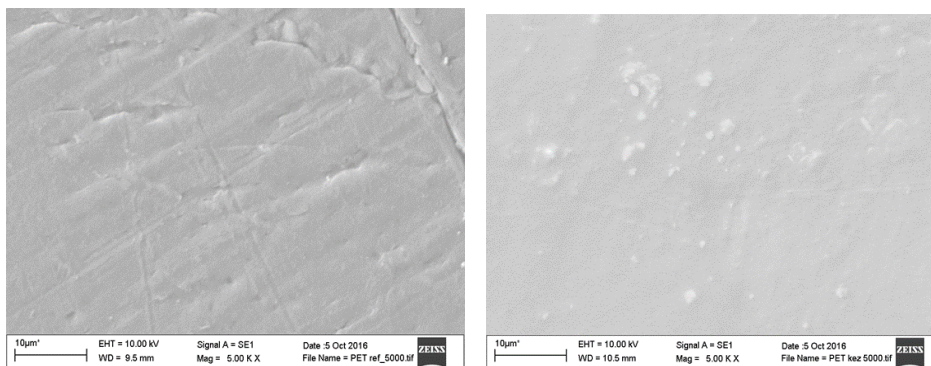


Figure 7. Surface morphology for PETP, from SEM (magnification 5000X) where to the left side is the pristine surface and to the right side is the treated one

## Conclusion

We can summarize this work as two commercial extruded polymers represent two different groups of the polymer (polyolefin and engineering polymers) are polypropylene (PP), and Polyethylene terephthalate polyester (PETP) have treated by atmospheric DBD plasma with 1min exposure time. The surface chemical composition was analyzed by X-ray photoelectron spectroscopy (XPS). Whereas, surface morphology was scanned by scanning electron microscopy SEM. The XPS results show a variation in the surface contains, but in general, the surface oxygen content was enhanced and the carbon content was dropped which introduce increasing in O/C atomic ratio and presents polar groups into the surface which substantially reinforce the surface wettability. In the same context, the surface morphology scan exposes a rise in the surface roughness due to DBD plasma treatment for both polymers, especially, for pp where a sharp edge could be seen. On the other hand, PP showed a decline in surface coherence while PETP cohesion was enhanced upon plasma treatment.

## Acknowledgements

The research is supported by OTKA K 113039.

## References

- [1] Prat, R., Koh, Y.J., Babukutty, Y., Kogoma, M., Okazaki, S., and Kodama, M. (2000), Polymer deposition using atmospheric pressure plasma glow (APG) discharge, *Polymer*, Vol. 41, PP. 7355–7360.

- [2] Duran, M., Massines, F., Teysse, G., and Laurent, C. (2001), Luminescence of plasma-treated polymer surfaces at ambient temperature, *Surface and Coatings Technology*, Vol. 142, pp. 743-747.
- [3] Toshifuji, J., Katsumata, T., Takikawa, H., Sakakibara, T., and Shimizu, I. (2003), Cold arc-plasma jet under atmospheric pressure for surface modification, *Surface and Coatings Technology*, Vol. 171, pp. 302-306.
- [4] Nishime, T. M. C., Toth, A., Hein, L. R. O., and Kostov, K. G. (2012), Surface characteristics analysis of polypropylene treated by dielectric barrier discharge at atmospheric pressure, *Journal of Physics: Conference Series*, Vol. 370, p. 012025. IOP Publishing.
- [5] Kostov, K. G., Nishime, T. M. C., Hein, L. R. O., and Toth, A. (2013), Study of polypropylene surface modification by air dielectric barrier discharge operated at two different frequencies, *Surface and Coatings Technology*, Vol. 234, pp. 60-66.
- [6] Kostov, K. G., Nishime, T. M. C., Castro, A. H. R., Toth, A., and Hein, L. R. D. O. (2014), Surface modification of polymeric materials by cold atmospheric plasma jet, *Applied Surface Science*, Vol. 314, pp. 367-375.
- [7] Gotoh, K., Kobayashi, Y., Yasukawa, A., and Ishigami, Y. (2012), Surface modification of PET films by atmospheric pressure plasma exposure with three reactive gas sources, *Colloid and Polymer Science*, Vol. 290, pp. 1005-1014.
- [8] Esena, P., Riccardi, C., Zanini, S., Tontini, M., Poletti, G., and Orsini, F. (2005), Surface modification of PET film by a DBD device at atmospheric pressure. *Surface and Coatings Technology*, Vol. 200, pp. 664-667.
- [9] Rashed, U. M., Ahmed, H., Al-Halwagy, A., and Garamoon, A. A. (2009), Surface characteristics and printing properties of PET fabric treated by atmospheric dielectric barrier discharge plasma, *The European Physical Journal-Applied Physics*, Vol. 45.
- [10] Liu, C., Brown, N. M., and Meenan, B. J. (2006), Uniformity analysis of dielectric barrier discharge (DBD) processed polyethylene terephthalate (PET) surface, *Applied surface science*, Vol. 252, pp. 2297-2310.
- [11] Onsuratoom, S., Rujiravanit, R., Sreethawong, T., Tokura, S., and Chavadej, S. (2010), Silver loading on DBD plasma-modified woven PET surface for antimicrobial property improvement, *Plasma Chemistry and Plasma Processing*, Vol. 30, pp. 191-206.
- [12] Černák, M., Černáková, L., Hudec, I., Kováčik, D., and Zahoranová, A. (2009), Diffuse Coplanar Surface Barrier Discharge and its applications for in-line processing of low-added-value materials, *European Physical Journal, Applied Physics*, Vol. 47, pp. 22806.
- [13] Mohai, M. (2004), XPS MultiQuant: Multimodel XPS Quantification Software, *Surface and Interface Analysis*, Vol. 36, pp. 828-832.
- [14] Evans, S., Pritchard, R. G., and Thomas, J. M. (1978), Relative Differential Subshell Photoionization Cross-sections (Mg K $\alpha$ ) from Lithium to Uranium, *Journal of Electron Spectroscopy and Related Phenomena*, Vol. 14, pp. 341-358.

- [15] Reilman, R. F., Msezane, A., and Manson S. T. (1976), Relative Intensities in Photoelectron Spectroscopy of Atoms and Molecules, *Journal of Electron Spectroscopy and Related Phenomena*, Vol. 8, pp. 389–394.
- [16] Bertóti, I., Mohai, M., and László, K. (2015), Surface modification of graphene and graphite by nitrogen plasma: Determination of chemical state alterations and assignments by quantitative X-ray photoelectron spectroscopy, *Carbon*, Vol. 84, pp. 185-196.
- [17] Al-Maliki, H., Zsidai, L., Samyn, p., Szakál, Z., Keresztes, R. and Kalácska, G. (2017a), Effects of atmospheric plasma treatment on adhesion and tribology of aromatic thermoplastic polymers, *Polymer Engineering and Science*. doi: 10.1002/pen.24689
- [18] Al-Maliki, H., Sukumaran, J., Kalacska, A., and Kalacska, G. (2017b), Influence of atmospheric DBD plasma on 3D topography of polymer, Danube Vltava Sava Polymer Meeting, Vienna, Austria, September 5-8.

## **The effect of sizes of the cast Polyamide 6 rods upon impact strength**

Miklós ODRÓBINA<sup>1</sup>, Zoltán SZAKÁL<sup>1</sup>, Gábor KALÁCSKA<sup>1</sup>, Róbert KERESZTES<sup>1</sup>, Otto EBERST<sup>2</sup>, Sever POP<sup>2</sup>

<sup>1</sup>Institute for Mechanical Engineering Technology,  
Szent István University, Páter K. u. 1., Gödöllő, H-2100, Hungary,

<sup>2</sup>Proned Control Srl, and Facultatea de Inginerie,  
Centrul Universitar Nord din Baia Mare,  
Universitatea Tehnica din Cluj Napoca (RO)

### **Abstract**

We have studied the impact strength of the magnesium catalysed cast polyamide 6 (PA6) rods according to the EN ISO 179-2:1999/A1:2012 standard. The goal of our research was that the mechanical properties of rods with different diameters are mapped beside same casting technological process. We have compared the received results with each other than have searched differences. We examined cylindrical product (rod) in diameter ranging from 40 mm to 300 mm in seven dimensional steps. We have found out that in this size range, semi-finished products can be divided into two groups typically in case of their impact strengths. In case of the products with a diameter of less than 100 mm the impact strength is higher and it is smaller in the larger dimension range. Thus, the minimum impact strength can be determined in case of the semi-finished natural PA6 rods that each rod performs independently of size. Furthermore, a range can be determined, which the impact strength values of product are scattered according to the manufacturing size.

### **Keywords**

cast polyamide 6, PA6, charpy impact test, mechanical properties, semi-finished products

### **1. Introduction**

Due to the increasing supply of plastic industry, plastics are being used now not only in subordinate locations, such as packaging materials, but also as load-bearing machine element. One of the most commonly used technical plastics is polyamide, which is one of the oldest but continuously improved plastics. The most commonly used type is polyamide 6 (PA6), which has good mechanical (hardness, toughness, strength) and tribological (abrasion resistance, sliding and gliding) properties. Additionally, it is suitable for composite production as matrix and fiber [Máthé, 2011]. The properties of polyamide 6 finished products

depend on highly the manufacturing technology and the input material. The PA6 can also be used in mass production, such as casting and extrusion [Czikovszky, 2003].



Figure 1. Casting tools with different diameters

The cutting of several parts provides wide and flexible use from semi-finished products (rod, tube, plate), which is widespread worldwide. The production of semi-finished products can be done by extrusion and casting. Both engineering experience and laboratory measurements have shown that the mechanical properties of extruded and cast polyamide 6 rods are slightly different. The material of the extruded rods generally has a lower hardness, greater deformation capability, weaker dimensional stability and more difficult machinability. Therefore, the engineering practice concentrates primarily on cast PA6 products, whose casting technology, tools and composite versions are constantly being developed.

In earlier research work in Hungary, the industrial production technology of magnesium catalysed cast PA6 was developed in case of semi-finished products (Figure 1). The advantage of this process is that it has a more homogeneous structure than previously known sodium catalysed PA6 products, has a higher degree of crystallinity and less residual monomer content. In addition, the abrasion resistance is better, and the value of impact strength is higher.

It is strongly recommended to use the toughened cast PA 6 materials in areas where operating conditions differ from the average. Such areas include aeronautics, agricultural engineering, engineering of mining and road building, and some automotive applications.

If the design and manufacturing of the machine element take place according to the exactly knowledge of the properties of a given size semi-finished product, then we could guarantee a minimal deviation of the expected lifetime.

It is a fundamental question: How do the particularities of the polymer manufacturing technology influence the resulting mechanical properties? In this research we have studied the impact strength value of magnesium catalysed cast PA 6 rods.

In our tests, we find the answer to the question of whether there are differences in strength parameters for seven different diameters of magnesium catalysed cast polyamide 6 semi-finished products (rods). If there is, what is the extent of this difference?

## 2. Investigated material: Cast PA6 matrix

The selected material is the magnesium catalysed cast PA6, which is manufactured under the name DOCAMID 6G-H by Quattroplast Ltd. The present research materials are made by gravitational casting. Among the cast polyamides, thanks to the specially-catalysed manufacturing process, it is distinguished by its uniform structure and toughness. Compared with the extruded natural PA 6, it has a higher strength, dimensional stability and abrasion resistance.

The input material of product is caprolactam ( $C_6H_{11}NO$ ), which is available in trade.

The Quattroplast Ltd. produces magnesium catalysed cast polyamide 6 with a unique manufacturing technology. It makes use of advantage that in this type of catalysts the ring-opening polymerization takes place in anhydrous medium in minutes

The essence of the process is anionic ring-opening block polymerization in the presence of magnesium counterion and activator. During the process by-product does not arise, so the molecule chains are not produced by polycondensation but anionic polymerization. The molecular weight of the finished material can not be greater than 25,000 g/mol and its monomer content is only about 1% that follows from the casting technology (mainly the catalyst content) [Andó, 2010].

## 3. Charpy impact test

*The principle of the method is as follows:*

The notched (V or U-shaped) or non-notched specimen is positioned horizontally and is broken by a single-arm pendulum between the two supports. The notched specimen is hit at the lowest point of the pendulum oscillation against the notch. It is shown in Figure 2 [ISO 179-1, 2012].

*Equipment:*

The applied pendulum impact tester (Figure 3) is, a table-mounted measuring device, developed specifically to determine the value of the specific impact of thermoplastics. It is suitable for Charpy, Izod, Dynstat and Tensile Impact

method. Hammer energies are available from 0.5 to 50 J depending on the type of the test. At break time, the impact velocity is between 2.9 - 3.8 m/s depending on the hammer used [Link 1]. The Charpy method was performed with a 1 J (hammer energy) according to the measuring range necessary to break the polyamide specimen.

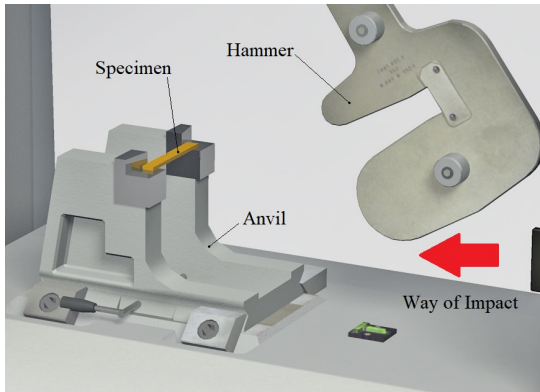


Figure 2. The position of specimen before the moment of impact



Figure 3. INSTRON CEAST 9050 impact tester

#### Specimen:

The specimen is a notched block. Its dimensions are prescribed by standard, and it is especially important to create a notch, and there are several possibilities.

For our measurements, the specimen is formed that the Figure 4 shows. The dimensions are in millimetres.

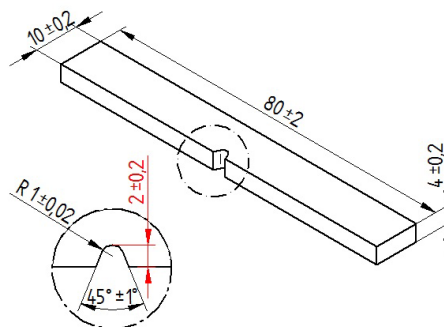


Figure 4. The sizes of specimen

The notch was constructed mechanically with a manual device manufactured by Instron. The notches were cut on the test specimens with a radius of  $1 \pm 0.02$  mm by a cutting knife what is selected in accordance with the standard.

Another important aspect is the location of the specimens inside the cast rods. The specimens required for the measurements were cut with axial orientation from the middle part of the rods, 9 pieces for each measurement. For our tests, the samples were taken from 7 different diameters of cast polyamide 6 rods (semi-finished product).

#### 4. The results of measurements

In the course of investigations we determined the value of the specific impact strength of the specimens belonging to each diameter. The value of the specific impact strength of unsaturated sodium-catalysed polyamides is below  $10 \text{ kJ/m}^2$  in the literature in case of the Charpy method [Kalácska, 2005]. The DOCAMID 6G-H that we measure has higher impact strength. Based on the measurements, the average value of the specific impact strength is  $15.89 \text{ kJ/m}^2$ . The Figure 5 illustrates the specific impact strength as a function of the diameter.

The chart shows that two types of trends can be distinguished. From 40 mm to 90 mm, a slight increase was observed in impact strength, which reached its maximum in case of 90 mm rod. Its average impact strength is  $18 \text{ kJ/m}^2$ . It is a very high value in case of various natural cast polyamide 6 materials in the world. Above 90 mm, a reduced impact strength is found at  $15\text{--}16 \text{ kJ/m}^2$ , which is still very high and favourable value up to 300 mm in diameter.

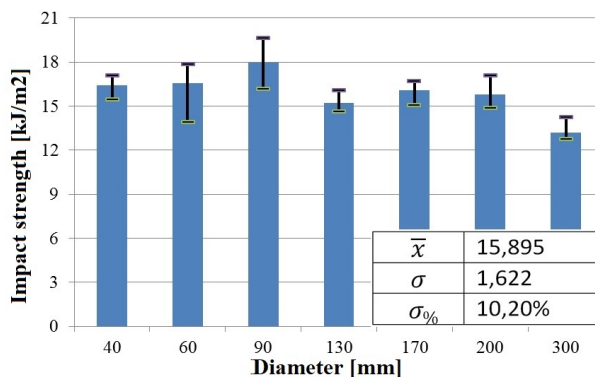


Figure 5. Measured impact strengths in case of rods with different diameter

The impact strength of rod with 300 mm is further reduced to around  $13 \text{ kJ/m}^2$ . This phenomenon draws attention to the further development of the casting technology of rods with diameters of 300 mm or more, and the expanding of the toughness.

It is typical of the whole series of measurements that the coefficient of variation is around 10%, which is very good in the case of dynamic tests. It suggests a homogeneous structure of the measured material.

## Conclusion

Based on the axial orientation samples taken from the centre of the rods with different diameters, it can be established that the impact strength is not constant in case of the natural cast PA6 rods that produced with a particular production technology.

In the 40 to 300 mm dimension range of magnesium catalysed PA6 (DOCAMID 6G-H), the impact strength is in the range of 13 to 18 kJ/m<sup>2</sup>.

After the casting of rods with a diameter of 300 mm or bigger, the technical reliability and the dynamic load capacity of larger machine components would be improved with a subsequent process (increasing impact strength), and the problems of cutting technology would reduce in case of the large-scale rods.

The reason of the differences of the coefficient of variation and impact strength can be found in the production technology in case of the measurements.

Ultimately, the thermal dynamics of the technology will determine the mechanical properties of the product, including the impact strength properties.

## References

- [1] Andó, M. (2010): Műszaki műanyagok kompozitok fejlesztése mezőgazdasági gépészeti alkalmazásokhoz. Ph.D értekezés, Gödöllő: Szent István Egyetem, Műszaki Tudományi Doktori Iskola
- [2] Czikovszky, T., Nagy, P., Gaál, J. (2003): A polimertechnika alapjai. Budapest: Műegyetemi Kiadó
- [3] Kalácska, G. (2005): Műszaki műanyag féltermék ismertető sorozat, 2. rész. Műanyagipari Szemle, 5, 2005.
- [4] Máthé Csabáné (2011): Műanyagok „igény szerint” – funkcionális töltőanyagokkal. Műanyagipari Szemle, 3, 2011.
- [5] MSZ EN ISO 179-1:1999/A1:2012 Műanyagok. A Charpy-féle ütési jellemzők meghatározása. 1.rész: Nem műszeres ütővizsgálat
- [6] Link 1: <http://www.instron.co.hu/wa/product/CEAST-9050-series-pendulums.aspx>

# Finite-element model development of single asperity scratch: a step-by-step approach

Kannaki PONDICHERRY<sup>1,2</sup>, Timothy GALLE<sup>1</sup>, Jacob SUKUMARAN<sup>1</sup>,  
Dieter FAUCONNIER, Stijn HERTELÉ<sup>1</sup>, Patrick. De BAETS<sup>1</sup>

<sup>1</sup>Soete Laboratory, Department of Electrical Energy, Metals,  
Mechanical Construction and Systems, Ghent University, Technologiepark,  
Zwijnaarde-903 Ghent, 9052, Belgium

Tel.: +32 9331 0489, E-mail: kannakishanmugham.pondicherry@ugent.be

<sup>2</sup>SIM vzw, Technologiepark 935, BE-9052 Zwijnaarde, Belgium

## Abstract

A roadmap and methodology to develop a three-dimensional (3D) finite-element model to simulate single asperity scratch is described in the present study. The step by step evolution from a two-dimensional (2D) static implicit Hertzian line contact model to 3D quasi-static explicit load controlled scratch model is explained. Each step is validated either by analytical models or by experiments. At every step, the model has shown a considerable agreement with the analytical solutions or experimental results. Therefore, scratch depth of metals can be predicted reasonably using the current model. Future work involves an extensive study of the influence of various parameters like indenter geometry, friction, etc.

## Keywords

Finite-element modelling, 3D scratch model, quasi-static-explicit, Hertzian contact

## 1. Introduction

A wide variety of research applications such as aerospace, ballistics, welding, fracture and failure analysis, etc. extensively use finite-element modelling as an efficient and effective tool to simulate response of material behaviour under operating conditions of respective fields (Gerbig, Srivastava, Osovski, Hector, & Bower, 2017; Jankowiak, Rusinek, Kpenyigba, & Pesci, 2014; Mason & Warren, 2017; Ni & Abdel Wahab, 2017). Finite-element modelling has also been used to study tribological phenomenon such as wear response of the material and influence of friction (Tobi, Sun, & Shipway, 2017; Yue & Wahab, 2017). Wear is one of the most common causes for component failure in real time applications. Among various types of wear, e.g., erosive, adhesive, fretting; etc., abrasive wear is of significant interest. According to an estimation, abrasive wear is responsible for almost 80-90% of all wear encountered in machine components whereas, fatigue wear follows at far distance with only 8%. Other

types of wear are even less common (Zmitrowicz, 2006). Abrasive wear is defined as, wear due to hard particles or hard protuberances forced against and moving along a solid surface (ASTM, 1987). The real system of abrasive wear is too complicated to be simulated using FE modelling. Therefore, a single scratch is the simplest and the most fundamental abstraction of abrasive wear that can be simulated with relatively less hardship.

Scratch indentation has been studied using Finite-Element Modelling (FEM) by many researchers from the perspective of various aspects such as, the influence of indenter geometry, friction coefficient at the contact, dynamic loading conditions etc. (Elwasli, Zemzemi, Mkaddem, Mzali, & Mezlini, 2015; Li & Beres, 2006; Subhash & Zhang, 2002). Many a times, the model development stage lacks a comprehensive description in literature. Hence, in the present work we focus on the methodology and process of model development itself. Therefore, a roadmap and methodology to develop a 3D finite-element model to simulate single asperity scratch is described in the present study. The present paper consists of the roadmap of finite-element scratch model development. The step by step evolution of the model from a simple 2D contact model to a 3D scratch model is explained in detail. Each step is validated either by analytical model or experimental results and the model has shown a considerable agreement.

## 2. Finite-element model development

### *Roadmap*

The present research aims at describing the development strategy of a finite-element model for scratch using ABAQUS (6.14). Hence, the path to achieve this goal was divided into four easy and simple steps of evolution listed below. The roadmap is laid out schematically in Table 1. These steps serve as building blocks aiding to learn and understand the process of model development, data extraction and analysis and the process of validation.

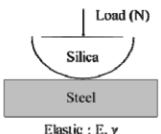
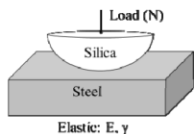
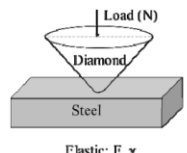
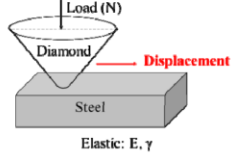
- i 2D Hertzian line contact
- ii 3D Hertzian point contact
- iii 3D Indentation
- iv 3D Scratch

Based on the type of problem we are trying to solve, two types of problem solving algorithms can be implemented in ABAQUS, namely, implicit and explicit. The fundamental difference in both the approaches is that in explicit scheme of analysis the values at time,  $t + \Delta t$  are calculated based entirely on time  $t$  whereas in the implicit scheme the value at  $t + \Delta t$  is obtained based on  $t$  and  $t + \Delta t$  which results in solving a set of non-linear equations (Chapra & Canale, 1988). Further details regarding these two schemes can be found in ABAQUS theory guide ("Abaqus documentation 6.14 ", 2014) The first two models are static processes, as they do not require time dependent material response and the inertial effects were insignificant. Therefore, they are solved

using the implicit scheme in ABAQUS/Standard. The third model of 3D indentation can be considered either as a static or a quasi-static process (inertial effects can be neglected but time-dependent material response is of interest). Thus, this model is solved using both implicit and explicit scheme by implementing ABAQUS/Standard and ABAQUS/Explicit respectively. This exercise helps not only to understand the nuances of the two approaches in detail, but also serves as a foundation for the development of the next step. The subsequent addition to the explicit 3D indentation model is to introduce the displacement of the indenter in order to achieve the scratch model.

The evolution of each stage of model development with respect to the type of process, model, etc., is summarized in Table 1. The first row describes the type of process and the solution scheme adopted to solve the model. The second row describes the type of model developed and the third row contains schematic representation of the models. The novelty of each stage is mentioned clearly in the figures. For example, the difference between the first two models is due to the dimensions, that is, the first model is a two-dimensional model whereas the second model was three-dimensional. Plasticity was introduced in the third model and displacement of the indenter was the uniqueness of the fourth model.

Table 1. Roadmap of scratch model development.

STATIC-IMPLICIT		QUASI-STATIC-EXPLICIT	
2D Hertzian line contact	3D Hertzian point contact	3D Indentation	3D Scratch
 <p>Elastic: E, <math>\gamma</math></p>	 <p>Elastic: E, <math>\gamma</math> 3D model</p>	 <p>Elastic: E, <math>\gamma</math> Plastic: True stress, true strain</p>	 <p>Elastic: E, <math>\gamma</math> Plastic: True stress, true strain</p>

### 2D Hertzian line contact model

The first step was to develop a simple two-dimensional finite-element model. The purpose of the two-dimensional model was to get acquainted with the process of model development, result extraction and analysis followed by verification of the model using analytical solutions. The model consisted of two deformable parts with semicircular ( $\Phi 1$  mm) and rectangular geometry (0.5 mm x 1 mm). The material properties listed in Table 2 were used to define the materials. The properties of silica and steel were assigned to the semicircular and rectangular parts respectively. In order to extract contact pressure from the model, plastic properties of the parts is not required. Therefore, only the elastic properties of the materials of the materials were used. The parts were partitioned appropriately and the area of contact being the region of interest was meshed

finer than the rest of the model. The finest element size was 1  $\mu\text{m}$ . A 4-node bilinear plane strain quadrilateral (CPE4) element type was used.

Table 1. Material properties of Silica and Steel

	Elastic modulus, GPa	Poisson's ratio
Silica	73	0.17
Steel	210	0.3

A frictionless, surface-to-surface contact was defined. The harder surface, silica, was defined as the master and the surface of the steel part was defined as the slave. A concentrated force was applied normal to the area of contact. Appropriate boundary condition of restricting the motions of the nodes on the side edges and the bottom of the specimen were imposed ( $U_1=U_2=U_3=0$ ). The semicircular part was also restricted to move in the X direction ( $U_1 = 0$ ). The von-Mises stresses (S) developed in the model are shown in Figure 1.

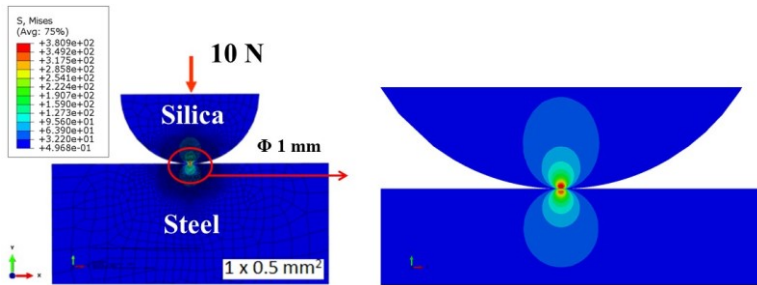


Figure 1. Two-dimensional Hertzian line contact model showing the von-Mises stress (S) distribution in the model

### 3D Hertzian point contact

The two-dimensional model developed in the previous step was further extended into a three-dimensional model. The three-dimensional model consists of two parts a hemisphere ( $\Phi 1\text{ mm}$ ) and a cube ( $0.5\text{ mm} \times 0.5\text{ mm} \times 0.5\text{ mm}$ ) as shown in Figure 2. The hemisphere was assigned the properties of silica whereas the cube was defined with the properties of steel. Since, contact pressure was being evaluated in this case too, only elastic properties were sufficient for material model definition. The region of interest being the point of contact had been finely meshed with an element size of 5  $\mu\text{m}$ . A similar surface contact, load and boundary conditions were implemented in the three-dimensional model as the two-dimensional model. The four side faces and the bottom of the specimen were bounded and the hemisphere was allowed only to move in the Y-direction. The contact stress distribution along the surface is shown in Figure 2 (b). The maximum contact pressure is 2.884 GPa.

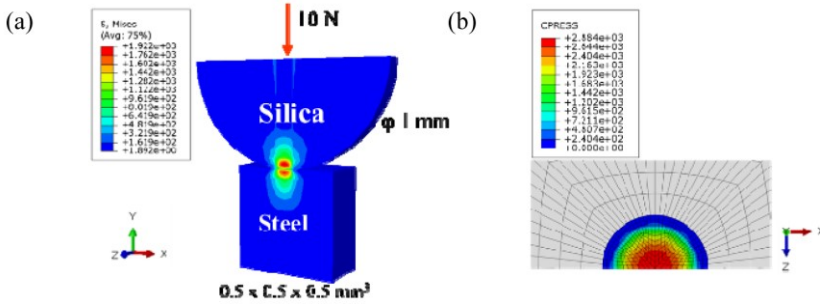


Figure 2. Three-dimensional Hertzian point contact model. (a) von-Mises stress (S) distribution in the model; (b) Contact pressure (CPRESS) distribution across the surface. The maximum contact pressure being 2.884 GPa.

### 3D indentation model

The three-dimensional indentation model simulates experimental microhardness indentation. The novelty of this model is the introduction of plasticity into the material definition of the specimen. Therefore, the specimen was defined as homogenous elasto-plastic deformable material. The elastic properties as shown in Table 2 were used whereas experimentally obtained true stress-true strain properties were used to define the plasticity of the steel specimen. The indenter was defined as analytically rigid cone of 120° included angle and a tip radius of 0.1 mm. A concentrated normal load of 25 N was applied on the indenter (see Figure 3). The increase in indentation depth with increase in applied load was plotted (see Figure 6 (a)). The residual depth of indentation after elastic recovery was observed to be 20.8 μm.

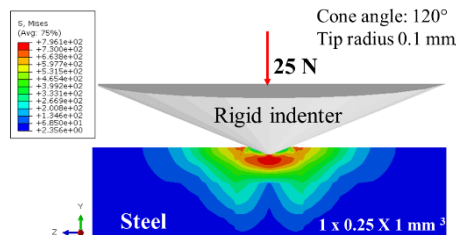


Figure 3. Three-dimensional indentation model involving a rigid cone with cone angle of 120° and a tip radius of 0.1 mm and an elasto-plastic deformable steel specimen (1 mm x 0.25 mm x 1 mm)

### 3D scratch model

The final step was to develop a finite-element model to simulate scratch. Scratch simulation involves the tangential movement of the indenter with respect to the specimen. In the present simulation the indenter is subjected to a displacement equal to the scratch length. The indenter geometry was similar to the previous

indentation model. The specimen dimensions of the elasto-plastic deformable material were 3 mm x 0.5 mm x 1 mm (see Figure 4). The scratch length was 2.5 mm. Mean scratch depth is defined the average displacement of the nodes along -Y axis between the scratch length of 1 to 2 mm. The mean scratch depth obtained for different scratch loads is plotted in Figure 6(b).

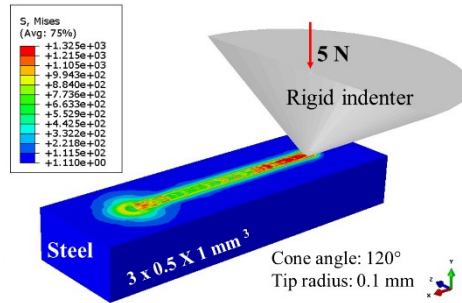


Figure 4. Scratch model involving a rigid conical indenter and an elasto-plastic deformable steel specimen.

### 3. Validation

The finite-element models developed were verified using analytical equations or validated using experimental results at each step. The verification of two-dimensional Hertzian line contact model was done using analytical equations of Hertz contact model (Bhushan, 2013). The analytical equations to calculate the effective contact radius ( $R^*$ ) and effective Young’s modulus ( $E^*$ ) are given in equation (1) and (2) respectively.  $R_1$  and  $R_2$  are the radii,  $E_1$  and  $E_2$  are the elastic moduli and  $\nu_1$  and  $\nu_2$  are Poisson’s ratio of the two surfaces in contact.  $W$  is the normal load applied. The maximum contact pressure  $p_{max}$  is calculated using equation (3) for Hertzian line contact.

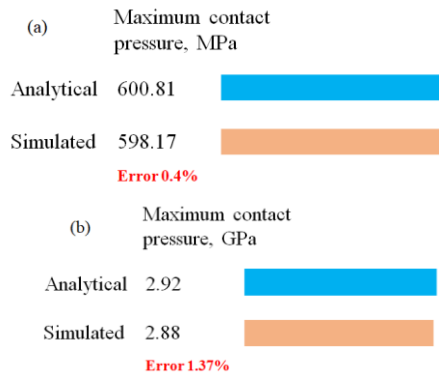


Figure 5. Comparison of analytical and simulated results;  
 (a) Hertzian line contact (b) Hertzian point contact

The comparison between the results obtained from the analytical solution and simulation is shown in Figure 5 (a). The maximum contact pressure was 600.81 and 598.17 MPa from analytical and simulated results respectively with an error of 0.4 %. Similarly, the three-dimensional Hertzian point contact model was verified using equations (1), (2) and (4). The equation of the maximum contact pressures varies in this case due to the change in the contact configuration. The maximum contact pressure obtained using analytical and simulations were 2.92 and 2.88 GPa with an error of 1.37 % as shown in Figure 5 (b).

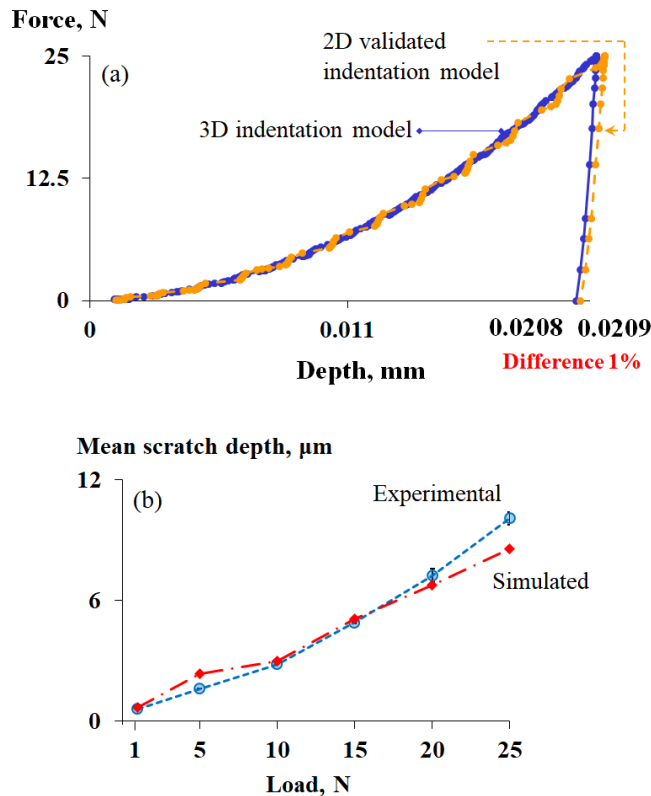


Figure 6. Validation of indentation and scratch models;  
 (a) Comparison of force-depth curve of the 3D indentation model developed and 2D validated model. The residual depth is showing a difference of 1 %.  
 (b) Comparison of experimental and simulated scratch results; Increase in the mean scratch depth with load is plotted. Simulated results are in good agreement with experiments.

The indentation model was validated indirectly using experimental results. A two-dimensional indentation model which was validated against experimental results was already available. Therefore, this two-dimensional model was used

to validate the 3D model developed. The increase in force with increase in scratch depth for both the two-dimensional and three-dimensional indentation models is plotted in Figure 6 (a). The difference between the residual depth of the 2D and 3D model is 1 %. The scratch model developed were validated using experimental results as shown in Figure 6 (b). The experiments were carried out using CSM scratch tester and details of the test procedure and equipment can be found elsewhere (Xu, van der Zwaag, & Xu, 2015). Mean scratch depth at 6 different scratch loads is plotted for simulated and experimental results and it can be seen that the simulated results are in good agreement with experimental results.

$$\frac{1}{R^*} = \frac{1}{R_1} + \frac{1}{R_2} \quad (1)$$

$$\frac{1}{E^*} = \frac{1-\nu_1^2}{E_1} + \frac{1-\nu_2^2}{E_2} \quad (2)$$

$$\text{Hertzian line contact, } p_{\max} = \left( \frac{WE^*}{\pi R^*} \right)^{1/2} \quad (3)$$

$$\text{Hertzian point contact, } p_{\max} = \left( \frac{6WE^{*2}}{\pi^3 R^{*2}} \right)^{1/3} \quad (4)$$

## Conclusions

The goal of finite-element model development for scratch has been successfully achieved with the help of the roadmap laid out. At each stage of evolution, the model has been successfully validated. The contact models both two-dimensional and three-dimensional are verified by analytical solutions. The indentation model also shows good agreement with a previously validated two-dimensional model. The results from the scratch tests and scratch simulations are in good agreement with each other. Future work involves understanding the effects of various parameters such as indenter geometry, sliding velocity, etc.

## Acknowledgements

I would like to express my deepest gratitude to Dr. ir. Tonyan Yue and Mrs. Kyvia Pereira for their valuable advice and support during the initial stages of

model development. I would like to thank Dr. Ir. Xiaojun Xu for conducting the validation experiments for scratch tests at NOVAM group, TU Delft. The research has been carried out in the frame work of MaDurOS program financed by SIM and VLAIO-Flanders.

## References

- [1] Abaqus documentation 6.14 (2014). from Dassault Systems, SIMULIA Corp.
- [2] ASTM. (1987). Annual book of standards *ASTM G40, Standard terminology relating to wear and erosion* (pp. 243-250). West Conshohocken.
- [3] Bhushan, B. (2013). *Introduction to tribology*: John Wiley & Sons.
- [4] Chapra, S. C., & Canale, R. P. (1988). *Numerical methods for engineers*: McGraw-Hill New York.
- [5] Elwasli, F., Zenzemi, F., Mkaddem, A., Mzali, S., & Mezlini, S. (2015). A 3D multi-scratch test model for characterizing material removal regimes in 5083-Al alloy. *Materials & Design*, 87, 352-362.
- [6] Gerbig, D., Srivastava, A., Osovski, S., Hector, L. G., & Bower, A. (2017). Analysis and design of dual-phase steel microstructure for enhanced ductile fracture resistance. *International Journal of Fracture*, 1-24.
- [7] Jankowiak, T., Rusinek, A., Kpenyigba, K. M., & Pesci, R. (2014). Ballistic behavior of steel sheet subjected to impact and perforation. *Steel and Composite Structures*, 16(6), 595-609. doi:10.12989/scs.2014.16.6.595
- [8] Li, J., & Beres, W. (2006). Three-dimensional finite element modelling of the scratch test for a TiN coated titanium alloy substrate. *Wear*, 260(11-12), 1232-1242. doi:http://dx.doi.org/10.1016/j.wear.2005.08.008
- [9] Mason, B. H., & Warren, J. (2017). Finite Element Simulation of Three Full-Scale Crash Tests for Cessna 172 Aircraft *58th AIAA/ASCE/AHS/ASC Structures, Structural Dynamics, and Materials Conference*: American Institute of Aeronautics and Astronautics.
- [10] Ni, J., & Abdel Wahab, M. (2017). A numerical kinematic model of welding process for low carbon steels. *Computers & Structures*, 186, 35-49. doi:http://dx.doi.org/10.1016/j.compstruc.2017.03.009
- [11] Subhash, G., & Zhang, W. (2002). Investigation of the overall friction coefficient in single-pass scratch test. *Wear*, 252(1-2), 123-134. doi:http://dx.doi.org/10.1016/S0043-1648(01)00852-3
- [12] Tobi, A. M., Sun, W., & Shipway, P. (2017). Investigation on the plasticity accumulation of Ti-6Al-4V fretting wear by decoupling the effects of wear and surface profile in finite element modelling. *Tribology International*, 113, 448-459.
- [13] Xu, X., van der Zwaag, S., & Xu, W. (2015). A novel multi-pass dual-indenter scratch test to unravel abrasion damage formation in construction steels. *Wear*, 322-323, 51-60. doi:http://dx.doi.org/10.1016/j.wear.2014.10.011

- [14] Yue, T., & Wahab, M. A. (2017). Finite element analysis of fretting wear under variable coefficient of friction and different contact regimes. *Tribology International*, 107, 274-282.
- [15] Zmitrowicz, A. (2006). Wear patterns and laws of wear - A review. *Journal of Theoretical and Applied Mechanics*, 44(2), 219.

# **Development of polymer gear test rig for loadbearing examination**

Róbert Zsolt KERESZTES, Miklós ODROBINA,  
Gábor KALÁCSKA, Fledrich GELLÉRT  
Institute for Mechanical Engineering Technology,  
Szent István University, Páter K. u. 1., Gödöllő, H-2100, Hungary,

## **Abstract**

In many areas of the industry the manufactures is commonly applied the plastic gears today, however, the failure processes of these plastic gears are not completely clear yet. The types of the tooth breakage are summarized briefly in case of occurring plastic gears. In addition, we designed and manufactured a real gear test rig, which is suitable for accurate determination of tooth damage in case of variable load (torque) conditions and stress speeds, as well as different modules. The load capacity of the gear has to be meant complex about point of view mechanics and tribology. The article releases the family of the gear test equipment and their operation.

## **Keywords**

polymer, gear, gear tooth, gear failure, test rig, gear test rig

## **1. Introduction**

These days there is very wide range of use of the plastics in such a manner, can be found in many areas of the industry, agriculture, space research, medical devices or the home and garden tools. At first they supplied in their uses secondary role as packing materials, handles. However, in the last decades more and more places appeared the plastic machine components which supplied structural function. For example: the belt pulleys, supporting rollers, different sliding plates, plain bearings and gears.

A number of plastic parts perform their task reliably in thousands ways of construction environment for a long time. In addition to the plastics have many benefits in front of metals such as the fewer weight, corrosion resistance, the great design flexibility, damping capacity, favourable tribological properties and the dry run (without lubrication).

Additional benefits that they were well machinable therefore individual components can be produced from them. Because of the reason mentioned above, it is also possible that the metal parts replacement with plastics much commoner. An appropriate example is for this phenomenon that the plastic gears gain ground much better certain areas.

However, the constructor has to pay attention to the disadvantages of plastics during planning which follows from structure of plastic.

We have designed and developed a plastic gear test rig, which can be used to investigate the teeth of plastic gears under extreme load conditions with different stress speed. We can get information from the brakeage and deformation of teeth, which few of scientific knowledge is available from. Like researcher, these may interest challenge to the detection.

## 2. Plastic gears in general

The gear drive is the most common among the mechanical drives, which is used expansively [Bártfai et. Al. 2017]. The materials, sizes and forming of gears hang on the parameters of the drive system, as the power, the temperature, etc.

These days the technical plastic gears are applied to less load transfer increasingly. Thermoplastic materials with a semi-crystalline morphology are most commonly used as gear wheel materials. Thermoplastics commonly used for gears include: Polyamides (PA), Polyoxymethylene (POM), Polybutylene terephthalate (PBT), High molecular weight, high-density polyethylene (HDPE), Polyaryl ether ketone (PEEK), Polyphenylene sulfide (PPS) and Polyurethane (PU) [Erhard, 2006; Melick, 2007; Paquet, 1989].

Certainly, the plastic gears have their own limitations in terms of temperature and load capacity. It is not worth manufacturing the heavy load, small size plastic gears because their strengths don't bear it. We can reckon it as a rule of thumb. Therefore, firstly they spread widely such areas, where their bearing capacities are enough and their advantageous properties can be used.

The load distribution of the plastic gear is an important factor from the point of view of its bearing capacity. The tooth-contact areas can be divided into three phases in case of the most widespread spur gear with involute profile, which is shown in Figure 2. When more than one pair of teeth is in contact, the load is shared among the pairs. Figure 2 illustrates the load-sharing characteristics between two pairs of teeth in contact. In Fig. 2, point E indicates the beginning of gear teeth meshing, point D is a transition point from double tooth to single tooth mesh, point B is a transition point from a single tooth to a double tooth mesh, and point A indicates the end of the mesh, while P is the pitch point of the gear. Section E-D and B-A indicate double tooth contact, whereas Section D-B is a single tooth contact area. The pitch value influences the boundaries of these sections considerably. The machinability and processing accuracy of different polymers are unlike, it follows that processing inaccuracy can create during production. If the pitch value is greater than the theoretical value, then the next gear tooth will connect later and thus the one tooth-contact area will be longer [Bárány, 1967; Melick, 2007].

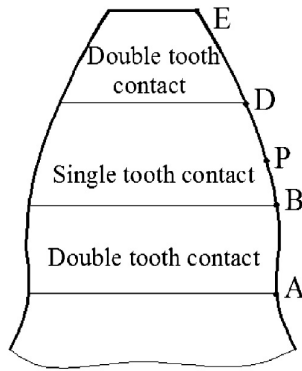


Figure 2. Tooth contact ares and limits [Hüseyin, 2009]

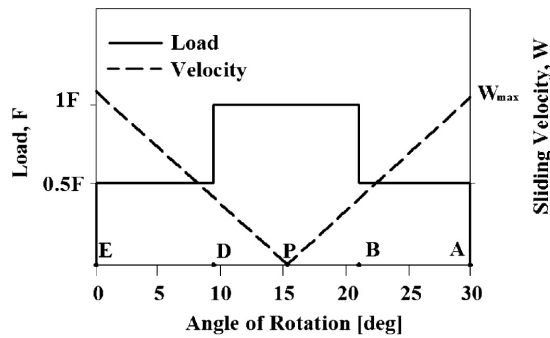


Figure 3. Theoretical load distribution and sliding velocity distribution along meshing axis [Hüseyin, 2009]

The Figure 3 illustrates the load distribution and the sliding velocity in case of various points of tooth contact. The load ( $F$ ) in the single tooth meshing area is higher when compared to that in the other sections. The sliding velocity is largest in the end points but zero in the pitch point.

In the course of the single and double tooth contact the theoretical load distribution changes according to  $F$  and  $F/2$ . However, some studies have pointed out that the above-mentioned phenomenon isn't true absolutely in the reality as a result of elastic deformation. The load of gear tooth hangs on the materials of the gear.

In case of the metals this change is almost linear but it isn't linear in case of the polymers [Erney, 1983; Melick, 2007].

### Tooth damage

The experienced failure forms of the metal gears are different as the plastic gears. The generally occurring damage of the plastic gears are as follows: tooth

fracture, surface fatigue (pitting), excessive wear and local plastic flow. The type of failure depends on the operating conditions and the type of polymer depends on the actually. Inner heat generation is created at the tooth of thermoplastic gear under repetitive high-speed stress therefore the whole cross section is able to strongly to warm up. This may cause softening of the teeth, and results in tooth failure finally. [Antal, 1987; Erhard, 2006; Senthilvelan, 2004; Senthilvelan, 2005]. The wear is created stronger at the face and flank of gear tooth than in case of area of pitch point due to the larger sliding velocity [Terashima, 1986]. The wear process will contribute to the formation of the larger friction heat as a result the material can soften and increases the load on the teeth due to the decreasing cross-section. For this reason the tooth of gear can be loaded to bending and it can cause the flow and whole breakage of the teeth.

The most common form of the surface fatigue is the pitting (Figure 4), which is created when the material has reached or exceeded the fatigue limit.

The tooth flank receives the maximum stress therefore this section is the most susceptible to pitting but this phenomenon is rare in case of the polymers, however, it may occur in special cases [Erhard, 2006].

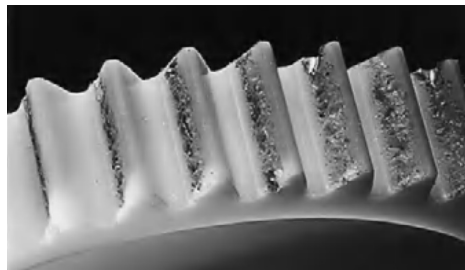


Figure 4. Pitting shortly before failure of the gear wheel [Erhard, 2006]

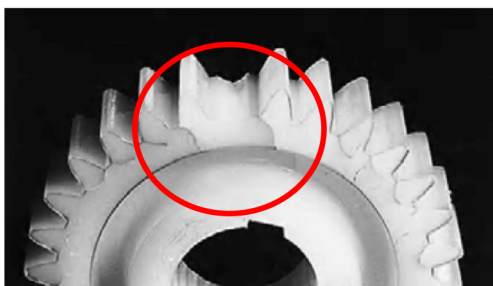


Figure 5. Fracture at the base of the tooth [Erhard, 2006]



Figure 6. Cracks emanating from the tooth flank close to the pitch diameter [Erhard, 2006]

Whereas the plastics conduct the heat badly and have low melting point compared with metals therefore they can melt in such a circumstances where the metals work appropriately [Terashima, 1986].

The ultimate state of any form of failure is a fracture, which means breaking the whole or part of the tooth. The fracture of plastic gear tooth occurs typically in two places. One of these areas is the tooth root (Figure 5). The crack occurs at fillet radius in general, and spreads along the fillet due to the deformation what causes the excessive load. The fracture at the fillet is not too common to occur typically when the plastic gear is loaded with high loads at low speed.

Another typical area is the environment of the pitch point (Figure 6) where the fracture can occur. This can be traced back to a higher load resulting from single tooth contact [Erhard, 2006].

According to the research of Terashima the type of failures was broken 92% in case of unmodified plastic gears which is caused by abnormal wear. 62% of the fractures were created in the environment of pitch point, and 30% of the fractures started directly from the pitch point. From this it can be concluded that the fracture usually occurs due to the single tooth contact [Terashima, 1986].

### 3. Material and forming of plastic gear specimen

The gears were machined an E 400 type lathe machine and a TOS OH-4 gear shaping machine which shown before and after shaping in Figure 7.

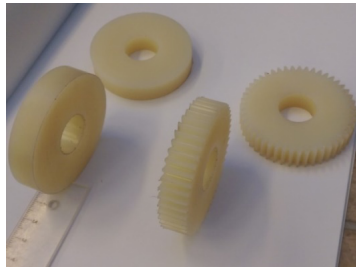


Figure 7. Semi-finished and finished plastic gears

Table 1. Parameters of plastic gears used for the test

Gear parameters	Value
Module, mm	1,25
Number of teeth	47
Face width, mm	12
Pressure angle	20
Base tangent length, (3)	21,119
Pitch circle diameter, mm	58,75
Abbandum circle diameter (theoretical), mm	61,25
Abbandum circle diameter (compensated), mm	61,04
Root circle diameter, mm	55,63
Transverse contact ratio	1,614

The tooth profile of the gears used for the measurements is involute without undercut. We decided this tooth profile because it is the most widely used in the world. The material of the plastic gear is the magnesium catalysed cast polyamide 6 (DOCAMID 6G-H). The material of the metal gears is a general purpose non-alloy structural steel (S355JR).

#### 4. Gear test rig for the test of the gear teeth fracture

The plastic gear test rig was developed in order to determine the load and deformation during the test and the moment of fracture in case of the relationship of polymer and steel gears (Figure 8). We used the Spider8 amplifier developed by HBM to process the signals of the measuring sensors. In case of the measurements the load can be generated by manual force, with a smaller and slower pre-load, followed by a uniformly increasing main load.

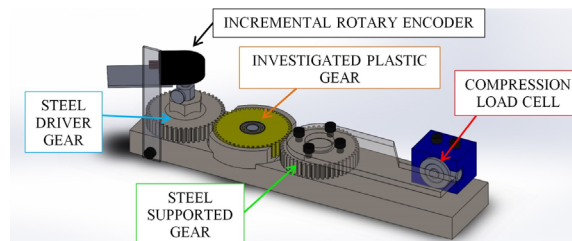


Figure 8. Gear Test Rig

The first step of the device application is that we have to reset which means that the load arm mounted on the supported gear is rotated until it reaches the compression load cell. The next step is that the torque is applied to the steel driver gear using a wrench. Meanwhile, the angular displacement of the driver gear is recorded continuously by the incremental encoder. The generated torque is passed through the teeth of the driver gear to the polymer gear. However, the supported gear is obstructed by the load arm through the load cell fixed to the frame.

Since there is a forced connection between the supported gear and the plastic gear, the load must be tolerated by the plastic gear until the moment of breakage what is recorded by the incremental encoder during the measurement. The distance is 100 mm between the centre of the supported gear and the load cell, so the torque is calculated easily.

In the course of test we can directly measure the angular displacement of the plastic gear as the angular displacement of the driver gear is measured as well as the rotation of the supported gear is negligibly small, therefore it can be zero so that the angular displacement of the plastic gear is equal to the angular displacement of the driver gear. The gear test rig is designed to connect two

tooth pairs simultaneously during the tests (Figure 9). However, due to the high elasticity of the plastics, the load distribution can be formed up to three tooth pairs.

The deformation of the steel driver gear and steel supported gear are negligible during the test compared to the polymer gear, so the angular displacement of the driver gear equals to the angular displacement of the plastic gear.



Figure 9. The gear test rig during the measurement

### 5. Test equipment for the tests of gear teeth connection

The contacting teeth surfaces are subjected to a complex tribological effect due to rolling and sliding with changing loads during gearmesh. The theories of transmitted mechanical power and teeth contact are clearly written in the literature, however, the friction phenomena is introduced with simplified condition, mainly taking the friction constant. A test equipment is developed for study of the real friction along the action line of mating gear teeth.

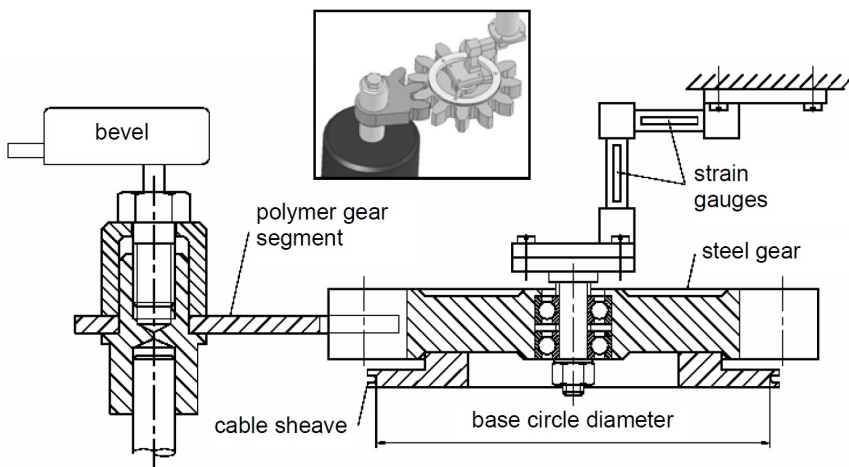


Figure 10. Draft of teeth contact tester for friction measurements [Keresztes, 2009]

Figure 10 illustrates the instrument for the tests concerning tooth contact. We can measure the teeth friction force and coefficient with this instrument, which are changing continuously along the action line [Keresztes, 2009].

## 6. Results

We determined the required torque and deformation for the fracture of the gear tooth in case of DOCAMID 6G-H. Figure 11 shows the measurement result of one sample in the form of a curve diagram. The diagram shows the values of torque and angular displacement as a function of time. Actual tooth fracture of the cast PA6 gear was effected by 119.5 Nm torque and the driver gear was angled approximately 9.45 °.

Basically, two speeds were used for the measurements, a slower pre-load at the beginning, and a faster main load, illustrated by  $v_1$  and  $v_2$  in the Figure 11. The behaviour of torque is important considering the angular displacement because these cohere with each other.

The line diagram shows that the speed of the pre-load and then the main load change during the measurement, so the angular displacement is not constant under the given time.

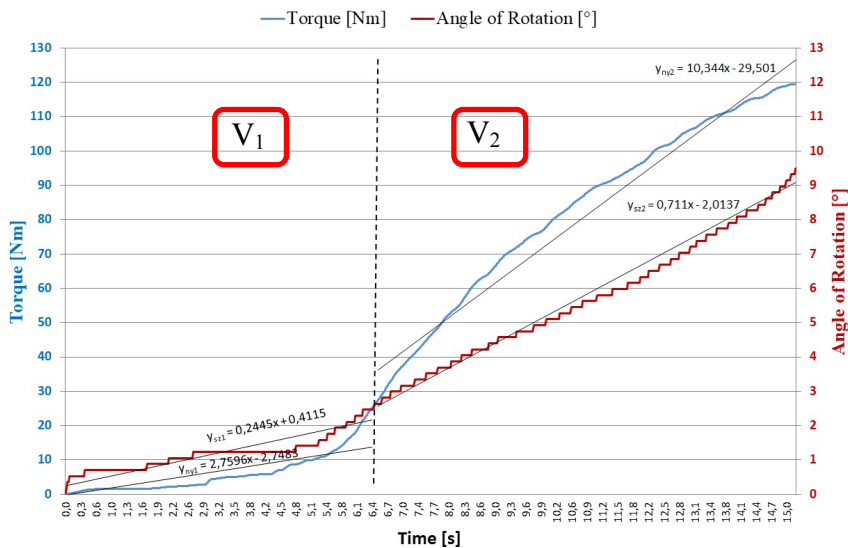


Figure 11. The curve diagram of the measurement

## Conclusion

Considering the diagram, it is also clear that a hardening is created, when the speed of load begins to increase than the material responds with hardening. It is similar to a tensile test. So the speed of test is an important factor.

In the course of our previous research, we executed more impact tests in case of the magnesium catalyzed cast polyamide 6 on a number of test specimens, and the results also showed a relatively uniform structure of material which the test of plastic gear confirmed [Odrobina, 2015].

## References

- [1] Bárány, J. (1967): Fogaskerékszámítás a TMK-ban, Műszaki Kiadó, Budapest.
- [2] Bártfai Z.-Blahunka Z.-Bácskai I.-Hartdégén G.: Biogázüzemben alkalmazott szilárdanyag aprító berendezés kopási tulajdonságainak javítása Mezőgazdasági Technika Különszám, No5/2017 p:32-36, HU ISSN 00261890
- [3] Erhard, G. (2006): Designing with Plastics. Hanser Publishers, Munich.
- [4] Erney, Gy. (1983): Fogaskerekek. Műszaki Könyvkiadó, Budapest.
- [5] Hüseyin, I. (2009): Performance improvement method for Nylon 6 spur gears. Tribology International, 42, 503-510., 2009.
- [6] Keresztes, R. Zs. (2009): Tribology Research of Engineering Plastics/Steel Friction Pairs.
- [7] Melick, Ir H.G. H. (2007): Tooth-Bending Effects in Plastic Spur Gears. Geartechnology, 9/10, 58-66., 2007.
- [8] Odrobina, M. (2015): Öntött PA6 gyártástechnológiai sajátosságai: anyag-szerkezet és mechanikai tulajdonságok kapcsolata. TDK dolgozat, Gödöllő.
- [9] Paquet, R. M. (1989): Systematic Approach to Designing Plastic Spur and Helical Gears. Geartechnology, 11/12, 12-27., 1989.
- [10] Senthilvelan, S; Gnanamoorthy, R. (2004): Damage mechanisms in injection molded unreinforced glass and carbon reinforced Nylon 66 spur gears. Appl Compos Mater, 11, 377-397., 2004.
- [11] Senthilvelan, S; Gnanamoorthy, R. (2005): Reinforced polymer gear fatigue and failure analysis. Trans Indian Inst Met, 58, 249-253., 2005.
- [12] Terashima, K; Tsukamoto, N; Nishida, N. (1986): Development of plastic gears for power transmission. Bulletin of JSME, 29, 1326-1329., 1986.

## Some recent tribological results from eco-friendly vegetal lubricants

Alessandro RUGGERO<sup>1</sup>, Nicolae UNGUREANU<sup>2</sup>, Radu COTETIU<sup>2</sup>

<sup>1</sup>Department of Industrial Engineering, University of Salerno (IT)

<sup>2</sup>Technical University of Cluj-Napoca, North University Center of Baia Mare

### Abstract

Growing environmental concerns provide motivation to increase the demand and use of environmentally friendly lubricants in many industrial sectors especially regarding the “Cleaner Production” purposes. Biodegradability, good lubricating properties and low production costs are the reasons to consider the plant oils a good alternative as reference to replace the petroleum-based oils that have limited resources. The aim of this work is to show some tribological results on the wear ability performances, regarding steel/steel contacts, of three investigated vegetal basestock oils. Object of investigation were the following vegetal oils: *Rapeseed Methyl Esther (RME) oil*, *Hydrotreated Vegetable Oil of Rapeseed (HVO)* and *raw Jatropha curcas L. oil (JCL)*. The experimental results are reported in terms of optical surface analysis after the execution of reciprocating tribological tests in presence of the investigated lubricants, under several normal load conditions in order to cover boundary, mixed and EHD lubrication regimes.

### Keywords

Cleaner Production; Vegetal Lubricants; Biodegradability; Tribology; Surface Analysis; Wear.

### 1. Introduction

Over the years a lubricant has been viewed as a fluid substance or mixture capable of reducing friction, adhesion, heat, wear and corrosion when introduced between two solid surfaces in relative motion. The most common constituent substances are base fluids and additives. Actually, many lubricants are mineral oil-based. They are obtained primarily from petroleum derivatives, but unfortunately, due to their low biodegradability and high toxicity, these oils are not convenient for environmental protection. In the last years, the environment protection activity provides motivation to push the use of environmentally “friendly” fluids in many industrial sectors. In this framework the vegetable oils seem to be attractive fluids for innovative lubricants formulations, since, in general, vegetable base oils have advantages due to their renewable origin and their higher biodegradability.

In fact, thanks to several advantages [1, 2], such as low environmental pollution, biodegradability, low toxicity, low production costs, low volatility and high viscosity indices, high flash points, the plant oils represents a good alternative to petroleum oils. Moreover, plant oils have greater anticorrosion properties for metal surface and higher viscosity indices. “Life Cycle Assessment” comparative studies indicate lower energy consumption during processing and lower impacts for the global warming potential than mineral and synthetic oils [3].

Actually, most of the crude materials for the preparation of vegetable oils are obtained from oleaginous plants: sunflower, rape seed, soybean, cotton and from palms, *Jatropha curcas* L, coconut tree [4,5].

The use of vegetable oils as lubricants under boundary and hydrodynamic/elasto-hydrodynamic lubrication regime is corroborated by their chemical structure with long fatty acid chains and adequate values of dynamic viscosity.

With the purpose to investigate on the wear protection ability of vegetal base stock oils, in this research are shown some results obtained on the surface analysis of tribosystems operating under several lubricating conditions.

## 2. Material and methods

In this paper three vegetal oils were investigated: Rapeseed Methyl Esther (RME) oil, Hydrotreated Vegetable Oil of Rapeseed (HVO) and raw *Jatropha curcas* L. (JCL). The experimental investigation was conducted in the Applied Mechanics Lab of the Department of Industrial Engineering of the University of Salerno –Italy-. In order to obtain results on the oils performance in a wide range of relative velocities of investigated tribo-pair, we selected an alternative motion tribometer apparatus. Thus, tests were carried out using a ball-on-flat *Reciprocatory Friction Monitor TR-BIO 282 (Ducom Instruments, Bangalore, India)*, following a consolidate test procedure [1]

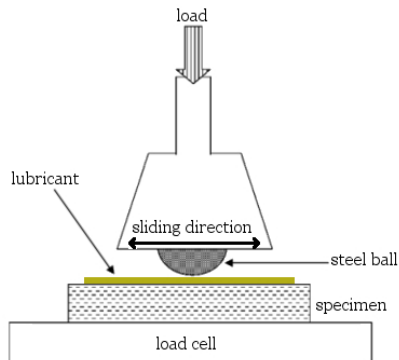


Figure 1. Schematic representation of the reciprocating apparatus.

In Figure 1 the schematic apparatus is represented. An AISI E52100 steel sphere (Young modulus  $E = 200$  GPa), Poisson modulus  $\nu=0.28$ ), 8 mm of diameter, was used in contact against a flat specimen of X210Cr12 steel (Young modulus  $E = 210$  GPa), Poisson modulus  $\nu=0.3$ ).

In the interface between these two elements, three analysed lubricant were deposited. Imposed normal loads were 6N and 12N, equivalent to a mean Hertz contact pressure respectively of 0.65 GPa, and 0.81 GPa and to a maximum values respectively of 0.97 GPa and 1.22 GPa. The tests lasted 20 minutes (with a frequency of 20 Hz and a stroke of 8 mm), enough to gain a steady state value of the friction coefficient.

To obtaining first information on the wear of the sliding surfaces, after the tests, an optical investigation was performed through a topographic surface acquisition. We used a 3D non-contact optical profilometer, *PLu Neox* (*Sensofar, Terrassa, Spain*), which can be used either as a confocal microscope or as a white light interferometer.

The worn surfaces, were previously cleaned from debris, washed with ethanol and dried, were scanned using a confocal lens with magnification of 20 $\times$ .

The analysis allowed to visualize the morphology of the spheres worn surfaces comparing the effects induced by RME, HVO and JCL lubricants.

About the used oils, in a previous research [1,2] the Authors, according to the standard ASTM D445 determined experimentally the kinematic viscosity, dynamic viscosity, density, flash point and total acid number (Table 1).

Table 1. Physicochemical properties of RME, HVO and  
Jatropha Curcas L. base oils [1]

Properties	RME	HVO	Jatropha Curcas L. oil
Density at 15°C (kg/m <sup>3</sup> )	884.5	780.7	916.9
Kinematic viscosity at 40°C (cSt)	2.829	4.679	36.605
Flash point at 760 mmHg (°C)	234 $\pm$ 0.5	245 $\pm$ 0.5	263 $\pm$ 0.5
TAN (mg KOH/g)	0.22	0.08	21.4

### 3. Results

The obtained results are shown in terms of 3D topographies. In this case we gained information on the wear of the spheres, but no remarkable wear information were found on the harder surface of the X210Cr12 flat specimens.

In Figs. 2–4, the worn surfaces and the impression average diameters “ $d_m$ ” of the AISI E52100 spheres, after tribotests, are reported by using HVO, JCL and RME as lubricants, respectively. Each figure shows the 3D topographies under several conditions: a) Load 6 N and frequency 20 Hz; b) Load 12 N and frequency 20 Hz.

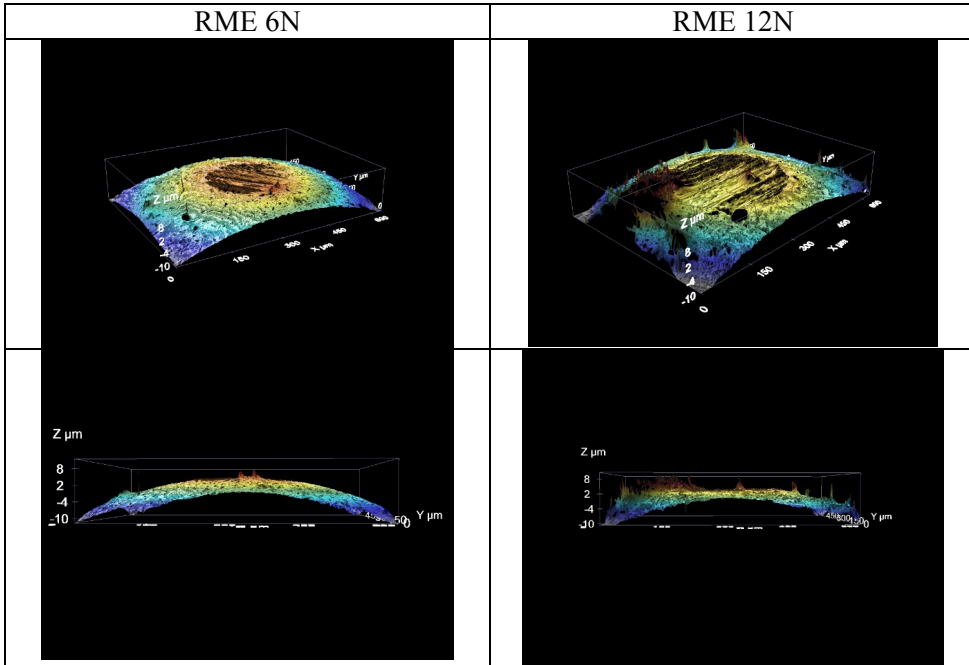


Figure 2. Surface analysis of 8mm sphere in presence of RME base stock with a normal load of 6N and 12N.

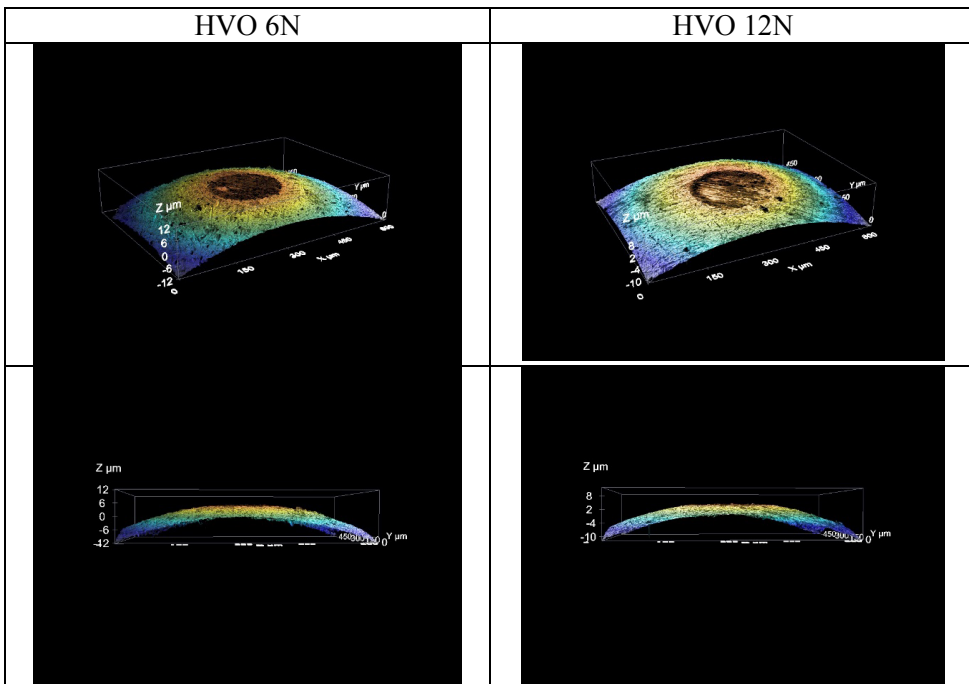


Figure 3. Surface analysis of 8mm sphere in presence of HVO base stock with a normal load of 6N and 12N.

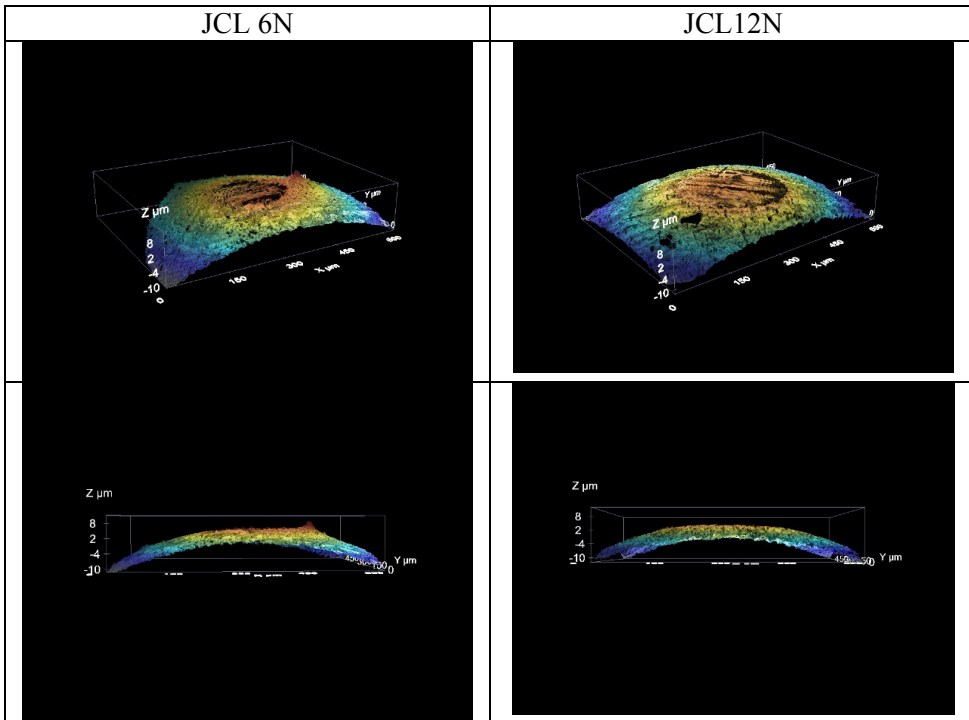


Figure 4. Surface analysis of 8mm sphere in presence of JCL base stock with a normal load of 6N and 12N

In Table 2 are summarized the calculated results.

Table 2. Wear impression diameter of the worn AISI E52100 spheres after tribotests with three lubricants.

	6N		12N	
	$d_m$ (mm)	std	$d_m$ (mm)	std
HVO	0,465	0,0052	0,482	0,0061
RME	0,601	0,0091	0,808	0,0083
JCL	0,651	0,0092	0,906	0,0062

## Conclusion

In this paper, some results on the tribological performances of three kind of base stock vegetal lubricants were investigated, by topographic observation of worn surfaces of the tripo pairs. The oil under investigation were raw *Jatropha curcas* L. seeds oil, Rapeseed Methyl Ester oil and Hydrotreated Rapeseed oil, while the the lubricated contact was a pair of AISI E52100 steel sliding spheres against

X210Cr12 steel. First obtained results showed a sensible lower wear of the sphere lubricated by HVO, at the same time these spheres presented the highest roughness values. This suggests a prevalence of adhesive wear, as the lubricant failed to separate the surfaces at low speed according with previous researches reported in [1,2]. More investigations have to be conducted in order to focus wear phenomena connected with boundary and mixed lubrication regime, in order to propose an optimal additive blend for allowing the correct utilization of these lubricants in many industrial applications.

## References

- [1] Ruggiero, A., D'Amato, R., Merola, M., Valášek, P., & Müller, M.. Tribological characterization of vegetal lubricants: Comparative experimental investigation on *Jatropha curcas* L. oil, Rapeseed Methyl Ester oil, Hydrotreated Rapeseed oil. *Tribology International*, 109 (2017): 529-540.
- [2] Ruggiero, A., D'Amato, R., Merola, M., Valášek, P., & Müller, M. (2016). On the tribological performance of vegetal lubricants: experimental investigation on *Jatropha Curcas* L. oil. *Procedia Engineering*, 149, 431-437.
- [3] Frijns, Jos, and Bas Van Vliet. "Small-scale industry and cleaner production strategies." *World Development* 27.6 (1999): 967-983.
- [4] Bartz, Wilfried J. "Lubricants and the environment." *Tribology international* 31.1 (1998): 35-47.
- [5] Nagendramma, Ponnekanti, and Savita Kaul. "Development of ecofriendly/biodegradable lubricants: An overview." *Renewable and Sustainable Energy Reviews* 16.1 (2012): 764-774.

## Wear mechanisms prevalent in agricultural tines

Jacob SUKUMARAN, Adam KALACSKA, Kannaki PONDICHERRY,  
Patrick De BAETS

Soete Laboratory, Department of Electrical Energy, Metals,  
Mechanical Construction and Systems,  
Ghent University, Technologiepark, Zwijnaarde-903 Ghent, 9052, Belgium  
Tel.:+32 9331 0489, E-mail: jacobpremkumar.sukumaran@ugent.be

### Abstract

The wear of soil engaging tools is of high importance considering the required increase of agricultural produce to meet the growing population. Considering wear studies, the wear mechanism is the key factor to equate between wear parts and lab-scale coupon specimens. In the present investigation symmetrical skew wedge tines were considered for investigation. An in-field test was performed for the wear investigation. Subsequently, the tines were investigated for wear mechanism, linear dimensional change and mass loss. It is evident from the investigation that the mass loss of the tine follows a linear trend as a function of ploughing distance. The thickness reduction and also the tip length of the tine shows a running-in behaviour. One of the important findings is that the linear dimensional losses are larger than the thickness losses which indicate the priority to study the wear mechanisms prevalent on the cutting side. Furthermore, two different micro-mechanisms were prevalent in the cutting side (micro-cutting and micro-ploughing). An segment specific map based on the different micro-mechanism is drawn for the investigated tines.

### Keywords

wear mechanism, soil engaging tools, micro-mechanism and abrasion

### 1. Introduction

Wear of agricultural parts may play an important role in the future where the productivity of the food has to meet the growing population. Beside the productivity, the cost involved in the wear of agricultural tool is also significantly high. For example, according to National Research Council of Canada, in the agriculture sector a total annual losses due to wear is accounted for \$ 940 million in the year 1986 (NRC, 1986). Also, another statistical data from Australian farmers clearly points out an expenditure of 40 million dollar a year on replacing and buying sweep shares (Fitzpatrick et al., 1990). Downtime due to the replacement of tines affects the production and influences the lead time in the season of seeding and planting crops (NRC, 1986, Fitzpatrick et al.,

1990, Ferguson et al., 1989). Existing researches try to understand the wear resistance of materials used in agricultural application however, their reports present limited information on the prevalent surface characteristics which indicate the micro-mechanism (Ferguson et al., 1989; Owsiak, 1997; Natsis et al., 2007; Fielke, 1996; Fielke, et al., 1993; Yu et al., 1990). The wear rate is frequently used for the tribological ranking of different materials. However, this ranking may mislead if the wear mechanism between the real application and the lab-scale tests vary with respect to each other. Considering the wear mechanism in agricultural tools, abrasive wear is a major concern for farmers. Soil engaging tools which is typically steels are soft material when compared with the hard sand/soil. The steels are abraded by the hard sand particles during the course of interaction in the ploughing operation. In the present investigation we focus primarily on the wear of tillage tools.

Amongst different abrasion mechanism the tillage wear is commonly classified as open three-body low-stress abrasion [8]. However, this is not straight forward considering the different modes of wear within a single tine. It is possible that different state of stress is exerted on the different segments of the tine. This also influences the flow of the abrasive particles over/under the tine during the ploughing process and also the compaction of the soil. This may result in different micro-mechanisms such as micro-cutting, micro-fatigue and micro-ploughing on the different segments of the soil engaging tools. It is well known that the wear rate is different with respect to the wear mechanisms and hence a clear understanding of the micro-mechanism is necessary for tribological characterization. With the limited information on the segment specific wear mechanisms in soil engaging tools the present research aims to elucidate the various micro-mechanisms incurred in different segments of the agricultural tine. Thus new material design can be aimed to overcome the particular wear mechanism which is responsible for the severe wear.

## 2. Materials and methods

In-field wear testing was conducted in Braunschweig, Germany using a commercially available symmetrical skew wedge tine provided by Köckerling, Germany (Köckerling, 2016). Tines were tested within the range of 8 to 12 km/h sliding speed and the operation depth ranged between 5 and 8 cm for a total sliding distance of 140 km. Thirteen intermediate pauses were made to extract wear data of tines for different ploughing distances. Two different soil types were engaged: clay and sand soil. After the in-field testing, the tines were measured for its wear characteristics using a protocol developed in-house. In the first stage of measurement, the tines were cleaned in order to remove the rust and remaining soil particles. Following the cleaning process, the linear dimensional measurement, mass loss measurement, surface characterization and the microscopy was performed. Literature clearly points out that linear measurement of geometrical dimensions is widely used in order to extract wear

data. The methodology and template for wear measurement of average cutting edge thickness, tip length, width and edge length were adapted from Natsis *et al* (Natsis et al.2007). The template for measuring the thickness and edge reduction is shown in *Figure 1a*.

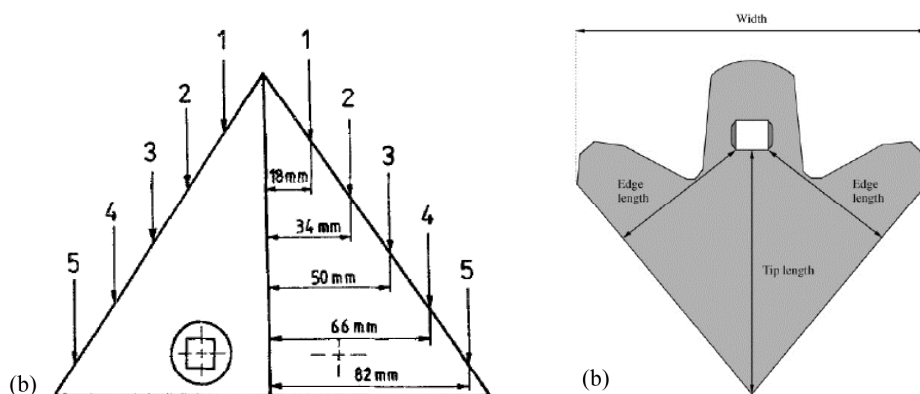


*Figure 1.* (a) Measurement points and (b) definition of tip length, width and edge length (Natsis et al.2007).

The micro-mechanisms were monitored using two different techniques for understanding the surface morphology and topography. Initially, a digital camera was used for visual inspection and the micro-mechanism were studied using a digital microscope at 400 X magnification. The optical system merely explicates the qualitative nature of the wear mechanism, however, this is validated using the stylus surface profilometry. A systematic tracing of profile was made using the profilometer (Somicronic® EMS Surfscan 3D, type SM3, needle type ST305) equipped with modules for contour analysis, surface texture analysis and 3D form. In the surface characterization, Gaussian filtering with cut-off lengths of 2.5 mm and 0.8 mm was performed for sampling lengths of respectively 5 mm and 4 mm. Based on a calibrated groove, the three-dimensional instruments conformity certificate (Hommel Somicronic) has an absolute error depth of 0.186  $\mu\text{m}$  on 110.00  $\mu\text{m}$  full scale and independently to this 1  $\mu\text{m}$  in the positioning direction. These region of interest (ROI) for these three investigations were performed based on the wear results from the linear dimensional change.

### 3. Results and discussion

After 140 km of ploughing distance, the tines were measured for its dimensional change and also the mass loss to understand the wear behaviour. In regards to the mass loss, a linear trend as a function of ploughing distance was evidenced

(See *Figure 2*). From the linear trend a constant wear rate of 3.24 g/km is noticed, similar tendency was reported in earlier studies (Ferguson, et al., 1989). However, in case of literature the wear rate is significantly higher which can be attributed to the soil condition (dry stony soil with 10% gravel content). In case of tip length measurement a clear distinction between running-in wear and steady state wear was observed. From the tip length measurement it is evident that running-in period persists up to 50 km ploughing distance. While comparing the three factors which are tip length, edge length and the half width, it is evident that the tip length undergoes significant amount of wear. Thus, it is noteworthy to give priority on the cutting side for further analysis on the wear mechanism. Besides, the length the thickness at various location were studied, which in-turn validates the two regimes of wear (running-in and steady state period). However, the thickness reduction (max: approximately 7 mm) was not significant when compared to the reduction in tip length. This also concludes that one has to prioritize on the cutting side instead of the top surface.

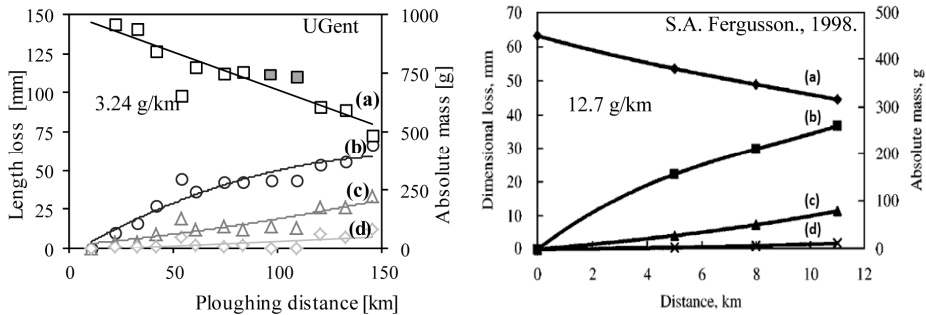


Figure 2. Wear as function of ploughing distance (a) absolute mass, (b) Tip length loss, (c) edge length and (d) half width

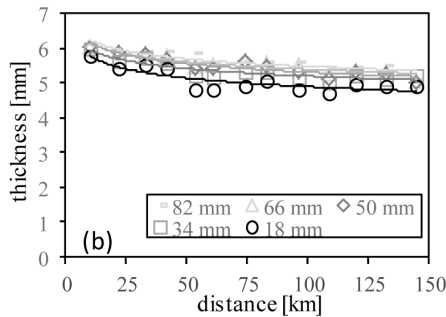


Figure 3. Thickness measurements at different location.

From the dimensional losses two region of interests were selected for further investigation (region 1: topside and region 2: cutting side. The topside often

experiences the rolling of abrasive particles, this is because the sand/soil is already loosened by the action of the cutting side. Subsequent motion of the tine leads to the rolling of the loosened particles. On investigating the topside for microscopy and surface roughness: micro-cutting mechanism was evidenced. Figure 4 shows the macroscopic view of the topside where narrow deep grooves with the absence of ridges on the contact surface. Such mechanism can be attributed to the micro-cutting of abrasive particles on the tine surface. In regards to the cutting side there are two distinct micro-mechanisms observed from the wear pattern. The region close to the topside shows wide grooves with plastically deformed ridges, such features indicate micro-ploughing. The groove widths are much larger than the size of the soil particles. Only the presence of gravel in the soil can cause these kind of grooves. The lower region of the cutting side has a more uniform wear pattern with narrow parallel grooves and a continuous chip formation are clearly seen. These features are typical for micro-cutting mechanism (see Figure 5). A major portion of the cutting side experiences micro-cutting mechanism which results in the reduction of the tip length. However, there is also a certain zone with micro-ploughing mechanism in the cutting side. The measurements made are rather qualitative and the region of interest (ROI) is partly local in nature. Though the present investigation aids to elucidate the micro-mechanism from the surface morphology and partly from surface topography, the global presence of these mechanisms are still questionable. A quantitative value to indicate the micro-mechanism is more appropriate where literature clearly points out the degree of penetration ( $D_p$ ) to study the micro-mechanism. In literature the characteristics feature for  $D_p$  were studied from the viewpoint of single asperity (Hokkirigawa, K. and Kato, K., 1988). However, in real application multiple scratches will be present. The measurement of roughness parameter can be foreseen to extract the wavelength and the amplitude profile of the surface which in-turn may aid to estimate the  $D_p$  of the worn surface. The roughness parameters from the stylus profilometry is more appropriate however, the 2D profile measured using a stylus has its limitation from the view point of nose radius. Hence for future investigation a more robust statistical evaluation from 3D profiles measured using non-contact optical method is proposed for surface characterisation.

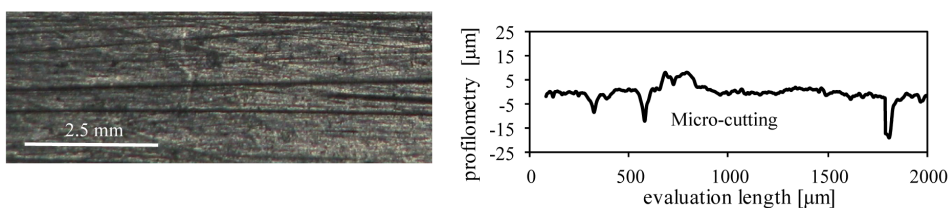


Figure 4. Microscopy and stylus profilometry of topside

Based on the above investigation it is evident that two regions within the same tine pertaining to different contact conditions leads to different micro-

mechanism. The two regions are the topside of the tine and the cutting side. Within the cutting side further segmentation can be made based on the micro-mechanism. In the cutting side two different zones were present for micro-cutting and the micro-ploughing as shown in the *Figure 6*. From the current investigation a clear picture of the wear mechanism prevalent in different segments are studied. However, the dominant mechanism responsible for the material removal process is still unknown. This can be studied by means of a cross sectional analysis where factors such as hardness and tribo-layer formation can aid more information.

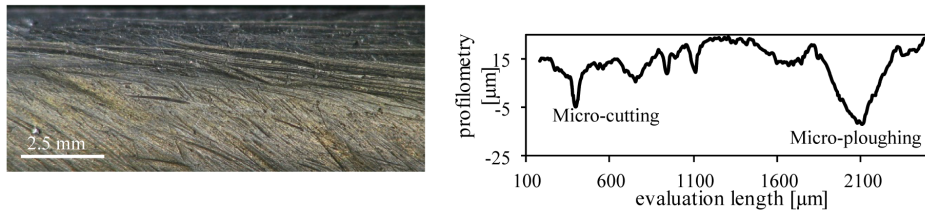


Figure 5. Microscopy and stylus profilometry of cutting side



Figure 6. Segment specific wear mechanism for the agricultural tines used ploughing process

## Conclusions

In the present investigation symmetrical skew wedge tines were investigated for the segment specific wear mechanism. The following conclusions were drawn from the above investigations:

1. The wear rate from the mass loss observation as a function ploughing distance follows a linear trend.
2. Both the tip length reduction and the thickness reduction measurements shows a running-in behaviour which is prevalent until 50 km.
3. In regards to the wear mechanism, the tine by itself can be divided in to two regions based on the dominant micro-mechanism which is the top side and the cutting side.
4. Furthermore the cutting side can be divided in a micro-ploughing and micro-cutting zone.

## Acknowledgements

This investigation was supported and funded by European commission research and innovation, research fund for coal and steel. Laboratory Soete acknowledges the material support received from Köckerling, Germany. The authors are grateful to Mr. Florian Schramm and Mr. Sebastian Kemper from Technische Universität Braunschweig, Germany for their support on experimental activities in-field tests.

## References

- [1] Ferguson, S. A., Fielke, J.M., Riley., T. W. (1989), Wear of Cultivator Shares in Abrasive South Australian Soils, *Journal of Agricultural Engineering Research*. Vol.69: pp. 99-105.
- [2] Fitzpatrick R. W., R.T.W., Wright M. J. (1990), End of Grant Report (1988-1990) for the Australian Wheat Research council (Project No. SAIT 1W). Australian Wheat Research council.
- [3] Fielke, J.M., (1996), Interactions of the Cutting Edge of Tillage Implements with Soil. *Journal of Agricultural Engineering Research*. Vol. 63: pp. 61-72.
- [4] Fielke, J. M., Riley, T.W., Slattery, M. G., Fitzpatrick, R. W. (1993), Comparison of tillage forces and wear rates of pressed and cast cultivator shares. *Soil & Tillage Research*, Vol. 25: pp. 317-328.
- [5] Hokkirigawa, K, Kato, K., (1988), An experimental and theoretical investigation of ploughing, cutting and wedge formation during abrasive wear, *Tribology International*, Vol. 21, pp. 51-57.
- [6] Natsis, A., Petropoulos, G., Pandazaras C., (2007), Influence of local soil conditions on mouldboard ploughshare abrasive wear. *Tribology International*. Vol. 41: pp. 151-157.
- [7] N.R.C. (1986), A strategy for tribology in Canada: enhancing reliability and efficiency through the reduction of wear and friction. National Research Council Canada.
- [8] Owsiak, Z. (1997), Wear of symmetrical wedge-shaped tillage tools. *Soil & Tillage Research*, Vol. 43: pp. 295-308.
- [9] Verschleissteile, (2016), Köckerling.
- [10] Yu, H. J., Bhole, S. D., (1990), Development of a prototype abrasive wear tester for tillage tool materials, *Tribology International*, Vol. 23: pp. 309-316.

# **Pin-on-disc tribology test of dry sliding frictional hybrid woven composite material samples cut with abrasive water jet machining**

Roland BICZÓ<sup>1</sup>, Mátyás ANDÓ<sup>2</sup>, Róbert KERESZTES<sup>1</sup>,  
Gábor KALÁCSKA<sup>1</sup>

<sup>1</sup>Institute for Mechanical Engineering Technology,  
Szent István University, Páter K. u. 1., Gödöllő, H-2100, Hungary,

<sup>2</sup>Savaria Technical Institute, ELTE, Szombathely

## **Abstract**

In our present paper we are introducing and investigating ways to create test specimens from hybrid composite friction material of a dry sliding clutch to perform pin-on-disc tribology tests in order to support material and finite element model development. The applicability of samples is tested through a tensile test performed according to DIN 53455. Then test samples are created with the approved machining method, and tested in pin-on-disc system. Results show good correlation with awaited values.

## **Keywords**

hybrid woven composite, friction, abrasive water jet machining, pin-on-disc system

## **1. Introduction**

The field of friction materials for vehicle industry has gone through a fascinating development throughout the last century due to the utilized novel composite materials. However, there are still open questions about friction behavior under different conditions, wear characteristic sensitivity, thermal loads and responses, manufacturing steps etc. [Biczó *et al* 2016] Today's investigations are circling around three basic topics in accordance with the requirements, loads and operating conditions, namely mechanical properties, thermal phenomena and tribology, and parameters influencing and governing them. [Biczó, Kalácska, 2016] All tests of these fields require test specimens machined from the investigated friction parts with unchanged properties compared to the whole product. Tribology tests are usually carried out on test samples with small friction areas. Creating such pieces require accurate and careful machining controlled by a reliable system.

## 2. Sample creation with composite failure modes in mind

Fiber reinforced composites has some dangerous failure modes, from which fiber pull-out represents the damage in adhesion between the fibers and the matrix. Utilizing some machining methods, such as sawing, etching etc. for sample creation, could result in fibers pulled out of the matrix, hence a mechanically modified test piece. Laser cutting could also harm the whole product, since it's flammable. Abrasive water jet machining on the other hand could serve as a solution.

## 3. Abrasive water jet machining

Abrasive water jet machining is amongst the newest machining techniques used in many industrial applications. It is a non-conventional machining process where material is removed by impact erosion of high pressure high velocity of water and entrained high velocity of grit abrasives on a work piece. [Relekar *et al* 2015] Machining with abrasive waterjets has many advantages over other technologies: no heat is generated in the work piece, low machining forces on the workpiece, machining of a wide range of materials is possible and free contouring possibilities without the need of material or geometry specific tools. [Hoogstrate *et al* 1997]

Many has studied the effects of water jetting parameters on polymer material properties pre and post manufacturing, finding that setup values of the technic has an effect on the final topology and mechanical properties. [Ramulu, Arola, 1993] Others found, that the manufacturability, hence the effects are dependent on the machined material. [Alberdi *et al* 2013]

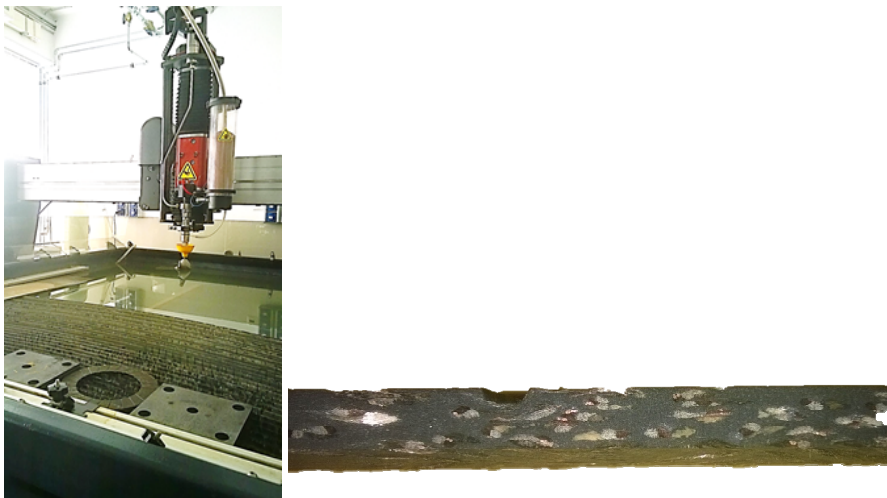


*Figure 1.* The 1515 MAXIEM OMAX abrasive water jet cutting machine and the smooth cutting edge of a test specimen

One fact to be taken additionally into account, that this technique utilizes water as it's transfer medium. However moisture is one thing to be avoided when designing the environment for a dry sliding clutch disk. A well-known phenomena is the cold judder of the discs especially among humid circumstances that definitely changes the frictional and mechanical parameters of the clutch facings. Idea is to compare one group of these parameters to determine if water jet cutting is appropriate for such test specimen creation.

As fiber reinforcement gives a privileged orientation to the composite materials, tensile test provides an opportunity, to decide whether abrasive water jet machining is able to be utilized to create samples for tribotests or not.

Therefore a tensile test was carried out according to DIN 53455 investigating three groups of specimens with different moisture levels. Specimens were created by 1515 MAXIEM OMAX abrasive water jet cutting machine shown on Figure 1. and then sorted into three groups. The first group of samples went under a slight heat treatment, drying (15 minutes, 150 °C), to give results of specimens left long untouched. The second group was placed between moist layers for 15 minutes. The third group remained untreated. The force-deflection curves of three test samples with different moisture levels can be seen on Figure 2. However no significant difference can be detected that would have been the result of the harmed structure. As a consequence, water jet cutting has not modified the material properties of the dry friction clutch facing. As a conclusion abrasive water jet machining turned out to be a useful method for creation of test specimens for dry friction hybrid composite facing mechanical and tribological investigations.

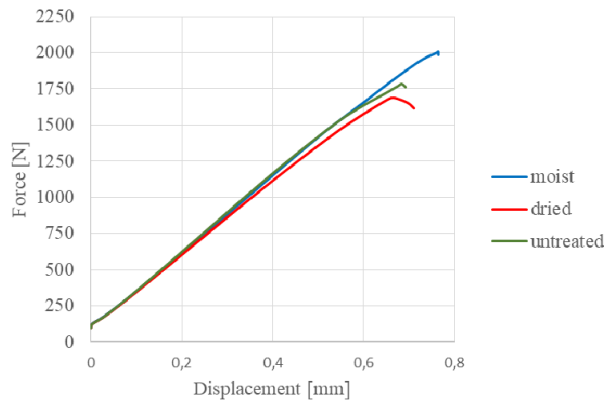


Figure 2. Force-displacement curves of test samples with different moisture levels

#### 4. Pin-on-disc test setup and early results

Continuous friction sliding rises between the surfaces of the fixed Ø10 mm hybrid composite test samples and the rotating disc made of GG25 in the pin-on-

disc tribological system that works without lubrication, among adhesive circumstances.

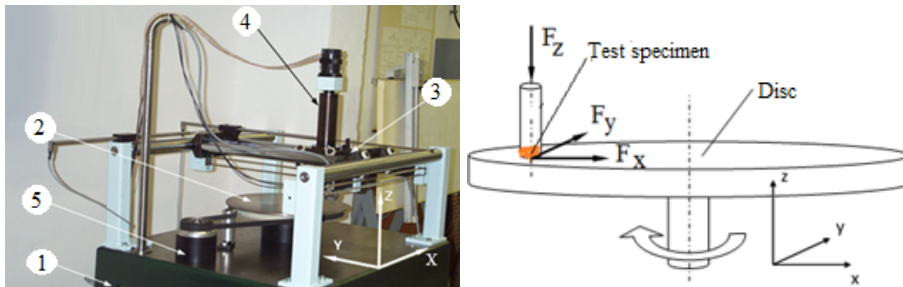


Figure 3. Pin-on-disc dynamic tribological material investigation system, a sketch of the system with forces rising on the test specimen

Figure 3 shows the main units of the test system: (1) table, (2) disc, (3) positioning system, (4) loading system, (5) electric motor with speed setting rotating the disc. The attachment of the test specimen required machining of additional steel pins that can be seen on Figure 4. The bond between composite and steel is guaranteed by universal superglue.



Figure 4. Test specimens cut out from friction facing, additional steel pins for attaching test samples to the system, attached pin

The surface roughness of the disc is determined with Mitutoyo SJ-201P application. Its value lies in the range of Ra 4 – 7.

During the tribology test sliding speed, the timeframe of the procedure, the normal load, the friction radius, the surface roughness of the disc and the environmental temperature play as parameters. Result parameters that we seek are the dynamic friction coefficient from the loads and forces, the temperature of the composite at 1 mm depth from the friction surface, wear and deformation. Parallel with the friction surface,  $F_s$  friction force rises while  $F_n$  normal force acts.  $F_x$  and  $F_y$  are force components parallel with the friction surface. Hence the dynamic friction coefficients can be determined as:

$$\mu = \frac{F_s}{F_n} = \frac{\sqrt{F_x^2 + F_y^2}}{F_z} \quad (1)$$

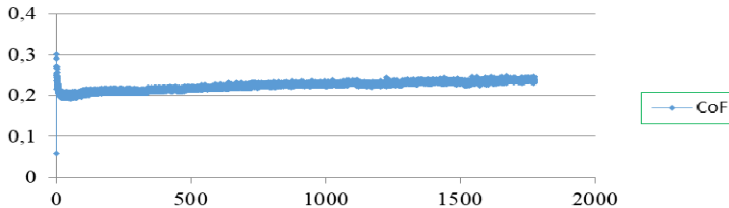


Figure 5. Coefficient of friction during a test run

An awaited dynamic friction coefficient curve can be seen on Figure 5 from a test run with the pin-on-disc tribology system. With different disc materials utilized, the sensitivity of the friction coefficient on the tribo-pair material can be determined giving a benchmark for planned industrial measurements and tests.

## Conclusion

Novel composite materials started great development trends among friction materials utilized in vehicles opening newer and newer topics for the engineers and scientists dealing with such materials. With possible damages in mind abrasive water jet machining turned out to be an efficient application for the creation of test samples of mechanical and tribological investigations of hybrid composite friction materials. These samples serve as essential units of tribo systems that are to aid material development.

## Acknowledgement

Many thanks to LuK Savaria Kft in Szombathely, Hungary for providing clutch facings and measurement opportunities and ELTE Savaria Egyetemi Központ (SEK) for test sample cutting.

## References

- [1] Alberdi A., Suárez A., Artaza T., Escobar-Palafox G.A., Ridgway K. (2013): Composite Cutting with Abrasive Water Jet, *Procedia Engineering*, 63,, pp. 421-429
- [2] Biczó R., Kalácska G., Szakál Z., Fledrich G. (2016): Composite Friction Materials for Brakes and Clutches, *The international conference of the*

- carpathian euro-region's specialists in industrial systems- 11th edition-, pp. 32-37, ISBN 978-606-737-166-6.
- [3] Biczó R., Kalácska G. (2016): Composite friction materials of couplings, Proceedings of the 4th international scientific conference on advances in mechanical engineering (ISCAME 2016), pp. 40-45, ISBN 978-963-473-944-9
- [4] Hoogstrate, A. M., Van Luttervelt, C. A., Gosger, P., Momber, A. W., Tönshoff, H. K., Louis, H., ... Leu, M. C. (1997). Opportunities in abrasive water-jet machining. CIRP Annals - Manufacturing Technology, 46(2), pp. 697-714.
- [5] Ramulu M., Arola D. (1993): Water jet and abrasive water jet cutting of unidirectional graphite/epoxy composite, Composites, 24/4, pp. 299-308
- [6] Relekar K. M., Kalase A. B., Dubal S. P. (2015): Abrasive water jet machining, International Journal of Innovations in Engineering Research and Technology 2/10

# Comparison of lab-scale erosion testing machines

Ádám KALÁCSKA, Jacob SUKUMARAN,  
Patrick DE BAETS

Department of Electrical energy, metals, mechanical constructions and systems,  
Faculty of Engineering and Architecture, Ghent University

## Abstract

In this paper a brief overview and a comparison regarding specific machine advantages and disadvantages are given about the possible test rigs that could be used for tribological modelling of erosion. The two most commonly used erosion testers, – the gas-blast (sand-blast) tester and the centrifugal-accelerator (or rotating-disc) tester – were highlighted with the prominent parameters that effect erosion e.g. the impact angle, the velocity of solid particles and the particle size and shape in focus.

From the review it is evident, that the sand/gas blast testers have an advantage in quick, simple and single sample testing at low erodent concentration, however there is an inadequate grasp and control on particle impact condition. The centrifugal accelerator testers have the advantage of testing multiple samples in parallel, as well as controlled impact conditions with adjustable impact angle and velocity of particle.

## Keywords

Tribology, wear, erosion tester, comparison

## 1. Introduction

Erosive wear is the phenomenon of removal of the surface of any component based on different conditions due to high-speed impact of solid, liquid or gaseous particles. The impacting particles gradually remove material from the surface through repeated deformations and cutting actions [1].

The factors which significantly affect the rate of erosive wear :[2]

- Impingement angle: the angle at which a particle hits the surface. By the experience it was found that the wear rate was high at an angle of 30° for ductile material and 90° angle for brittle materials.
- Impact speed: high speed particles impacts cause more damage than low speed collisions.
- Particle properties: particle properties were more important in erosive wear phenomenon, sharp and hard particles causes more wear rate.
- Temperature: High temperatures cause high erosive wear because increase in softness of material in high temperatures

- Particle flux rate: Particle flux rate is the mass of particles hitting an area of surface per unit of time, which can vary greatly from 100 kg/m<sup>2</sup>/s to 10,000 kg/m<sup>2</sup>/s [2].

In a tribosystem, where the major wear mechanisms are reviewed in the wear analysis process, the proper model of the wear system requires modelling such test rigs that are capable of controlling the dominant system variables. In industry, especially farm engineering, erosion is one of the main wear mechanisms. In the following an overview and a comparison of erosion testers will be made to study the advantages and disadvantages. This will allow us to make an appropriate choice for testing applications in lab-scale.

## 2. Erosion testing devices

The standardization of methodology and design of equipment for erosion testing is difficult to achieve considering the complexity of the problem. Literature review was done on methodology and design of erosion testers. Various types of erosion test rigs used so far for determination of erosion rate in different conditions can be listed as linear gas gun, slurry pot erosion tester, contra rotating disc tester, slurry jet erosion wear test rig, sliding bed erosion test fixture, flow-through slurry wear tester and sliding bed wear test and closed hydraulic loop tester. These different types of testers are further classified into four types:

- sand or gas-blast rig,
- re-circulating liquid slurry loop,
- centrifugal accelerator
- whirling arm rig [3].

In the gas-blast rig, particles are introduced into a fast-moving gas-stream and are accelerated down in an acceleration tube, before particles impact on the test piece. This equipment is widely used (figure 1)

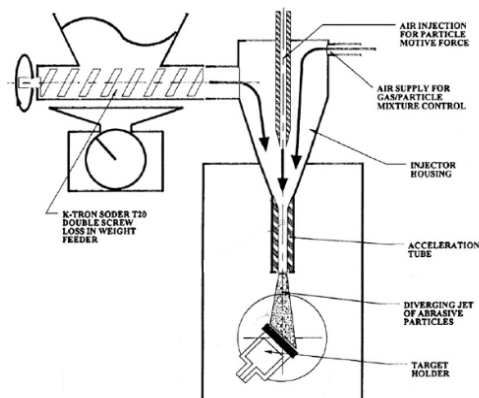


Figure 1. Schematic diagram of a gas-blast erosion tester [4]

Gas-blast erosion tester allows testing of specimen one by one. Particle velocity is taken to be equal with the velocity of a gas stream because the latter is easy to determine. However, the actual impact velocity depends on the size and shape of the particles and on the length of the acceleration distance. The test process is running in one impact condition on a single sample, hence the productivity of this configuration is low. In some cases, the gas-stream has been replaced with a water jet. Slurry erosion is caused by the interaction of solid particles suspended in a liquid and a surface which experiences mass loss by the repeated impacts of particles. Slurry erosion is a complex phenomenon, and is influenced by many factors, which include flow field parameters, target material properties and erodent particle characteristics [5].

Besides being inexpensive and easy to operate, slurry pot tester can provide a rapid ranking of the erosion resistance of different materials [6]. However the investigation on the effect of particle size, impact velocity and impact angle cannot be undertaken with slurry pot tester [3].

Also, some study classifies free particle fall in vacuum type of laboratory test equipment. This type of machine has very limited application, with a particle velocity  $< 5$  m/s [7].

The main parts of the centrifugal erosion tester are the feeder, an accelerating rotating disc and a sample holding system. The centrifugal accelerator (figure 2) and whirling arm types of erosion testers use different motion to deliver the erodent to the test surface.

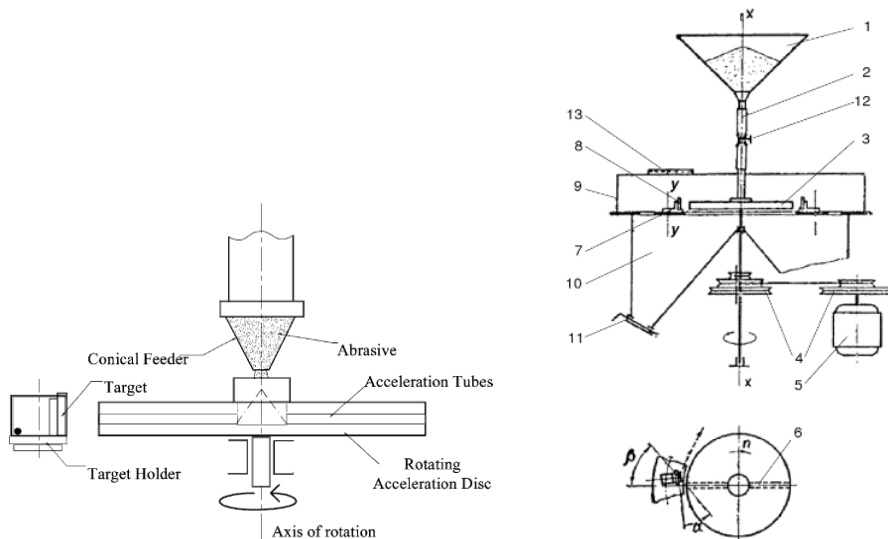


Figure 2. Schematic diagram of centrifugal accelerator [8] [9]

Both of these involve circular motion which is in contrast to the gas-blast rig described above, where linear motion is used. In the centrifugal accelerator test

samples are held stationary at the rim of the rotor and the sand particles are fed into the centre before being accelerated radially onto the target surfaces. The particles change the specimen surface geometry (deformation), and/or they also remove material from the specimen (wear). The target specimen could be reoriented relative to the direction of parallel flow by ejecting particles. The target holder is the main equipment that is used for changing the angle of attack of the particles that are fed into the system. The impact angle and velocity of the erodent could be easily changed and held on a constant value in this type of test rig. These parameters are crucial in this configuration, to determine erosion wear rate. The angular velocity effects the exit angle of the particle when it leaves the disc. A study was made [10] to model in ANSYS CFX the examined material loss.

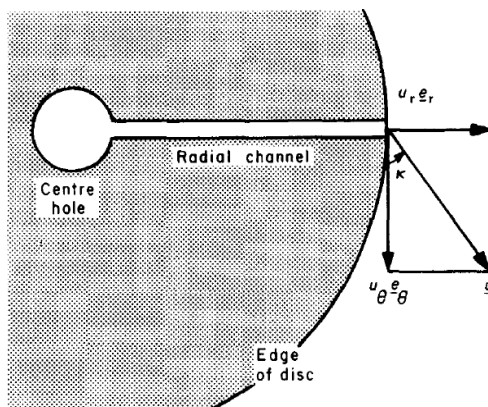


Figure 3. Radial and tangential velocity of exiting particle [10]

For summary, the velocity of particle is:

$$v = \sqrt{v_t^2 + (k \cdot v_t)^2}$$

where  $v$  velocity of particle;  $v_t$  tangential velocity,  $k$  is a constant ( $0 < k < 1$ ), which depends on the friction coefficient between the tube wall and the particle ( $\mu$ ):

$$k = 1 - \mu$$

The exit angle of the particle is also dependent on the friction coefficient between tube wall and particle:

$$\alpha = \arctg(k)$$

The material and shape of the particle effect the angular velocity of particle.

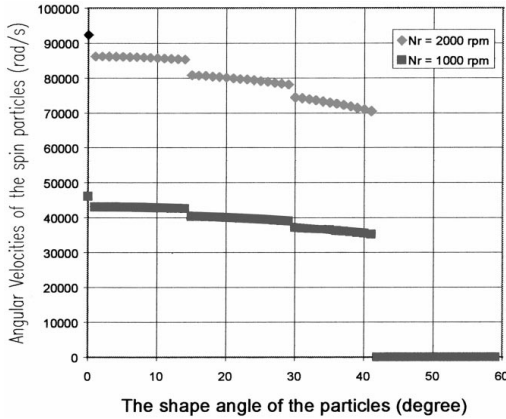


Figure 4. The effect of the shape angle of particles on the angular velocity [9]

The prominent parameter that effect erosion next to the impact angle and the velocity of solid particles is the particle size and shape of the test material as well as the erodent mass that hits the specimen. A study was made to define the dispersion angle [9], in case of centrifugal erosion tester the  $\Theta/2$  (half dispersion) angle is between 3,5 and 4,5°. The dispersion depends on the distance between the specimen and the place where the particle leaves the disc. The erosive wear increases with increase in particle size according to power law relationship. The effect of particle shape on the erosion is not very well established due to difficulties in defining the different shape features. Generally roundness factor is taken into consideration. If roundness factor is one then the particles are perfectly spheres and a lower values show the particle angularity [11]. Different particle rotation results change in the mass flux of particles at the target surface (figure 5)

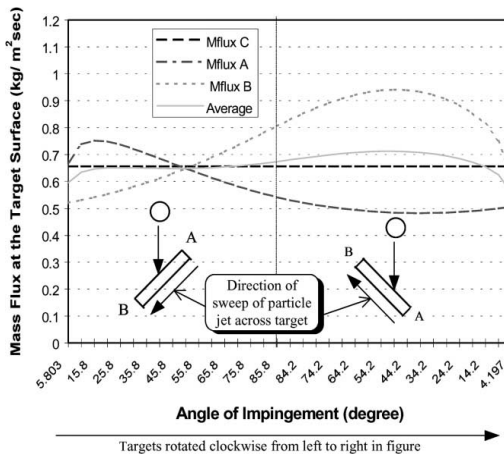


Figure 5. Direction of particle rotation effect to mass flux [9]

In the centrifugal erosion testers multiple tests can be conducted simultaneously with the samples arranged around the periphery of the rotor. Velocity determination is also simple as it can be considered to be that of the rotor velocity. However, test duration is often long and difficulties can occur in quantifying the mass of abrasive that strikes the target. A related rig is that of the whirling arm design. Here, the samples are mounted onto the end of arms which are attached to a rotor. This is rotated at high speed and erodent is fed onto the target surface [12].

### 3. Comparison of erosion testing devices

The two most commonly used erosion testers are the gas-blast (sand-blast) tester and the centrifugal-accelerator (or rotating-disc) tester (figure 6a). The most commonly used bench scale test rigs to evaluate the erosive wear at an accelerated rate are the slurry pot tester (a variant of whirling arm rig, figure 6b) and the jet impingement tester (JIT) (sand blast type) [1].

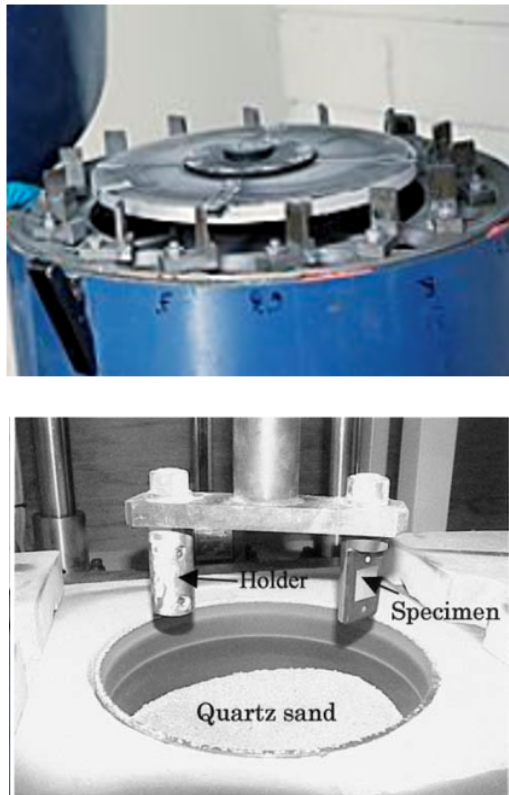


Figure 6. Different erosion test rigs:  
a) Centrifugal erosion tester, b) Slurry pot tester [13]

The general response of the particles to the accelerating forces will be different in each of the apparatus. Not only that, but within each tester the response of an individual particle will vary depending on its particular characteristics (particle size, shape, etc.) and its interaction with the apparatus. This may lead to differences between the gas-blast and centrifugal-accelerator testers in, for instance, the distribution of particle velocities and trajectories [9]. Erosion tester types and their specifications are summed up in Table 1 [12].

Table 1. Summary on specifications of erosion tester types

Type of erosion tester	+Pros/Usage	-Contra
Sand/gas blast rig (Jet Impingement tester)	<ul style="list-style-type: none"> <li>+ Determine the variation of wear with impact angle at low solid concentration</li> <li>+ Quick</li> <li>+ Eroduct delivery: linear motion</li> <li>+ Simple result analysis</li> </ul>	<ul style="list-style-type: none"> <li>- Impact angle, impact velocity changes during test</li> <li>- Inadequate grasp and control on particle impact condition</li> <li>- Eroduct not recycled</li> <li>- Advert gas/particle interaction could occur</li> </ul>
Re-circulating liquid slurry loop	<ul style="list-style-type: none"> <li>+ Rapid ranking of erosion resistance</li> <li>+ Inexpensive</li> <li>+ Easy to operate</li> <li>+ Eroduct recycled</li> <li>+ Eroduct delivery: linear motion</li> </ul>	<ul style="list-style-type: none"> <li>- Particle size, impact velocity, impact angle cannot be undertaken</li> <li>- Eroduct particle degradation</li> </ul>
Whirling arm	<ul style="list-style-type: none"> <li>+ Eroduct delivery: circular motion</li> </ul>	<ul style="list-style-type: none"> <li>- Vacuum needed to eliminate aerodynamic effects on particles, and reduce rotor power needs</li> <li>- Complex equipment</li> </ul>
Centrifugal accelerator	<ul style="list-style-type: none"> <li>+ Easy to determine erodent velocity</li> <li>+ Inexpensive</li> <li>+ Easy to operate</li> <li>+ Eroduct delivery: circular motion</li> <li>+ Multiple tests simultaneously in same condition</li> <li>+ Particle/gas interaction is minimal</li> </ul>	<ul style="list-style-type: none"> <li>- Longer procedure</li> <li>- Difficulties quantifying erodent mass, that strikes each target</li> </ul>

## Conclusion

- The prominent parameters that effect erosion e.g. the impact angle, the velocity of solid particles and the particle size and shape were highlighted.

- It was found, that the sand/gas blast testers have an advantage in quick, simple and single sample testing at low erodent concentration, however the impact angle as well as the velocity changes during the tests. There is an inadequate grasp and control on particle impact condition. Advert gas/particle interaction could occur.
- The centrifugal accelerator testers have the advantage of testing multiple samples in parallel, as well as controlled impact conditions with adjustable impact angle and velocity of particle. The main disadvantage of this machine is the difficulty in quantifying erodent mass that hits the target specimen.

## Acknowledgement

The study was created for the project PR000050 - Centrifugal erosion tester, Ghent University - Laboratory Soete.

## References

- [1] Mamata, K. P. (2008). "A review on silt erosion in hydro turbines." *Renewable & sustainable energy reviews* 12(7): 1974.
- [2] Dr. Dmitri Kopeliovich. Mechanisms of wear (2009). Available: <http://www.substech.com> (2017.02.14)
- [3] A. A. Gadhikar, A. Sharma, D. B. Goel, and C. P. Sharma, "Fabrication and Testing of Slurry Pot Erosion Tester," *Trans. Indian Inst. Met.*, vol. 64, no. 4–5, pp. 493–500, Oct. 2011.
- [4] T. Deng, M. Bingley and M. S. A. Bradley, "Understanding particle dynamics in erosion testers—A review of influences of particle movement on erosion test conditions" *Wear*, vol. 267, pp. 2132-2140, 2009
- [5] S. R. More, B. D. Nandre, and G. R. Desale, "Development of pot tester to simulate the erosion wear due to solid-liquid mixture," *Int. J. Reasearchers Sci. Dev.*, 2014.
- [6] J. A. Williams, "Wear and wear particles—some fundamentals," *Tribol. Int.*, vol. 38, no. 10, pp. 863–870, Oct. 2005.
- [7] S. Söderberg, S. Hogmark, U. Engman, and H. Swahn, "Erosion classification of materials using a centrifugal erosion tester," *Tribol. Int.*, vol. 14, no. 6, pp. 333–343, Dec. 1981.
- [8] I. Kleis and P. Kulu, *Solid Particle Erosion: Occurrence, Prediction and Control*. Springer Science & Business Media, 2007.
- [9] T. Deng, M. S. Bingley, and M. S. A. Bradley, "Influence of particle dynamics on erosion test conditions within the centrifugal accelerator type erosion tester," *Wear*, vol. 249, no. 12, pp. 1059–1069, 2001.
- [10] Mehdi Azimian, Hans-Jörg Bart (2015) 'Erosion investigations by means of a centrifugal accelerator erosion tester, *Wear* 328-329(2015)249–256

- [11] <https://writepass.com/journal/2012/12/to-investigate-erosive-characteristics-of-targets-by-using-a-small-centrifugal-accelerator-erosion-tester/> (2017.08.28)
- [12] R. J. K. Wood and D. W. Wheeler, “Design and performance of a high velocity air–sand jet impingement erosion facility,” *Wear*, vol. 220, no. 2, pp. 95–112, Oct. 1998.
- [13] <http://www.tut.fi/en/research/research-fields/materials-science/research-equipment/wear-research/erosion-tester/index.htm> (2017.04.16)
- [14] T. Deng, M. S. Bingley, M. S. A. Bradley, and S. R. De Silva, “A comparison of the gas-blast and centrifugal-accelerator erosion testers: The influence of particle dynamics,” *Wear*, vol. 265, no. 7–8, pp. 945–955, Sep. 2008.

## Wear mechanism classification by image processing

Klára BARTHA<sup>1</sup>, Jacob SUKUMARAN<sup>1</sup>, Dieter FAUCONNIER<sup>1</sup>,  
Jozef VLEUGELS<sup>2</sup>, Shuigen HUANG<sup>2</sup>, Patrick DE BAETS<sup>1</sup>

<sup>1</sup>Department of Electrical energy, metals, mechanical constructions and systems,  
Faculty of Engineering and Architecture, Ghent University

<sup>2</sup>Department of Material Engineering, Catholic University of Leuven

### Abstract

Wear mechanism is the key for tool wear monitoring and fault detection of worn parts. In tool wear monitoring and fault detection, recognizing wear mechanisms acting on a surface is of great importance. Visual inspection is one of the non-contact methods for identifying wear patterns. However, this task is often carried out by technical experts, and therefore can be time consuming, subjective and expensive. In order to overcome such challenges, digital image processing techniques for surface pattern recognition has gained interest in the recent years. These techniques enable on-line monitoring of worn surfaces. In this article, an image processing method is proposed which applies the k-Nearest Neighbours machine learning algorithm for the identification of different wear mechanisms based on properties extracted from image contours. Such computer vision method allows automated classification of worn surfaces based on images without the presence of an expert. The proposed digital image processing tool was tested for classification of images showing abrasion, adhesion and pitting, and results show that it is able to classify wear mechanisms with 97.78% accuracy.

### Keywords

Wear mechanism classification, image processing, surface pattern recognition

### 1. Introduction

Identification of wear mechanisms from the worn surface may play an important role in tool wear monitoring. Investigation of different wear mechanisms is traditionally carried out by means of visual inspection. It is usually done by experts, and thus can be time consuming, and does not allow on-line monitoring of the systems. That is why digital image processing techniques for surface pattern recognition gained interest in recent years. Laghari used grey level co-occurrence matrices and neural networks for the classification of wear particles based on surface texture information and wear particle dimensions [1][2]. Stachowiak et al. proposed a combination of wavelet and fractal methods for extracting features from images of wear particles, and Support Vector Machine

learning algorithm for classifying the wear mechanisms [3]. Soleimani et al. applied grey-scale granulometry to images of worn surfaces, in order to gain quantitative information of wear, however they did not apply classification method [4]. Szydłowski et al. used wavelet-based extended depth of field technique and morphology operations in a machine vision system for micro-milling tool wear monitoring, but also without a classification method [5]. In present article, we propose an image processing method for wear mechanism recognition, where the images are characterized by different properties calculated from the object contours of the image. Then, these features are given to the k-Nearest Neighbours machine-learning algorithm, which enables automated classification of worn surfaces based on this data.

## 2. Methodology

Image classification by machine learning consists of two main phases. The first is a training phase where the program is provided with input images each with the label of the class it belongs to. The images are then enhanced, features are extracted from them and arranged to feature vectors representing the image. Based on these feature vectors and the corresponding labels the machine learning algorithm is trained. The second phase is the classification, the algorithm is given images again, however this time without labels indicating the classes. The images are enhanced and the features are extracted the same way as in training process, then the machine learning algorithms assigns each picture to a class based on the information obtained during the training phase. This kind of machine learning method is called supervised learning.

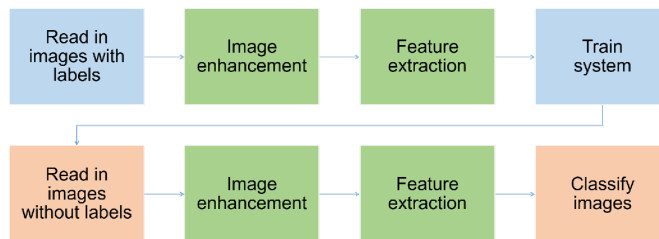


Figure 1. Process of image classification by supervised learning

In order to eliminate the effects of different illumination conditions and enhance the contrast of the images Contrast Limited Adaptive Histogram Equalization (CLAHE) [6] was applied. The CLAHE algorithm partitions the image to small tiles and for each tile, the histogram is equalized, then the border of the tiles is treated by means of bilinear interpolation. A limit value is used for the contrast to eliminate the enhancement of noise.

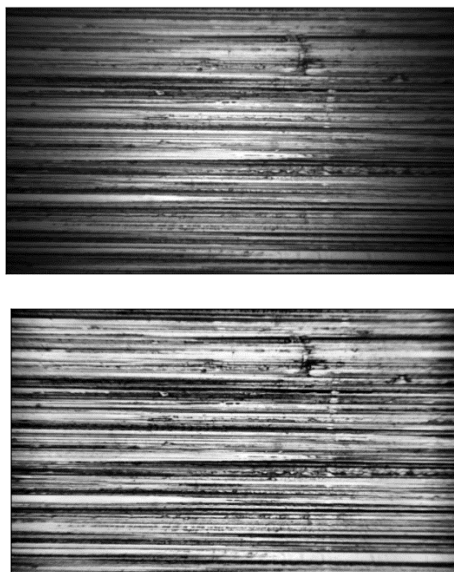


Figure 2. Original greyscale image (top) and the image after CLAHE (bottom)

Since most object detecting methods work better on binary pictures, after enhancement the images are converted to binary form by thresholding. Then, the images are further processed using binary morphology, which are mathematical operations that can be applied to pictures for making features more distinct. For each pixel  $x$  in the image a so-called structuring element  $B(x)$  is assigned. Then, following the notations of [7] [8], dilation of  $X$  with structuring element  $B$  can be defined as

$$D(X, B) = \{x | B(x) \cap X \neq \emptyset\}, \quad (1)$$

and erosion of  $X$  with respect to  $B$  is formulated as follows

$$\varepsilon(X, B) = \{x | B(x) \subseteq X\}. \quad (2)$$

However, in image processing generally these two operations are applied after each other, first with the structuring element  $B$ , than the other operation with  $-B$  defined as  $\{-b | b \in B\}$ . For symmetric structuring element, this set will yield  $B$  itself. Binary closing is the procedure of applying dilation first and then erosion

$$C(X, B) = \varepsilon(D(X, B), -B) \quad (3)$$

While erosion followed by dilation is called binary opening

$$O(X, B) = D(\varepsilon(X, B), -B) \tag{4}$$

The purpose of closing in the case of digital images is to fill small black holes on the front objects. Opening in turn discards small white spots and thus removes noise.

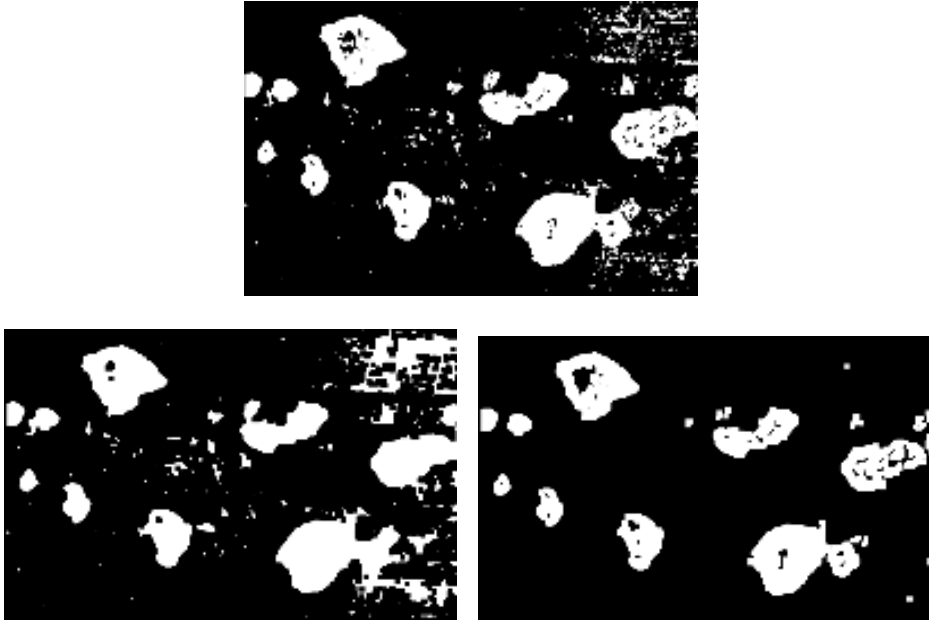


*Figure 3.* Binary image after thresholding (top), the image after binary closing (bottom left) and the image after binary opening (bottom right)

The next step is data acquisition. For this purpose, the contours of the processed images were detected. Contours are given by their constituting points therefore they allow the calculation of a variety of features. In order to find bright and dark objects as well, both the image and its inverse after enhancement are converted to binary form. Two types of contours are investigated: contours of bright blobs from the original image, and contours of dark blobs obtained from the inverted image. First, the elongation of the contours is investigated. Elongation is an invariant property that can be calculated from second order central moments of the object. Following the notations in [9], these moments for a pixel at  $(x,y)$  with greyscale value  $g(x,y)$  and object centroid  $(\bar{x}, \bar{y})$ , can be calculated by the following expressions

$$m_{2o} = \sum_y \sum_x (x - \bar{x})^2 g(x, y), \tag{5}$$

$$m_{20} = \sum_y \sum_x (y - \bar{y})^2 g(x, y), \quad (6)$$

$$m_{11} = \sum_y \sum_x (x - \bar{x})(y - \bar{y})g(x, y). \quad (7)$$

In the case of binary images  $g(x,y)$  can only have two values, 1 for pixels in front objects, and 0 for background pixels. From here, the elongation of a contour can be obtained from the formula

$$elong = \frac{a + b}{a - b} \quad (8)$$

where the terms a and b are given as relations of the contour moments

$$a = m_{20} + m_{02}, \quad (9)$$

$$b = (4m_{11}^2 + (m_{20} + m_{02})^2)^{1/2}. \quad (10)$$

Both the contours of bright and the contours of dark objects are divided to three groups according to their elongation. Contours with small elongation are then partitioned to three groups based on their area.

In the case of medium and largely elongated contours four groups are created by area. In addition, to each one of these blobs an ellipse is fitted which is defined by its major and minor axis and the angle formed by its major axis and the horizontal line. Then, the width of the contour is approximated by the minor axis of the ellipse, the length of the contour by the major axis, and the orientation of the blob by the angle. With the help of this information, additional subcategories are produced, four groups by width, four groups by length and six groups by orientation. The number of contours in each of the final categories is counted, and so they form the elements of the feature vectors, which are the inputs of the machine learning algorithm.

In this study the k-Nearest Neighbours [10] supervised learning method was used for the classification of the images. In this method, after the training of the system, each feature vector is represented by a point in feature space and is associated with the label of its class. When a new item is added, its distance is measured from each point of the training dataset in the feature space. The k points which has the closest distance to the new point are selected, and the new item will get the same label as the majority of these k nearest points.

### 3. Results

For the development of the proposed image processing tool Open CV was used which is an open source library containing various functions and algorithms for computer vision.

The program was tested for classification of images of three different wear mechanisms, namely abrasion, adhesion and pitting. The images used in the classification were all from experiments carried out in in Soete Laboratory, Ghent University. For abrasion, injection moulded PA6/6 and extruded PA6/6 materials were used in test procedure according to DIN 50322 (ASTM G132 category). The pictures of adhesion were acquired on a pin on plate test according to ASTM G133 standard on a PLINT 177 machine, and the used materials were zirconia against coated steel. In the case of pitting, the test conditions were: twin disc (Modified FZG), steel against steel, and dry contact condition.

The system was trained with 100 images. Then, 45 unlabelled images were used for testing, 15 pictures of each type of wear mechanism.

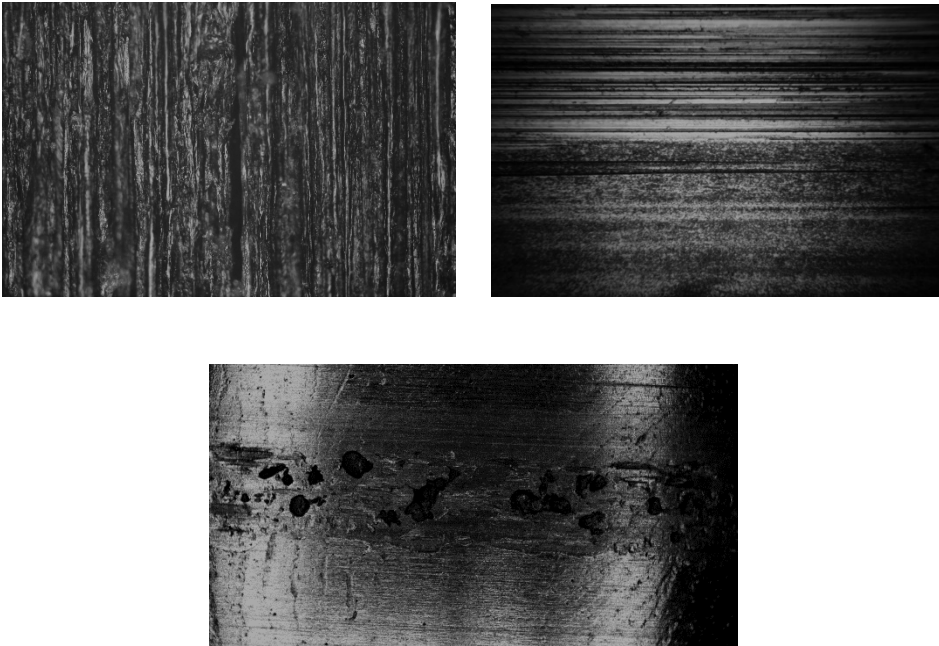


*Figure 4.* The three investigated wear mechanisms: abrasion (top left), adhesion (top right) and pitting (bottom)

For the enhancement by CLAHE  $6 \times 6$  pixel tiles and 6.0 clip limit were applied, the binary morphology operations were carried out using  $3 \times 3$  pixel square constructing elements. The k-Nearest Neighbours algorithm was applied with  $k = 3$ . The algorithm correctly classified all images of abrasion and pitting. In the case of adhesion, 14 images were assigned to the correct class, and the mechanism on one of these images was misclassified as pitting. Overall, the image processing tool could recognize the wear mechanism on the images with a probability of 97.78%.

## Conclusion

The proposed image processing method was able to classify wear mechanisms with 97.78% accuracy. The method uses properties of the image contours as image features and the k-Nearest Neighbours machine learning algorithm. It provides an automated method for qualitative investigation of worn surfaces. Such wear mechanism identification tool can be important in industry as it allows far field inspection of surfaces without the presence of an expert.

Further studies should consider the possibility of quantitative investigation by this technique. Also, other wear mechanisms should be included in the system, and based on huge database of images of different worn surfaces, an objective wear mechanism classification tool could be developed, which could eliminate the subjectivity of the classification of different experts.

## Acknowledgement

This investigation was supported and funded by Fonds Wetenschappelijk Onderzoek – Vlaanderen (FWO) G077216N. The research performed under a cooperative effort between Ghent University (Belgium) and Katholieke Universiteit Leuven, Department of Material Engineering (Belgium).

## References

- [1] Laghari, M. S. (2003): Recognition of texture types of wear particles. *Neural Computing & Applications*, 12(1), 18-25.
- [2] Laghari, M. S., Memon, Q. A., & Khuwaja, G. A. (2004): Knowledge based wear particle analysis. *International Journal of Information Technology*, 1(3), 91-95.
- [3] Stachowiak, G. W., & Podsiadlo, P. (2006): Towards the development of an automated wear particle classification system. *Tribology International*, 39(12), 1615-1623.
- [4] Soleimani, S., Sukumaran, J., Kumcu, A., De Baets, P., & Philips, W. (2014): Quantifying abrasion and micro-pits in polymer wear using image processing techniques. *Wear*, 319(1), 123-137.
- [5] Szydłowski, M., Powalka, B., Matuszak, M., & Kochmański, P. (2016): Machine vision micro-milling tool wear inspection by image reconstruction and light reflectance. *Precision Engineering*, 44, 236-244.
- [6] Pizer, S. M., et al. (1987): Adaptive histogram equalization and its variations. *Computer vision, graphics, and image processing*, 39(3), 355-368.
- [7] Serra, J. (1986): Introduction to mathematical morphology. *Computer vision, graphics, and image processing*, 35(3), 283-305.
- [8] Haralick, R. M., Sternberg, S. R., & Zhuang, X. (1987): Image analysis using mathematical morphology. *IEEE transactions on pattern analysis and machine intelligence*, (4), 532-550.

- [9] Guyer, D. E., Miles, G. E., Schreiber, M. M., Mitchell, O. R., & Vanderbilt, V. C. (1986): Machine vision and image processing for plant identification. *Transactions of the ASAE*, 29(6), 1500-1507.
- [10] Cover, T., & Hart, P. (1967). Nearest neighbor pattern classification. *IEEE transactions on information theory*, 13(1), 21-27.

## **Tribological characteristics of tailor made PTFE coated basalt/ vinyl ester composites for large scale system**

Karthikeyan SUBRAMANIAN<sup>1</sup>, Rajini NAGARAJAN<sup>1</sup>,  
Jacob SUKUMARAN<sup>2</sup>, Patrick De BAETS<sup>2</sup>,  
Gábor KALÁCSKA<sup>3</sup>

<sup>1</sup>Centre for Composite Materials, Department of Mechanical Engineering,  
Kalasalingam University, Krishnankoil,  
Tamilnadu, India – 626126.

<sup>2</sup>Department of Mechanical Construction and Production, Ghent University,  
Technologiepark, Zwijnaarde 903,  
Ghent, Belgium.

<sup>3</sup>Institute for Mechanical Engineering Technology, Szent István University,  
Páter K. u. 1., Gödöllő,  
H-2100, Hungary,

### **Abstract**

This work addresses the development of eco-friendly tribo-system using sustainable bio-degradable basalt fiber and thermoset vinyl ester matrix. Two different composite material design were used in this study i.e., one is basalt fiber/vinyl ester composite (BFVEC) and the other is PTFE (10 wt %) coated basalt fiber/vinyl ester composite (BFPTFEC). Static and dynamic mechanical properties of both the composites was studied in addition to the thermal properties. From the well-known fact of literature, the tailor made PTFE coated composite alone is considered to perform the tribological testing in higher loading condition. Accordingly, the tribo-test was performed for the selected PV limit of 400 MPa-mm/s (10 KN and 50 mm/s) in a flat-on-flat configuration. Infra-red thermal imager camera was employed to study the variation of contact temperature at the interface between composite and counterpart. The characterization techniques such as FTIR and XRD was performed to understand the changes in chemical composition before and after wear process. Only a slight change in mechanical property was noticed between the composites in both static and dynamic condition, however, the higher thermal conductivity value of 0.187 W/m-k was noticed in PTFE coated composites. The static and dynamic coefficient of friction of PTFE coated composites was found to be 0.12 and 0.19 respectively. To understand the failure mechanism of sliding wear, the morphology of worn out composite surface and counterpart was analyzed using SEM-EDX analysis. Wear mechanisms shows only the matrix failure by thermal degradation rather to have fiber breakage, fiber thinning and fiber separation which are usually noticed in the fiber reinforced composites. The present investigation suggested that the PTFE coated degradable basalt composites are to be considered as an alternative to the bearing materials working at higher contact pressure and low velocity.

## **Keywords**

Basalt fiber, Taylor made composite, PTFE, Friction

## **1. Introduction**

Development of novel tribo-composites with ecological benefits is always expected to be appreciable especially in the field of marine, aerospace and dam structure as a replacement of sliding bearing. In these application, to design a material with low frictional force and without sacrificing the mechanical strength is very important. However, these manmade composites leads to the increasing production cost and discover the landfill as decomposable product. Therefore, it is important to identify the alternative reinforcement with comparable and overcoming ability towards strength and environmental consciousness respectively. One such kind of reinforcement fabric is basalt fiber which is extracted from the origin of natural resources. Initial process of basalt fiber production originated from volcanic rock. Moreover, the basalt fiber can overcome the strength of glass fiber, however, it is only exhibit lower strength compared to carbon fiber. In order to develop a tribo component using the synergistic effect of filler and basalt fiber, the hybrid composite can be a better alternative for high cost tribo material system. The basalt fiber is selected as a reinforcing element in the present work due to its desirable degradability behavior. Moreover, the basalt fibers in the form of fabrics reinforcement in polymer composites can finds its attention towards a large scale and heavy-duty friction units requiring high strength.

At the same time, to attain the better tribological characteristics with the inclusion of lubricant additives is found to be the well known process implemented lot in the self lubricating polymers. Accordingly, the Polytetrafluoroethylene (PTFE) is the one, which was identified as a best solid lubricant additives suitable for all the high performance engineering polymer. Having all said, the explore of basalt fiber in the tribological application is found to be significant. However, there is no adequate works published by correlating the temperature dependent mechanical properties with the tribological aspects in large scale applications using basalt fiber based polymer composites. Hence, the mechanical strength of basalt/VE composite with and without the addition of PTFE was studied under static and dynamic condition for an alternative choice of ecological tribo product. Moreover, it is only limited works have been reported in the case of higher pv limit for the design of polymer based bearing material. Hence, a first time attempt has been done to study on frictional force and wear resistance properties of PTFE particle filled BFVECs under higher PV limit condition. Besides, other characterization techniques such as FTIR and XRD have also been studied. Further, the morphological analysis of worn out surfaces of sample and counterpart material was performed using SEM – EDX.

## 2. Experimental details

### *Materials Used*

The woven form of Basalt Fabric GSM (300±30) is used as a primary reinforcement. It was obtained in the form of roll from the Nickunj Eximp Entp P Ltd, Chennai, India.. The general purpose thermoset vinyl ester matrix was used as a binding material in composite. In addition, the tribo lubricant filler of PTFE was also used in the form of particles and applied at the top layer of the composites to provide the resistance against wear. The polymer resin, PTFE and all other chemicals such as Methyl Ethyl Ketone Peroxide (MEKP) and Cobalt Naphthenate taking part in the curing of polymer are all purchased from Sigma Aldrich (P) Ltd, Bangalore.

### *Fabrication of the tailor made composite*

A simple manufacturing technique of hand layup is only used for the fabrication of basalt/PTFE reinforced vinyl ester composites. Based on the literature survey in the aspect of mechanical strength, the 50 wt % of basalt fiber content is selected for the making of composites [15]. Firstly, the required quantity of vinyl ester resin was split into two halves out of which one half of the resin is mixed with the 10 wt % of PTFE content. The PTFE was thoroughly mixed with the resin using hand stirrer then it was subjected to the mechanical stirring at 500 rpm for about one hour with radial rotor blade. The resin-PTFE mixer was kept in the ultra-sonicator for about 15 minutes to distribute agglomerated particle of PTFE. Then, the mould cavity of 250 X 250 size was created using foam board and it was affixed with the glass plate to obtain the bottom surface of the composite with good surface finish. Finally, the resin was mixed with proportionate amount of (1.5 ml) curing agents and applied as a resin coating over the glass plate at inner region of mould cavity.

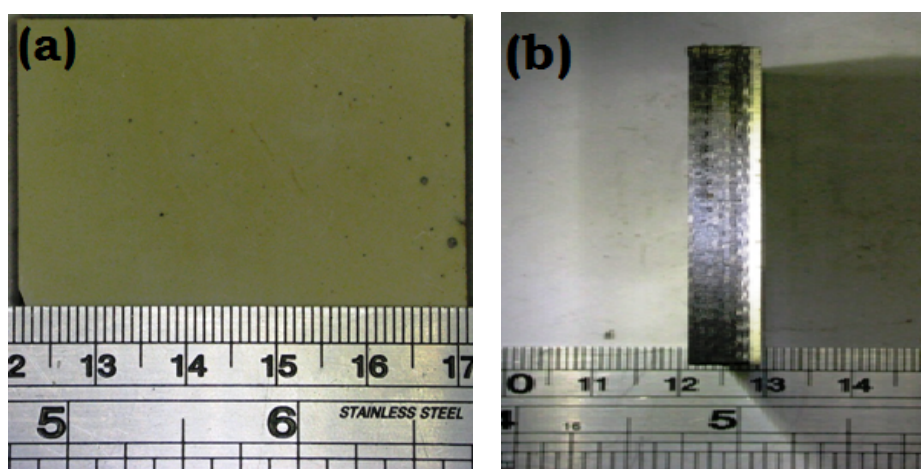


Figure 1. Fabricated BFPTFEC laminate using hand layup technique  
(a) top view (b) cross-sectional view

Then, the resin impregnated basalt fiber fabrics are placed one over another up to six layers with the application of roller. The rolling was done to remove the air bubbles and folding of fabric during the fabrication process. Before closing the mould, the remaining three layers of basalt fabric is placed on the top with the overlaying of PTFE filler. The closed mould was kept at room temperature curing for about 24 hours. After the curing, the laminate was subjected to post curing in hot air oven at 70°C for one hour. In similar manner, the tailor made composites were fabricated for two different thickness of 3 mm and 7 mm to perform the mechanical and tribological tests. The samples were cut for the required dimensions from the laminated composites and the photographic image of the same is shown in Fig. 1(a-b).

### *Density*

The density of BFVECs as well as BFPTFE hybrid composite is measured, using Archimedes's principle with the mettelro density measuring apparatus. Initially the weight of the specimen in air ( $W_a$ ) and weight in water ( $W_w$ ) are measured. The density ( $\rho_c$ ) of composites is measured using the equation (1).

$$\rho_c = \left[ \left( \frac{W_a}{W_a - W_w} \right) \right] \times \text{Density of water} \quad (1)$$

### *Characterization Studies*

In order to understand the presence of chemical compositions, the characterization studies such as X-ray diffraction (XRD) analysis, FTIR, and SEM-EDX was used. All the samples were subjected to these studies under before and after wear conditions. In XRD, the step scanning was employed at a scanning rate of 2°/min with Cu-K $\alpha$  radiation using a SHIMADZU, XD-DI X-ray diffractometer. The scanning angle ( $2\theta$ ) was taken from 3° to 80°. Scanning electron microscopy was performed for unworn, and worn out composite surfaces using Hitachi S-3000 model.

### *Static Mechanical Tests*

The static mechanical properties such as tensile, flexural and impact test were performed based on ASTM-D 3039, ASTM-D 790 and ASTM-D 256 respectively. Tensile and Flexural tests were conducted in (Instron, Series-3382) a universal testing machine. The rectangular specimens were cut by water jet machining with the dimensions of 200 mm X 20 mm X 3mm. In flexural testing, three-point bending was performed at room temperature on a specimen of 127 mm X 12.7 mm X 3mm dimension. For both tensile and flexural, the cross head speed of 5 mm/min was selected. The un-notched izod impact strength was performed with the rectangular specimen of dimensions 65 X 12 X 3 mm.

### *Dynamic Mechanical Analysis*

Dynamic mechanical properties such as the storage modulus ( $E'$ ), loss modulus ( $E''$ ) and mechanical damping parameter ( $\tan \delta$ ) were measured by using the SII EXSTAR DMS 6100 – DMA instrument. The rectangular hybrid composite specimens of size 50 X 10 X 3 mm<sup>3</sup> were used. The test was conducted by using a 3-point bending mode. The samples were tested in a nitrogen atmosphere in a fixed frequency mode of 20 Hz and a heating rate of 2° C/min. The measurements were taken over a temperature range of 20 °C-300 °C.

### *Roughness measurement*

The surface roughness was measured using a contact 2D profiler (MITUTOYO, SURFTEST SJ – 410). The average values of three measurements were recorded in each case as per ISO 1997. The distance travelled by the probe is 20 mm. The flatness of the samples were ensured from the surface plate, before taking the measurement on the surface of PTFE coating. The Gaussian filter was used in the process of roughness measurement. All the roughness parameters, related to 2D measurements were recorded.

### *Dry sliding wear testing details*

In this study only the BFPTFE hybrid composites was considered to perform the dry sliding wear test using medium scale flat (MSF) testing machine (Fig.2) at Laboratory Soete, Ghent University, Belgium. The specifications of the MSF machine is also presented in Table 1.



Figure 2. Medium scale experimental setup used for friction and wear measurement located in Laboratory soete, Ghent University, Belgium.

A 100 chromium steel was used as a counter plate on both of the sides of vertical actuator. Two identical wear samples of size 50 X 50 mm<sup>2</sup> at 7 mm thickness were used on both sides of the sample holders. A protruded length of 2 mm is the maximum allowable pre-defined thickness which can be removed in the wear testing. A k-type thermocouple was used at the rear side of the counter plate which was identified to be the place of maximum temperature accumulation.

*Table 1.* Specifications of the MSF wear testing machine

Property	Value
Normal load	Max 200 kN
Friction force (per interface)	Max 100 kN
Velocity	Max 50 mm/s
Stroke	Max 100 mm
Friction material dimensions	50 mm x 50 mm x 7 mm

The addition of a filler in the form of a particulate or fibers in the matrix can offer more resistance to the wear loss of the composites. Wear tests of BFPTFE hybrid composites was carried out as per the tribological testing conditions given in Table 2. The dry sliding properties such as wear, static and dynamic friction force and temperature at the counter plate were studied by online measurement system. The wear test was performed at a constant applied load of 10 kN and it was selected based on the contact pressure suitable for marine applications. The counter surface plate was made of 100 chromium steel having dimensions of 200 mm length, 20 mm thick and surface roughness (Ra) of 0.1 - 0.2 μm are shown in Fig.3. All the tests were conducted at ambient temperature. At least four tests with eight samples of composites were subjected to the wear test and the average value is reported.



*Figure 3.* Microscopic photograph of 100 chromium steel counter material after dry sliding

Table 2. Details of dry sliding wear testing conditions

Test Condition	Values
Stroke length	100 mm
Load	10 kN
Velocity	50 mm/ sec
Sliding distance	500 m

All the data were recorded at the frequency of 20000 Hz for friction force for the entire process. The static and dynamic coefficient were determined using the formula and it is given in equation (1). The average value of 0.12 and 0.19 for static and dynamic coefficient of friction was observed from the four repeated test with eight samples.

$$\mu_{static} = \frac{(|F_{T,min}| + |F_{T,max}|)}{2} \text{ (equation 1)}$$

$$\mu_{Dynamic} = \sqrt{\frac{1}{T} \int_0^T (F_T(t))^2 dt}$$

### 3. Results and discussions

#### *FTIR and XRD Characterization*

In order to understand the change in chemical proportions under before and after wear conditions, the FTIR spectra was present in all the three cases as shown in Fig. 4. Unanimously, all the composites exhibits a absorbance intensity peak at  $2950 \text{ cm}^{-1}$  ( $-\text{CH}_2$  vibration) and at  $1563 \text{ cm}^{-1}$  ( $-\text{NH}_2$  stretching). Results revealed that the vinyl ester polymer had interacted with the PTFE particle successfully. The presence of  $-\text{OH}-$  group appears between  $3400 \text{ cm}^{-1}$  and  $3600 \text{ cm}^{-1}$ , at the same time the broadness of peak depends on the concentration and it can happen due to hydrogen stretching. The other intensity peaks related to vinyl ester matrix and vinyl ester based filler composites were also found to be appeared at  $2920 \text{ cm}^{-1}$  (CH stretching),  $1620 \text{ cm}^{-1}$  (benzene rig) and  $950 \text{ cm}^{-1}$  (bending of C-H bonds). Similarly, X-ray diffraction patterns was carried out for unfilled and PTFE filled composites and that are shown in Fig.5. It can be clearly seen from the Fig.6, that all the curves are mapped at same 2 theta angle (at  $18^\circ$ ); though, the variation in intensity for unfilled and PTFE filled composites have been noticed. A large amorphous region can be seen in the case of X-ray pattern of unfilled BFVEC (a). Whereas, the shift in peak was observed at the lower angle side in pattern (b) and it indicates the presence of amorphous phase in

the worn out PTFE composites. It may happen in lieu of thermal degradation of PTFE due to the temperature rise in the contact temperature.

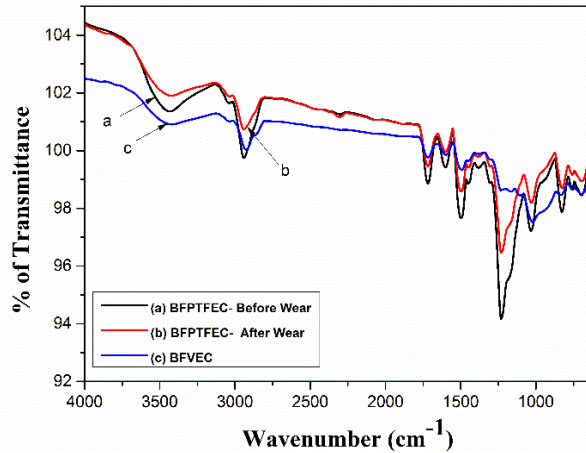


Figure 4. FTIR spectra of unfilled and PTFE filled composites in before and after wear condition

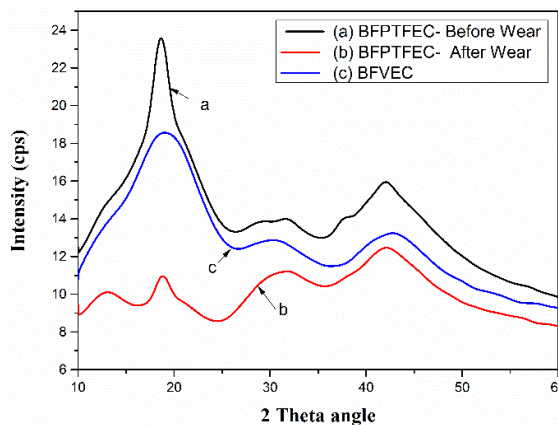


Figure 5. XRD pattern of unfilled and PTFE filled composites in before and after wear condition

### *Static Mechanical properties*

Before studying the tribological behavior of tribo-lubricant filled BFVE composites, all the fundamental mechanical properties were discussed and compared with the unfilled composite in the following section. Because, the deformation ability of material is one of the key parameter needs to be studied to realize the degree of asperity contact between the materials during sliding process. Fig.6a shows the tensile strength and modulus of BFVEC and BFPTFEC. Results

clearly shows that there is no significant variation in tensile strength between the composites. Whereas a slight variation in tensile modulus was observed between them. Because, the addition of filler as bulk can influence the dispersion ability of filler in matrix and it was observed as a critical factor to decide the strength of composites Fig.6b shows the flexural strength and modulus of unfilled and PTFE filled BFVEC. A significant improvement in flexural strength was observed in the case of BFPTFECs. Normally, it is a good sign for a tribo material used in the field of high loading conditions. About 41% of increment in flexural strength of BFPTFECs can increase the possibility of contact pressure in tribo testing. It can happen due to the resistance of shear offered by the particulate filled composites. However, the flexural failure of samples was not only decided from the resistance to shear and it also depends on the compressive strength of the material.

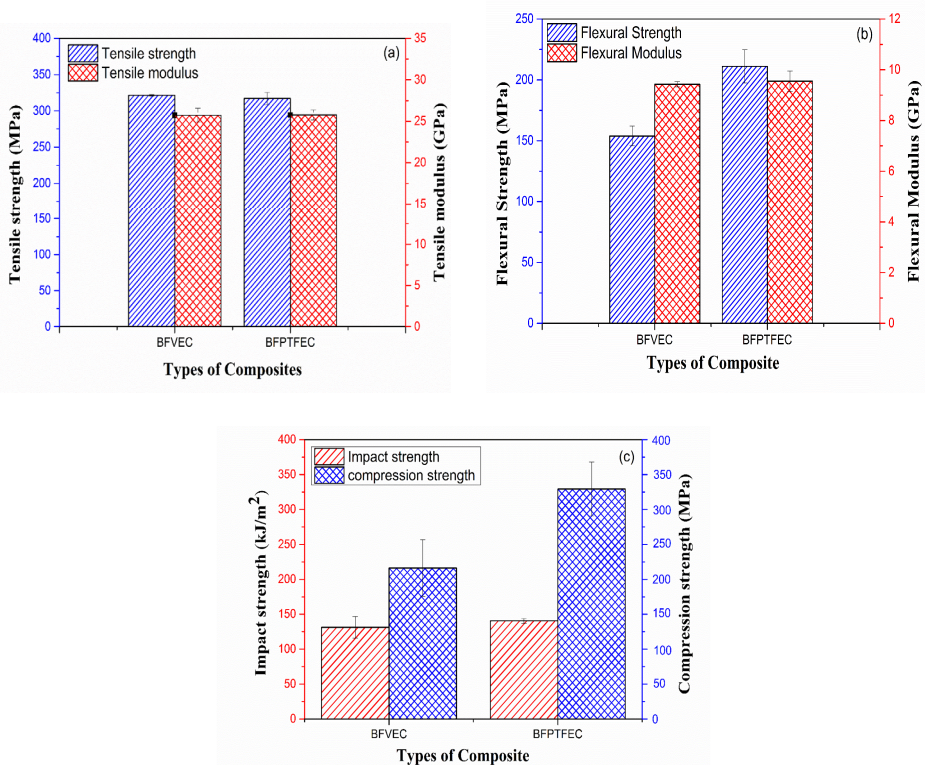


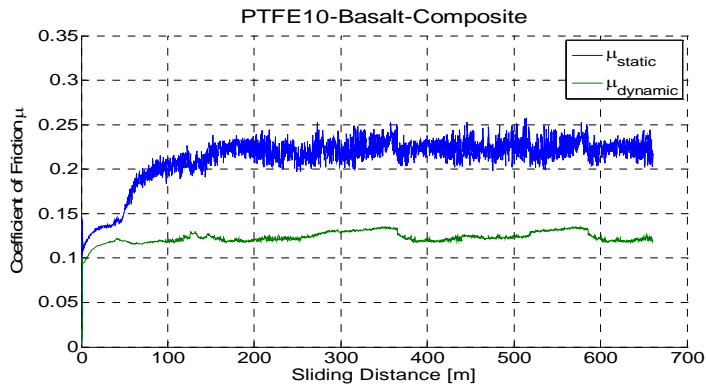
Figure 6. Mechanical strength and modulus of unfilled and PTFE filled BFVECs (a) tensile test (b) Flexural test and (c) Impact and compression test

The impact strength was studied with the application of sudden drop of hammer load on cantilever supported in notched specimen. From Fig.6c. it was observed that only a slight change in impact strength between the composites. However the PTFE coated composite exhibits a slight increase in impact strength. It implies that the particle inclusion can also impart to absorb energy.

### Friction and wear characteristics

In order to achieve the reliable data, there are four tests were conducted at the identical condition with 8 number of samples each at either side of the counter plate. For the data acquisition, a DEWESoft 8.0 software was used with the hardware systems of 8 channel NI DAQ card. The friction and wear data were recorded through online process using DEWESoft software at large sampling rate. Besides, the temperature data was recorded from the back side of the counter plate using k-type thermocouple at the same sampling rate using LABVIEW program. Further, thermal imager camera is employed to the side of the machine at 1m distance from the contact surface. It can show the temperature value at the contact surface (between counter plate and composite plate) through the online measurement system.

The samples are placed in the cylindrical holder on the both sides and the holders were affixed with the aid of rectangular pin in a cylindrical hole. The hydraulic cylinder is moved up and down in vertical direction for the sliding distance of 100 mm per stroke. The load is applied through the horizontal cylinder to holder and engaged the samples with counter face material. The tests were conducted for the period of 5 hours as per the wear testing condition given in Table 2. Fig. 7 shows the typical static and dynamic friction characteristic curves for test 1. Both running in and steady state condition of friction characteristics curve for all the tests exists at the same region. After the running in condition almost a constant friction curve was observed until the entire test was finished.



In the lieu of friction curve, the ductile nature of thermoplastic PTFE can exhibits elastic deformation at the asperity contact as soon as to reach the  $T_g$  value of polymer matrix at the flash contact temperature. Usually, if the plastic deformation exist, the un-recovery material expansion is takes place at the edges of the samples. But in this case, all the particles are subjected to the elastic shear and it regains original location; however the block traces on the damaged surface was clearly noticed. This visual inspection provides more emphasis on the failure of the

composites with respect to thermal degradation rather to analyze the failure due to contact pressure. The possibility of breakage in the cross linking density of polymer matrix due to thermal stresses was confirmed from the appearance of amorphous phase in the X-ray pattern after the wear test. It is a known fact that in the case of thermoset polymer, the contact temperature was found to be the critical factor constrained the crack propagation with the support of molecular immobility. The Shore-D hardness is obtained for pure BFVEC and PTFE filled BFVEC reinforced hybrid composites. It measures the resistance offered by the material against indentation. The tests were performed according to the ASTM D-2240. The measurement of the Shore-D hardness values are presented in Table 3. Generally, increase in hardness value indicate the brittle nature of material. Therefore, the lower hardness value of BFPTFECs indicates the ductility property than that of pure BFVEC. All these kind of results are the reason to choose the PTFE filled composite alone to study the tribological performance.

Table 3. Properties of non-layered and PTFE layered composites

Type of Composite	Density (g/cc <sup>3</sup> )	Shore – D Hardness	Thermal Conductivity (W/m-K)
BFVECs	1.2452	98	0.108
BFPTFECs	1.2924	87	0.187

Wear rate is a key parameter to study the tribological performance of the material, and it is defined as a volume of the material removed/unit time, and is calculated by measuring the weight loss of the specimen. The addition of a filler in the form of a particulate or fibers in the matrix can offer more resistance to the wear loss of the composites. For accurate and uniform results, it must be ensured that the surface flatness and roughness are perfect. The surfaces of both the sample were cleaned with a soft paper soaked in acetone before the test. Before the wear test, all the sample were kept inside the oven at 70°C for 12 hrs, because this is the optimum condition where the mass difference found to be zero. All the tests were conducted at ambient temperature. At the end of the test, the sample was again weighed in the same balance. The difference between the initial and final weights was a measure of the slide wear loss. In composite specimens, the basalt fabric mats are placed parallel to the sliding direction and normal to the applied force.

At least eight samples of composites are subjected to the wear test and the average value of two samples per test is reported. The wear was measured by the loss in weight, which was then converted into the wear volume using the measured density data presented in Table 3. After the wear test, the sample was again cleaned. The specific wear rate ( $K_s$ ) was calculated from the equation (2):

$$K_s = \frac{V}{PXD} \left( \frac{mm^3}{Nm} \right) \quad (2)$$

where  $V$  is the volume loss,  $L$  is the load and  $D$  is the abrading distance. The lower value of specific wear rate was found from all the specimens with the confidence interval of 95 % .

### *SEM micrograph analysis of Worn out Surfaces*

SEM micro graphical photograph of worn-out samples and counter plate is shown in the Figure. Matrix failure and removal of PTFE coating can be clearly seen in Fig.16a which was occurred due to the ploughing mechanism. The irregular crack was found to be grown and lead to the formation of irregular crack and it leads to the formation of networking between the branches of cracks. Along the direction of crack formation the removal of matrix was seen in the form of rectangular slots. The debonded PTFE particles and wear debris were found at the surface of worn-out samples. And also, in some regions the fine fragments of basalt fiber was noticed and it implies that the asperities of counter plate can plugged deep into the specified region and cuts the fiber into small fragments. But, it was not found to be true for the entire surface. Therefore, it ensure that the wear failure is based on the asperity contact, type of deformation and flash contact temperature at the localized regimes. The local deterioration may allow the crack to progress further while the contact temperature got increased. Hence, it is important to focus the mechanism of failures at the asperity contact. So that the rate of material removal can be reduced through proper asperity design with the aid of controlled surface temperature.

Fig.16b shows the SEM micrograph of BFPTFEC samples with side edges. In some situation, the failure was also found to be happened at edges due to the machining of samples with sharp corners. The fibres in the orthogonal direction shows the weft and warp direction of basalt fabric. The applied load can create more stresses at the edges where the stress concentration will be higher. The loosely separated basalt fibres was clearly seen in Fig.16b and it was happened due to the debonding between the matrix and fibre. Further, the crack formation at the interface and fibre fracture was also be observed.

Fig.16 (c-d) shows the worn-out surface of counter plate material with lower and higher magnification. Fig.16c shows the formation of orderly developed grooves parallel to the direction of wear track, the deposition of transfer film is clearly seen from the high magnification (Fig.16d) and it sealed the grooves in longitudinal and transverse direction. This result further evidenced from the surface roughness value along depth z-direction ( $R_z$ ). A significant reduction of surface roughness was noticed on both parallel and perpendicular directions. It happens due to the filling of valleys by the transfer films. A thick layer of transfer films on the counter face could be the reason for exhibit this lower coefficient friction and wear loss. The adhesion strength of PTFE on the counter plate also plays a role to decide the friction characteristics. In this case, a strong adhesion was found to be occurred between the PTFE and counter plate. It was confirmed from the thick patches of transfer film.

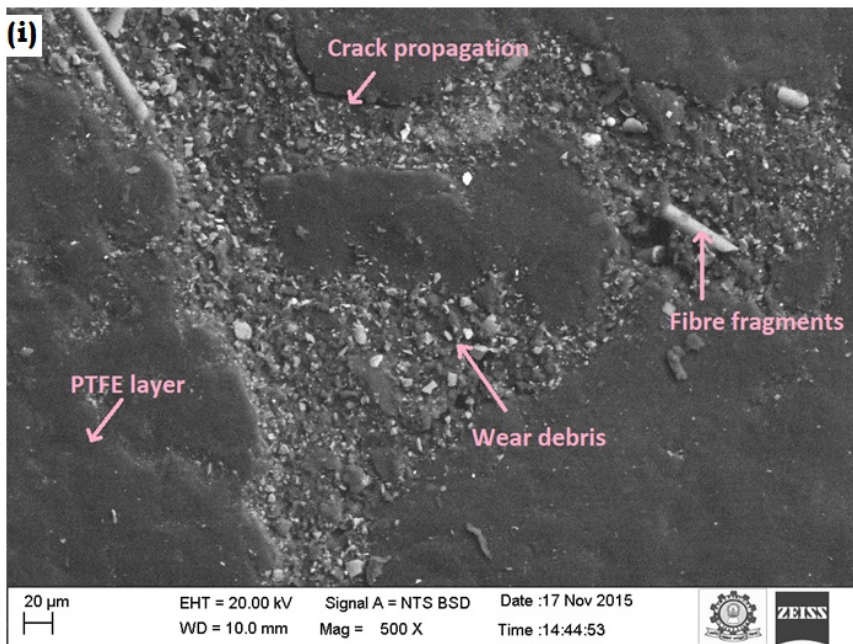


Figure 16a. SEM micrograph of worn out sample of PTFE coated BFVEC (i) top surface (ii) edge surface

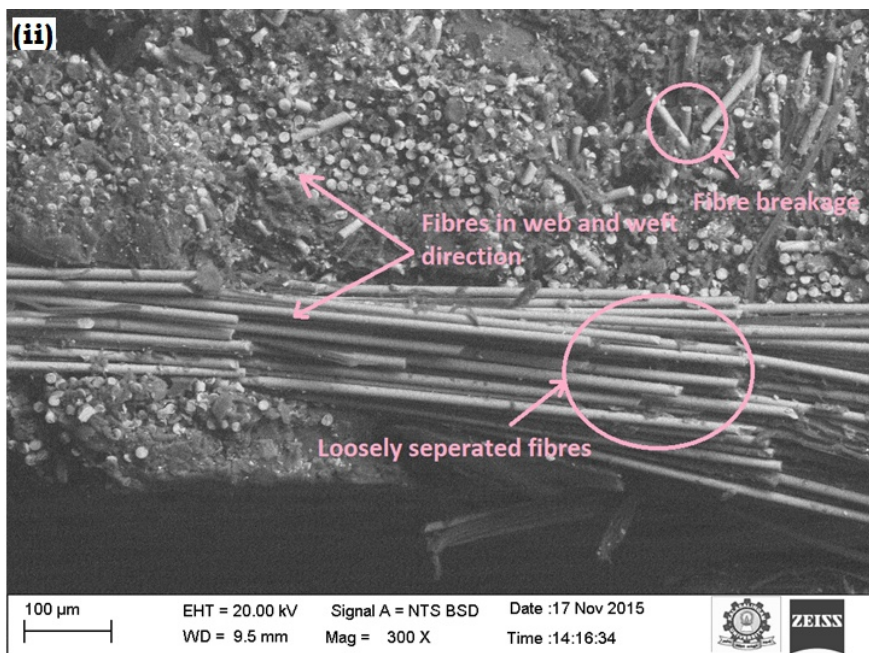


Figure 16b. SEM micrograph of worn out sample of PTFE coated BFVEC (i) top surface (ii) edge surface

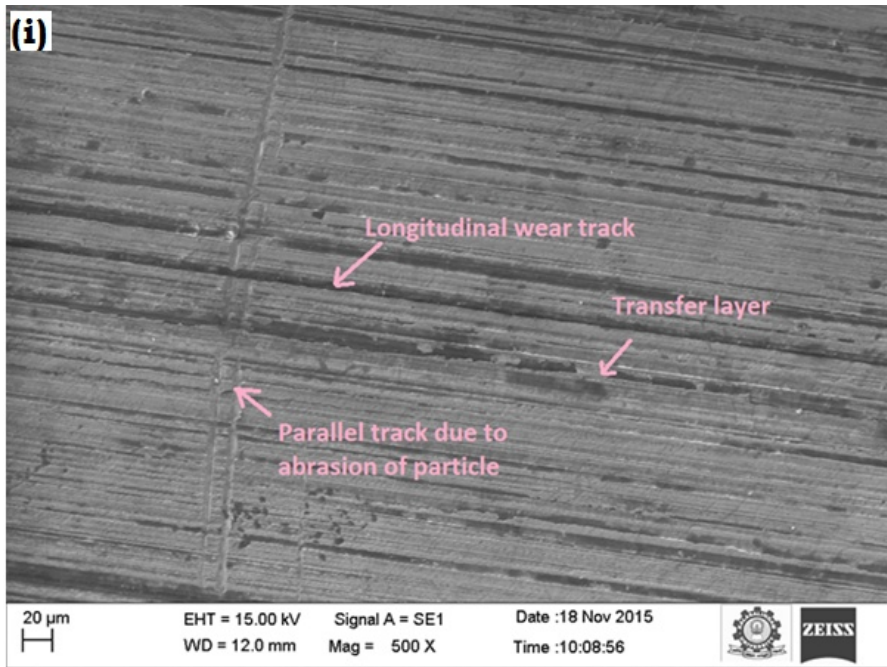


Figure 16c. SEM micrograph of counter face material after wear (i) at lower magnification (X 500) (ii) at higher magnification (X 2000).

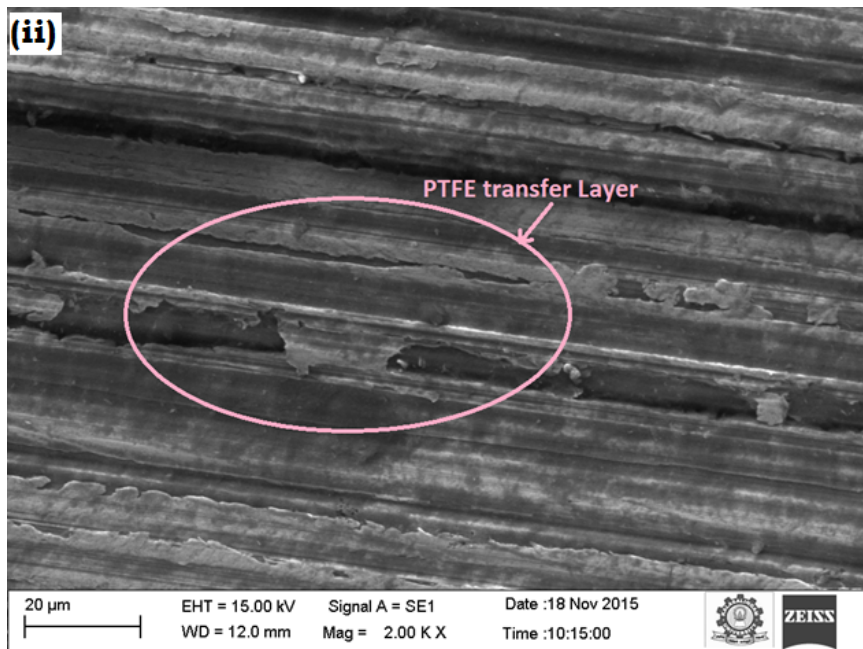


Figure 16d. SEM micrograph of counter face material after wear (i) at lower magnification (X 500) (ii) at higher magnification ( X 2000).

## Conclusions

The present research attempts to explore the likelihood of using eco-friendly fibers as reinforcement in tribological components. In this background, a novel material design was used where better tribological characteristics were observed without losing the mechanical strength. The following conclusions were drawn from the novel eco-friendly PTFE mono layered basalt fibre vinyl-ester composite:

- Regarding the mechanical properties an increase in flexural strength and compressive strength by 41 % and 60 % respectively was observed for the layered composite.
- The tensile strength, tensile modulus and the impact strength of the layered composites were comparable with the non-layered composites. However the Shore D hardness decreased by 11%.
- The thermal conductivity was improved significantly by 42% and this might have increased heat transfer capability. The measured contact temperature from the sub-surface ranges between 85-90°C and hence the operational regime of the novel composite is within this range.
- For the Novel composite a stable friction characteristics was clearly achieved in the steady state which implies the novel material suitable for tribological components such as plain bearings, sliders, hinges etc.
- The friction enhancer which is the transfer layer is clearly formed on the steel counter face.

On the whole the novel layered composite possessed superior mechanical characteristics when compared to the conventional non-layered materials. Moreover the friction values of 0.19 and 0.12 for the static and dynamic coefficient of friction are significantly lower than the values reported in the literature and hence the material is more suitable to be used in tribological composites.

# **Dynamic mechanical and thermogravimetric analysis of PTFE blended tailor made textile woven basalt/vinyl ester composite on tribological characteristics**

Karthikeyan SUBRAMANIAN<sup>1</sup>, Rajini NAGARAJAN<sup>1</sup>,  
Jacob SUKUMARAN<sup>2</sup>, Patrick De BAETS<sup>2</sup>, Gábor KALÁCSKA<sup>3</sup>

<sup>1</sup>Centre for Composite Materials, Department of Mechanical Engineering,  
Kalasalingam University, Krishnankoil, Tamilnadu, India – 626126.

<sup>2</sup>Department of Mechanical Construction and Production, Ghent University,  
Technologiepark, Zwijnaarde 903, Ghent, Belgium.

<sup>3</sup>Institute for Mechanical Engineering Technology, Szent István University,  
Páter K. u. 1., Gödöllő, H-2100, Hungary,

## **Abstract**

In this work, the authors prepared basalt/vinyl ester tailor made green composites with uncoated and Polytetrafluoroethylene (PTFE) coated basalt woven fiber. These composites were subjected to dynamic mechanical analysis (DMA) and Thermo gravimetric analysis (TGA). The DMA revealed that the dynamic mechanical properties of the composites were enhanced when the fillers were coated with PTFE at low temperature region. The TGA indicated a three stage degradation for the composites made with PTFE coated filler. The improved storage modulus, loss modulus and loss tangent manifested negative correlation with the friction characteristic in glassy region. Further the SEM coupled EDX spectral analysis was performed to understand the formation of transfer layer in counter surface.

## **Keywords**

Basalt woven fiber; PTFE coated composite; DMA; thermal decomposition

## **1. Introduction**

Advancement of Polymer bearing technology is identified as suitable alternative to the classical metal bearings used in the field of many engineering applications. Besides, the addition of reinforcement in the form of fillers, particulates and fibers were found to enhance the structural properties in addition to tribological performance. However, in polymer bearing industries the material failure occurs mainly due to the temperature raise at the interacting surfaces. From this, one can easily identify that the correlation exists between the temperature dependent material properties and the outcome of tribological

process. Accordingly, many studies have been carried out using polymer composites and their temperature dependent characteristics such as Dynamic Mechanical Analysis (DMA) and Thermo gravimetric analysis (TGA) with the combination of tribological properties. Moreover, the results of analysis revealed that the addition of reinforcements enhance the visco-elastic properties of polymers through rigid link mechanism. And also, they found that the smaller particle size exhibited the increased modulus due to better interaction between matrix and filler in large surface area.

Polytetrafluoroethylene (PTFE) is a widely used solid tribo-lubricant which exhibits better tribological performances which is used as bulk and surface layered reinforcement in different polymer systems. The addition of PTFE as bulk in nylon matrix showed enhanced thermal characteristics such as dynamic mechanical and thermo gravimetric analysis. However, the influence of visco elastic material properties of PTFE coated fiber reinforced composite with respect to varying temperature was not found explicitly. Further, this present work also describes the novel data processing approach to the tribological characteristics with the aid of Dewesoft data acquisition system. Moreover, the interaction of friction and wear characteristics curves with the temperature dependent elastic properties and mass loss through thermo gravimetric analysis were analyzed.

## **2. Fabrication and measurement techniques**

### *PTFE coated basalt/vinyl ester composite*

Both uncoated and PTFE coated basalt/vinyl ester composites were fabricated using hand layup techniques. The tailor made coated composites were fabricated based on tribologically optimized condition (PTFE 10 wt. %). The detailed step by step process of fabrication methodology was described in our previous work.

### *Measurements of DMA and TGA*

Dynamic mechanical properties such as the storage modulus ( $E'$ ), loss modulus ( $E''$ ) and mechanical damping parameter ( $\tan \delta$ ) were measured by using the SII EXSTAR DMS 6100 – DMA instrument. The rectangular composite specimens of size 50 X 10 X 3 mm<sup>3</sup> were used. The test was conducted by using a 3-point bending mode. The samples were tested in a nitrogen atmosphere in a fixed frequency mode of 20 Hz and a heating rate of 2 °C/min. The measurements were taken over a temperature range of 20 °C-300 °C.

### *Thermogravimetric analysis*

The thermal stability of the uncoated and PTFE coated basalt/vinyl ester composites was evaluated, using the SII EXSTAR TG 6000 module. About 3 - 6 mg of the sample was subjected to dynamic TGA scans at an increased heating

rate of 5 °C/min in the temperature range of ambient to 900 °C in N<sub>2</sub> atmosphere. The TG curves were analyzed as percentage of weight loss, as a function of temperature.

#### *Tribological evaluation*

Both wear and friction data was measured with the help of DEWEsoft data acquisition system at the higher sampling rate of 20 kHz. The tribological testing parameters and conditions were discussed in our previous publications. For the friction data processing, the NI-Lab VIEW program was used. The algorithm for computing the static coefficient of friction is divided into three parts. Accordingly, in the first part the entire data was segmented into number of subsections using the facility available in the DEWESoft software. Secondly, the maximum and minimum points of friction curve in every cycle were picked. Similarly, the concept of interpolation method in Lab VIEW software was used for the first time for data processing of dynamic coefficient of friction.

#### *Microscopic study*

SEM and their EDX spectra were also recorded using Zeiss 018 SEM model for pristine and worn out counter surface material to understand morphological changes and the presence of element over the counter surface.

### **3. Results and discussions**

#### *Dynamic mechanical properties*

The DMA is an analyser where a small deformation is applied to a sample in a cyclic manner. This allows the material's response to stress, temperature, frequency and other values to be studied. The term is also used to refer to the analyser that performs the test. The temperature dependence mechanical properties such as storage modulus, loss modulus and damping factor of uncoated and PTFE coated basalt/vinyl ester composites are shown in Fig.1 (a-b).

A similar kind of modulus pattern was observed for both the composites throughout the testing temperature range. However, a higher storage modulus was obtained for PTFE coated composite in the glassy region (<95 °C) since the PTFE particle deposition does not allow the molecular mobility in the polymer matrix in the lower temperature range. Hence, the accumulation of temperature takes place in each localized region until the molecular oscillation existence starts. Beyond a certain limit, the storage modulus of both composites was mapped with each other until the maximum experimental temperature (Fig.1a). Once the interaction of PTFE and matrix got separated by the temperature degradation, it behaves like an unfilled composite. During the temperature rise, the PTFE particle tends to oscillate and it increases the friction force at molecular level and exploit in the form of heat energy. Hence, in the lower temperature region, the loss modulus was found to be higher for coated

composite (Fig.1b). Although, after a certain temperature a steady state modulus value was observed in both  $E'$  and  $E''$  conditions. It is noteworthy that the change in modulus was not possible to appear while the contact temperature reached beyond 95 °C. It is a required property expected to have an all the bearing materials working at higher load with low velocity. Similarly, a small shift in peak value was noticed in the damping characteristic curve and it implies that the  $T_g$  value of coated composite was slightly higher than for the uncoated composites. As expected, a marginal increase in damping value was found in the case of coated composites (Fig.1c).

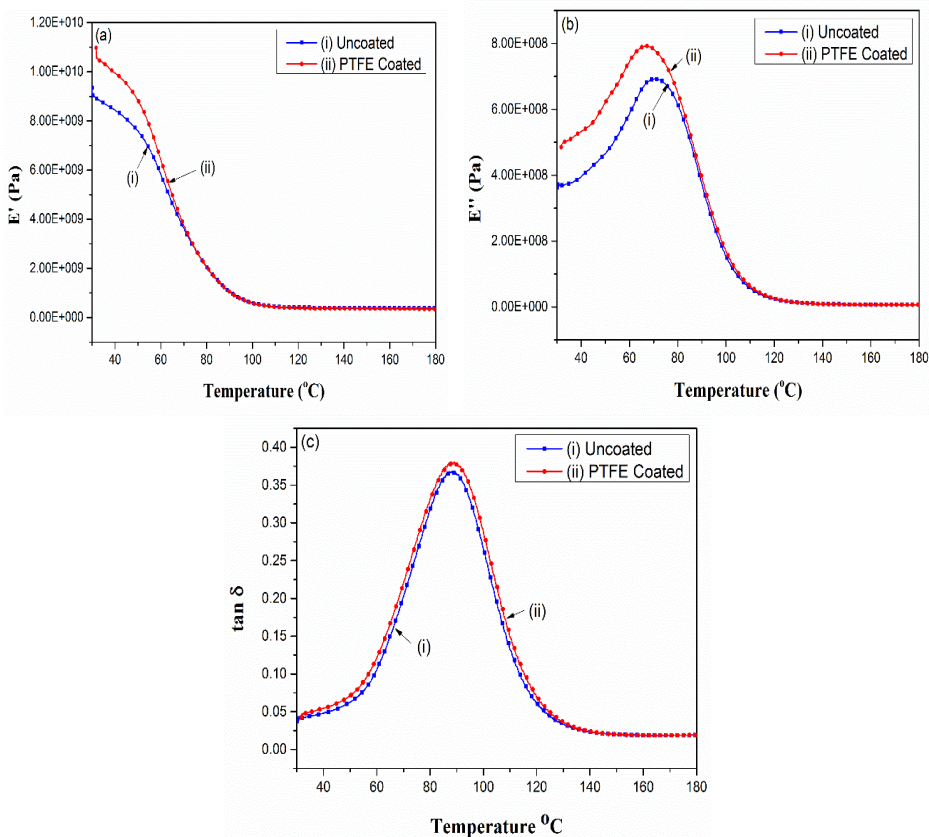


Figure 1. (a) Storage modulus, (b) Loss Modulus and (c)  $\tan \delta$  of uncoated and PTFE coated basalt/vinyl ester composites

### Thermo gravimetric Analysis

The thermal stability of uncoated and PTFE coated basalt fibers/vinyl ester composite under before wear (BW) and after wear (AF) conditions was studied using their primary thermograms shown in Fig.2a. In addition, the derivative

thermograms (DTG) for the same are also presented in Fig. 2b. From Fig. 2b, it can be seen that in the case of the composite with PTFE coated basalt exhibited three stages of mass loss either in the case of both before wear and after wear conditions. However, only the two stage mass loss was observed in the case of the composite with uncoated basalt fibers.

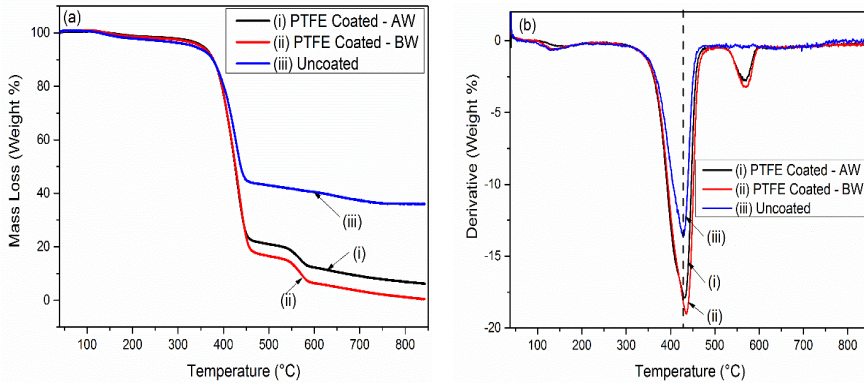


Figure 2. (a) Primary and (b) Derivative thermograms of uncoated and PTFE coated basalt/vinyl ester composite

During the initial stage of heating only a minimum mass loss was observed in the range of 30.8 °C to 140 °C due to the loss of absorbed moisture and other volatiles if any. Generally, this type of behavior is expected in all types of polymer based composites. From Fig. 2a, the initial decomposition of 10 % mass loss occurred in the 150 °C to 350 °C temperature range for the composite with uncoated basalt fibers and composites with PTFE coated reinforcement under before and after wear conditions. At 50 % of mass loss, the composite with uncoated basalt fibers possessed a slightly higher degradation temperature compared to PTFE coated composites. Thereafter, almost the constant thermogram plot was observed and it showed higher thermal stability in the case of composite with uncoated basalt fibers. It could be due to the presence of basalt fiber particles in the samples after the degradation of vinyl ester polymer. Hence, the degradation temperature has shown higher value in the case of uncoated composites. Further, the PTFE coated composite showed the third stage mass loss between the temperatures of 500 °C to 600 °C as the PTFE coating could degrade with the release of hydrofluoric acid at temperatures over 400 °C. Besides, the peaks were also found to appear in the temperature range of 500 °C to 600 °C in the derivative thermograms shown in Fig. 2b. Among the peaks in the 500 °C to 600 °C, the weight loss for the composite with PTFE coated basalt fiber under worn condition was less than that for the composites before wearing. This may be due to the removal of PTFE coating on the fibers present on the surface of the composites due to wearing out. These observations indicate that the thermal stability of the composites with uncoated basalt fiber and the composite with PTFE coated basalt fiber under wearing out condition was higher

than that of the composite with PTFE coated basalt fiber before wearing out condition.

### DMA Vs Friction coefficients

Fig.3 shows the static and dynamic coefficient of friction (COF) for varying contact temperature. The magnitude of dynamic COF was lower than the static COF throughout the testing period as seen in Fig 3(a-b). Since the dynamic COF was measured during the running condition where the surface morphology at contact surface was found to keep on changing. Similarly, the static COF was measured only in the starting of impending motion at the end of the every stroke. Though, the testing condition (load, boundary condition, environment, etc.) of DMA and tribological tests were different, the behavior of material property was compared only in the aspect of varying temperature.

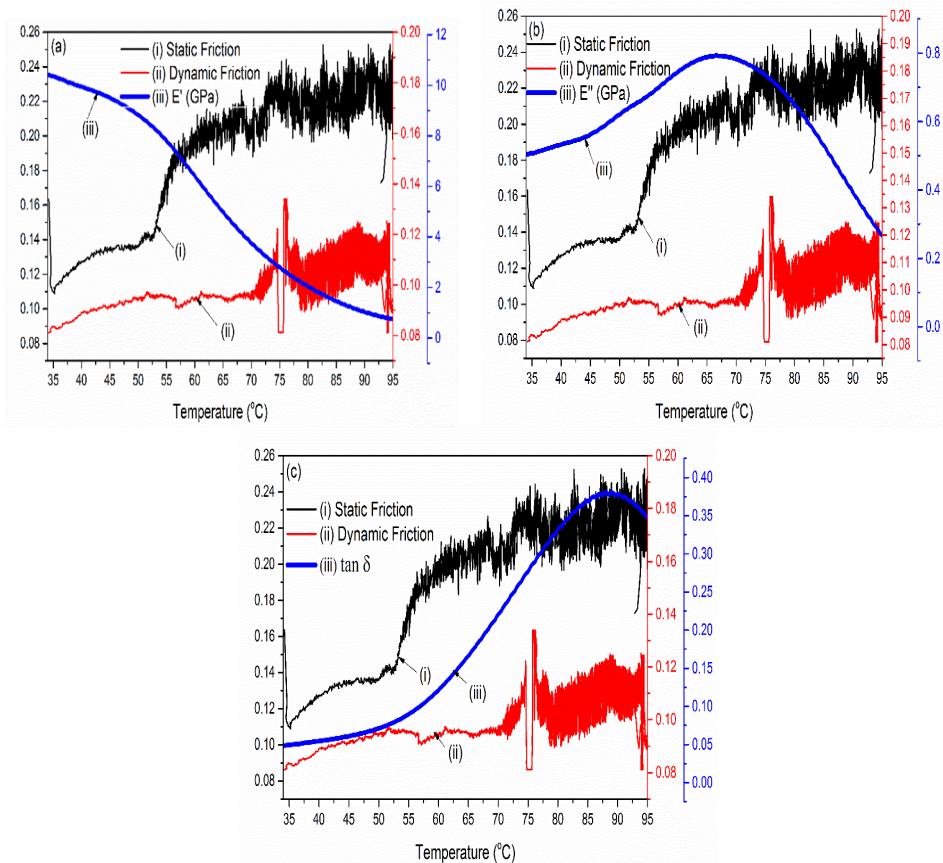


Figure 3. Comparison of (a) Storage modulus Vs static and dynamic COF  
(b) Loss modulus Vs static and dynamic COF  
(c) Damping factor Vs static and dynamic COF

Accordingly, Fig.3 (a-b) shows the correlation of storage modulus, loss modulus and  $\tan \delta$  with static and dynamic coefficient of friction. It can be clearly seen from the Fig.3a that the increasing COF was observed in the running in period while the storage modulus was decreased. After reaching the steady state condition, the friction curves seem to appear in constant pattern even at elevated contact temperature. However, the modulus was found to decrease continuously after the glassy region. In the case of loss modulus up to running in period, both friction and modulus were simultaneously increased. After the transition period, the loss modulus was found to decrease. The process of interfacial debonding between PTFE and VE matrix due to the increasing temperature could lead to the molecular mobility and in turn reduce the loss modulus also. Consequently, the depletion of PTFE layer can formulate the transfer layer over the counter face material. A linearly increased trend was observed in the case of damping factor ( $\tan \delta$ ) during the transition period of “running in” to “steady state” period. Thereafter, a sudden increase in value of  $\tan \delta$  was noticed in the steady state condition of friction. It implies that the rate of molecular displacement was not enough to break the polymer cross linking density. Hence, the energy dissipation was increased significantly due to the constrained atoms mobility. Once the existence of amorphous phase appeared with the increasing heat source, damping values were reduced.

#### TGA Vs wear

Fig 4 shows the mass loss and wear from thermo gravimetric analysis and friction test respectively. Even though, both of the curves were recorded in different conditions, the behavior of material seemed to be similar. Accordingly, the slop at any point in either curve exhibits very closer value. It also ensures that the change in behavior of polymeric materials mainly depends on the effect of varying temperature rather than on testing conditions.

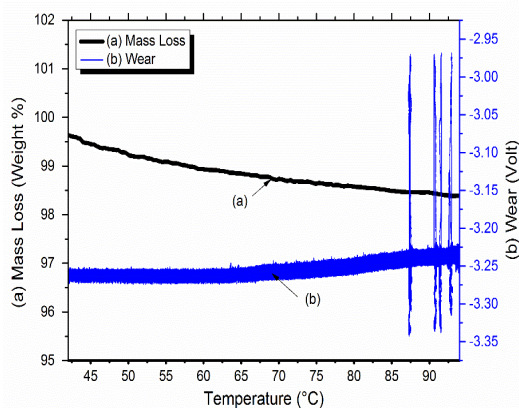


Figure 4. Comparison of mass loss and wear data with respect to change in temperature

### Morphological analysis of counter face material

SEM-EDX elemental analysis was performed on pure chromium steel counter face material prior to friction test as well as worn out counter face material and are shown in Fig. 5 (a-d). Before the friction test, the surface of the chromium steel was seemed to be clean and smooth as seen in Fig.5a. After the friction test, the formation of thin coated surface was noticed in the morphological analysis of SEM as shown in the Fig.5. To understand the chemical composition of surface at before and after wear conditions, the EDX elemental analysis was also performed on counter face material. Accordingly, the chemical substances such as Fe, Cr and C were found to be dominantly present in the virgin counter material (Fig.5c) before the friction test. On the other hand, for the other case the mass content of fluorine was increased (Fig.5d) which indicates that PTFE was transferred to the surface of the chromium steel during the friction test. The percentage of elements obtained from the EDX analysis is presented in Table 1 for both neat and worn out counter surface materials. It might have occurred due to the depletion of PTFE at higher contact temperature, so that the mobility of PTFE particle in viscous polymer matrix led to the transfer film and attributed to the lowering of friction at contact surface.

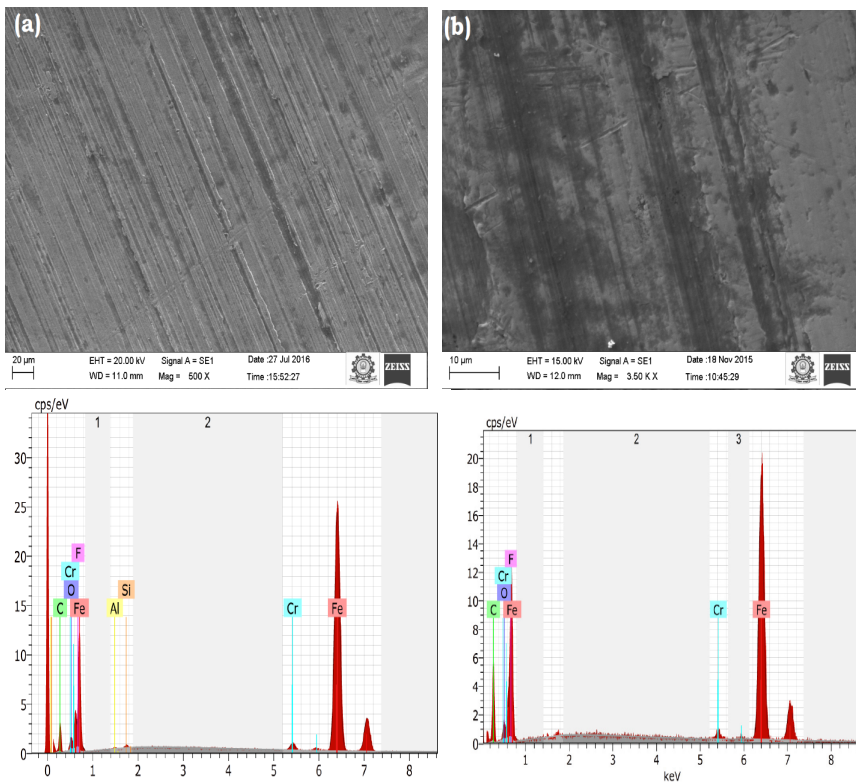


Figure 5. SEM micrographs and EDX spectra of the friction surface for 100 chromium steel (a) before and (b) after the friction test (load: 10kN, sliding speed: 50 mm/s).

Table 1. Composition of counter material before and after wear by EDX analysis

Composition	Counter plate Before Wear		Counter plate After wear	
	norm. C [wt %]	Atom. C [wt %]	norm. C [wt %]	Atom. C [wt %]
Iron	82.84	53.46	63.53	30.48
Carbon	13.53	40.59	22.63	50.49
Oxygen	1.69	3.81	1.56	2.61
Chromium	1.08	0.75	1.02	0.53
Fluorine	0.44	0.83	11.27	15.89

## Conclusion

The PTFE layered composites had shown significant improvement in DMA properties at the glassy region. The increase in these properties was due to the restriction of molecular mobility by the interaction between PTFE and vinyl ester matrix. In the case of thermal properties, increasing thermal stability was found for the uncoated composites and it could be due to the presence of fiber debris in the sample. The third stage thermal degradation in the coated composites exhibits the volatilization of fluorine content present in the PTFE. A steady state friction curve was obtained while the modulus was getting down with increasing temperature. It implies that the weakening of stiffness in the PTFE blended composites formulated the transfer layer coating on the counter surface of the material. SEM coupled EDX elemental analysis confirmed the transfer layer formation through the change in morphology and increasing fluorine content in the counter plate material after the wear testing.

# **Analysis of production and physical distribution of baked products at Andana Pan Bakery – Baia Mare, Romania**

Adrian Dan POP, Nicolae Stelian UNGUREANU  
Technical University of Cluj-Napoca, North University Center of Baia Mare

## **Abstract**

Bakery industry has no sufficient scientific research in order to support a real time decisional process of the managers who are most of the time also involved in the production process and all their knowledge is based on practical experience. Our purpose was to conduct an observatory analysis on Andana Pan Bakery from Baia Mare, Romania, and based on theoretical notions regarding the supply chain management was analysed step by step the production and distribution strategy and physical process. Our results indicate that bakery production and distribution is facing high challenges and high risks of low performance and profitability and a clear algorithm to correlate the distribution with production process and improve the distribution management, lowering the costs and increasing the profits would be a perfect tool for any small and medium size bakery

## **Keywords**

production, physical distribution, baked products, supply chain management

## **1. Introduction**

“Egyptians had invented leavened bread as well as the bakery. They established a hierarchy of breads: wheat for the rich, barley for the middle class, and sorghum for the poor. Centuries later, the English Parliament enacted a series of laws that limited the profits bakers could make from bread and required that every baker put his mark on his loaves. And that was the beginning of the trademark.” (Lynn, 2012)

Andana Pan bakery is a small-medium size bakery in Maramures area of North West of Romania, founded in 1996 and managed as a family business and it's development over the last 20 years was constant even if the Romanian economy had a difficult transition period and in the recent years a global crisis was manifesting in Romanian economy very strongly too. Andana Pan has a huge variety of products like bread, cookies, fancy cakes, donuts, pretzels, pies, and may other local traditional products and benefits from a good image on the local market, a strong brand and a vast network of owned food stores but as most

of the bakeries in Romania, it's management is mainly based on the experience of the responsible production manager. As a result, production planning happens more or less "chaotic", which often results in "bottle-necks", deficient dimensioning, ineffective staff allocation and operation problems. The aforementioned points cause a production environment in which factories are not able to achieve the best possible economical and ecological performance. (Hecker, Hussein, & Becker, 2010)

When started this research we had in mind some of the general aspects of the panification industry but we found out that the domain is mostly unexplored and distribution is one of the key aspects left out.

By the end of this research we build an affordable tool for small-medium business owners in bakery industry to correlate the production and distribution processes and maximize their profits by lowering the distribution costs and increasing the efficiency.

Based on theoretical notions regarding distribution and production management in general we conducted an exploratory research with the purpose to identify what are the most relevant aspects of the production and distribution process, the specificity of the bakery industry in few easy to follow stages.

## **2. Ingredients and production supplies acquisition**

“The production of bakery goods is strictly time sensitive due to the complex biochemical processes during dough fermentation, which leads to special requirements for production planning and scheduling.

Instead of mathematical methods scheduling is often completely based on the practical experience of the responsible employees in bakeries. This, sometimes inconsiderate scheduling approach often leads to sub-optimal performance of companies.” (Hecker F. , Hussein, Paquet-Durand, Hussein, & Becker, 2013)

This is also the case at Andana Pan Bakery in Baia Mare, Romania, where due to their own experience, among the six factors that influence the most the quality of fresh baked products, the quality of ingredients and production supplies is the most are vital in order to keep the constant quality of the products they put on the market. Without a constant and high quality of the raw materials, the output can't be expected to be at the requested standard.

Andana Pan states very clear from beginning to all its suppliers the demand for high quality ingredients and it's informing all the potential suppliers using an informative letter with precise specification of each product they intend to order. Along with the written requests, to the new partners and for the new products, the company is asking that the supplier will bring their own technicians and ingredients and test them in the factory together with the employees and equipment of the bakery. This kind of actions are also solicited by the new suppliers in order build trust with their customers.

All products must be delivered to the bakery storage directly, Andana Pan does not agree to develop relations with deposit or stores.

Based on experience, Andana Pan refuses to contract big quantities or unique supplier for any of the main raw materials used in production and it's always open for new ingredients, new technologies and is organizing frequent simulations and tests with new ingredients and new bakery products, and the only goal is to increase the quality of the products with the lowest costs possible.

"The challenging advantage of economic companies owed to innovation is an undisputed matter." (Drenta, Lobontiu, & Lobontiu, 2015)

Sometimes, Andana Pan is the one initiating the process to analyze the Supply Companies present on the market but more often, due to the image and national reputation of the local bakery, a large variety of suppliers are initiating the contact with Andana Pan, aiming for a strong partner in the area even if they haven't started the distribution in Baia Mare yet. Having in consideration the geographically position of the city of Baia Mare, the bakery has offers from Hungarian and Ukrainian companies.

The need for different types of raw-materials is established by the person responsible with acquisition, always with in the presence of the owner and the manager of the bakery. They choose to buy higher quantities for most of the ingredients as their valability term is not very short.

As an example, in order to produce the regular white bread, only 4 ingredients are needed including water: white flour(wheat flour), yeast and salt.

Water supply is directly from the city pipeline due to it's well known quality of mountain springs.

There are only two yeast suppliers in Romania and both of them represent international brands: Fala and Pakmaya. For short period of time, both types of yeast were used in the production but in the end a decision was made in favor of Fala Yeast Company. Due to special conditions required by yeast, it is delivered 3 times/week, every second working day.

Iodized salt is the one used in food production and the main suppliers are from Dej salt mine or the imported salt from Ukraine. The bakery storage allows a maximum of 500kg of salt at once.

The wheat flour suppliers are based as close to the factory as possible but the decision is made according to their production capacity and delivery requirements from Andana Pan. For short periods of time, Andana Pan did import wheat flour directly from Hungary, as neighbor country, very well developed on this sector of agriculture and cereal processing. "The impact of food transport can be partly offset if food is sourced locally or within a determined radius of the consumer. However, there are trade-offs to consider: imported food that has been produced more sustainably than the food available locally is an example." (Estrada-Flores & Larsen, 2010)

After choosing the right ingredients providers that can deliver the demanded quantities of contracted products, price negotiation is one of the most important part before closing the deal and signing the contracts. Andana Pan is very careful on it's image in front of the customers but also in the relation with it's suppliers and there were no situations without a mutual solution with it's partners.

### 3. Production process

In order to ensure the management quality, Andana Pan implemented an international standard for Food safety management system, a requirement for any organization in the food chain, ISO22000:2005.

Andana Pan fulfills the key criteria that are needed in order to obtain high quality products with minimum costs but all its strategy is based on experience and responsible management from its owners.

Before production starts, every Sunday evening, the company management is filling the product documentation, the technological form of each product and follows the production instructions, adjustment and control.

The technology that is now in place in Andana Pan bakery is 10 years old in average and the employees are highly experienced due to their interaction with the technology and production process.

In our analysis we followed the production process for this example:

Code: 6422608000017

Name on the market: White sliced bread 0,65 Kg

Ingredients: white flour (wheat flour), yeast, and water

Weight: 0,65 kg

*Flushing the flour and dosing of feedstocks.* The wheat flour used in this process is Type 550, Type 650 or mixt. To produce a quantity of 230 breads, 100 kg of flour will be mixed with 1.2 kg of salt and 2 kg of yeast and 55 liters of water on right temperature.

*Mixing process.* The mixing process of all ingredients is one of the most important stages during the whole process. The capacity of the mixer used in production is of 250 kg. There are two mixing stages: 1st speed stage is used for 3 minutes at the beginning of the process and then the mixer speeds up in the 2nd stage where it takes about 7 minutes. Before moving to next production stages, the dough must ferment for 10 minutes and mix again for 1 minute, right before moving it on the next machine.

*Portioning.* Portioning of the dough is done automatically by a volumetric divisor. Because after the mixing the dough is continuously fermenting, it is mandatory that the portioning is done exactly after the last step, because the volume of the dough is growing when is fermenting and the division would not be equal.

*Modeling round.* For this operation, the divisor is connected to a conic modeling machinery that transforming the dough in a round piece and goes on the working table where it has to wait around 13 minutes before the next step.

*Final modeling.* This operation is done manual by bakers working in the factory. They model each piece of round dough into a loaf shaped bread and then they put it on a conveyor belt on a bakery cart with 7-8 shelves. They must move quickly and finish all in the same time so all the products ferment and grow uniform. When the whole cart of modeled loafs is done, it will be deposited in a fermenting room.

*Fermentation.* Fermentation is done in a temperature and humidity controlled room where the temperature must be around 35-37 Celsius degrees and the humidity around 75 -77%. The fermentation time is about 18-20 minutes.

*Baking bread.* Baking time is about 28 minutes and it must be done at 220 Celsius degrees.

*Slicing and packaging.* For this product, the slicing and packaging is only one operation and it's done in the same time after the bread was baked and had at least 6 hours in a special room to cool.

#### **4. Marking, labeling, packaging, and storage of goods**

*Marking.* Andana Pan is a trademark and is registered in the Romanian Office for Inventions and Trademark. Also, the company has do product brands. Franzela Fermecata(The Magic Loaf) is the trademark for bakery products and Piticii lui Andana(Andana's Dwarves) is the trademark for all sweet goods. The sliced bread is packed in a plastic envelope, already printed with the Andana Pan trademark.

Special containers are used to pack 7 loafs of bread and prepare them for storage and transportation.

*Labeling.* Types of Information on Bakery Labels: Common name of the product (e.g. “Muffin”, “Croissant”, “Bagel”, etc.), Ingredients used, from the heaviest to the lightest ingredient, Nutrition facts, Net weight, Name and address of the manufacturer

*Packaging.* In order to ensure temporary physical, chemical, mechanical, biological protection and in order to maintain the quality and integrity of the products during transportation, handling or storage, Andana Pan uses individual packages of stretch film, polypropylene film and polyethylene foil. They are placed manually on the products to cover their surface.

For storage, transport and handling, packaged products are placed in plastic shuttles, easy to use. They are 30 cm wide, 30 cm high and 50 cm long. Their size and usage influence a lot the distribution process.

#### **5. Marketing, sale, distribution and after-sale customer service**

On small business level is not a common approach but marketing performance represents a "complex concept which sparked a considerable wave of interest in the last decade among both academicians and practitioners. Despite the numerous studies and researches dedicated to marketing performance, marketing specialists proposed a series of divergent points of view, which created more confusion around this subject rather than contributed to its clarification." (Bacali & Sava, 2013) This is how the analyzed bakery marketing strategy was developed:

The competition from hypermarkets that started in-store bakeries, almost all "bread only" bakeries disappeared from the local market or they had to develop a

more industrial concept of bakery and increase the distribution routes over 250 km.

Andana Pan decided that in addition to selling bread, to offer cakes, scones, bagels, coffee drinks and sandwiches in its own shops keeping the distribution of regular bread for the retail customers that are spread all over the city and 25-30 km around the city.

While a bakery tries to develop a particularly bakery concept, it has to keep in mind that is needed something to differentiate themselves from other bakeries in town.

Market survey is one of the most important ongoing activities. "People strongly prefer some breads over others. Age, income level, and ethnic background of your market are important considerations when deciding what breads and other items to offer." (Lynn, 2012)

Due to its own strategy and company ownership decision, Andana Pan does not deliver to any supermarket and hypermarkets and has its focus on small proximity stores.

The most important role in sales for Andana Pan bakery its on the distribution driver and sales department based in the factory office. The drivers are in contact with all the potential customers and they take the delivery orders for the next day directly from the market. By phone, e-mail or any other means, the office workers are organizing the deliveries according to the closest existent route.

The entire process is experience based and very approximate. There was never applied a study or a simulation model in order to verify the efficiency and profitability of each route/product/customer or if there is a correlation between them and production and how it could be improved.

Andana Pan also sale the products directly to the final consumers by using various ways as: home delivery, phone orders and direct pick-ups, and its own chain of local food stores.

Due to this variety of options and by keeping the standards very high, Andana Pan has a very strict price policy and is not very influenced by the other bakery products on the market.

"In predominantly service and information-based economies, the pivotal role food plays in the maintenance of life has arguably become neglected as an object of ethical and political contemplation. We often fail to realize that the incarceration of food by the commodity form degrades the food object itself as well as guaranteeing continued dependency on the wage. In a generalized commodity society, labor power is the only thing a person has to sell in order to buy her bread. This leaves us vulnerable in the event of an environmental crisis because we do not have direct access to food sources." (Watters, 2013) Andana Pan argues that the most valuable asset a person has to sell is its time and the company policy is to encourage home made products, offering its customers support and examples of homemade recipes but when it becomes too much time consuming, our offer is to save time by choosing Andana Pan fresh baked products.

## Conclusion

Taking in consideration the high variety of products Andana Pan has in production now, that were not part of this analysis, a similar attitude in its management may lead to sub-optimal performance of the company and a clear algorithm to correlate the distribution with production process and improve the distribution management, lowering the costs and increasing the profits would be a perfect tool for any small and medium size bakery.

## References

- [1] Bacali, L., & Sava, A. (2013). Assessment of the Importance of Market Performance Indicators for the Firms from the National TOP of Romania. *Actual Problems of Economics*, 236-245.
- [2] Drenta, R., Lobontiu, M., & Lobontiu, G. (2015). Difussion of Technology in SMEs. *Managing Intellectual Capital and Innovation for Sustainable and Inclusive Society*, Bari.
- [3] Estrada-Flores, S., & Larsen, K. (2010). *Best Practice Food Distribution Systems*. Sydney: Food Chain Intelligence.
- [4] Hecker, F., Hussein, W., & Becker, T. (2010). Analysis and Optimization of a Bakery Production Line using ARENA. *International Journal of Simulation Modelling*, 208-216.
- [5] Hecker, F., Hussein, W., Paquet-Durand, O., Hussein, M., & Becker, T. (2013). A case study on using evolutionary algorithms to optimize bakery. *Expert Systems with Applications*, 6837–6847.
- [6] Lynn, J. (2012). *Start Your Own Restaurant and More*. Entrepreneur Press.
- [7] Watters, S. M. (2013). *Food Ontology and Distribution: Ethical Perception and the Food Object*. London: The School of Graduate and Postdoctoral Studies, The University of Western Ontario.

# **Evaluation of PID-P cascade control algorithm used in positioned pneumatic drives**

Eszter SÁRKÖZI, László FÖLDI

Institute for Mechanical Engineering Technology, Szent István University,  
Páter K. u. 1., Gödöllő, H-2100, Hungary,

## **Abstract**

Due to the non-linear behaviour positioning of a servopneumatic system needs complex solutions. In this paper a cascade structured control algorithm was designed for servopneumatic drives, which contains PID outer loop and P inner loop with pressure difference feedback. The applied tuning method was model-based genetic algorithm combined with gradient minimum search. During the evaluation of the cascade control algorithm the optimized positioning task and the system respond of changing force load were examined.

## **Keywords**

Servopneumatic drive, Position control, Cascade controller, Genetic algorithm

## **1. Introduction**

In order to achieve linear motion pneumatic, electromagnetic and hydraulic actuators are typically used. Due to their advantageous characteristics in position controlled applications the latter two are more widespread, but also pneumatic actuators have several advantages: they are fast, cheap, have an outstanding power-to-weight ratio, are easily maintainable and they do not contaminate the work piece. The challenge to the use of pneumatic drives in positioned applications is that due to piston friction and the characteristics of compressed gas flow their behaviour is non-linear. As a result their typical industrial use is such applications which require linear motions between end positions.

In the last decades such industrial controllers became available which have adequate computing capacity for real-time usage. With the use of them servopneumatic systems are also capable for positioning purposes. There are several control methods used (e.g. PID variations, fuzzy logic, sliding mode, status controller) in pneumatic positioning, in this work cascade-structured control algorithm is designed and evaluated.

## **2. Objectives**

In this article our main objective was to design, apply and evaluate cascade-structured control algorithm, which is proper for servopneumatic systems for

positioning purposes. To achieve our objectives the following steps were implemented:

- selection and assembling of examined servopneumatic system,
- design and application of the used cascade control method,
- mathematical modelling of the examined system,
- identification of the model,
- tuning of the controller with genetic algorithm,
- evaluation of behaviour of tuned systems.

### 3. Experimental apparatus

As an actuator a Festo DGPL-25-450-PPV-A-KF-B double acting rodless pneumatic cylinder of 450mm stroke length was applied. A Festo MLO-POT-0450-TLF analogue displacement encoder was attached to the cylinder, which has a 0,01 mm travel resolution. The applied encoder is a potentiometer which provides a voltage signal in proportion to the displacement. The used way-valve was an MPYE-5-1/8-LF-010-B 5/3 proportional valve (Fig. 1).

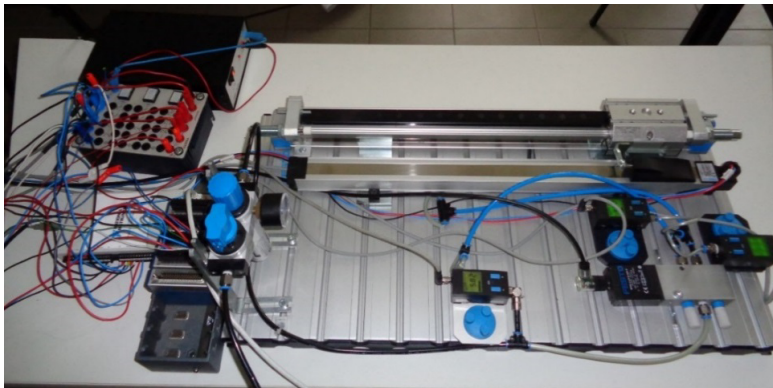


Figure 1. The experimental apparatus

The major elements of the electronic system are a 0-24 V direct current power supply (NI PS-15), an electronic instrument board (Festo), a NI CompactRIO™ (cRIO 9073) programmable automation controller and the already mentioned electro-pneumatic elements (displacement encoder, pressure sensors and proportional solenoid valve). The applied NI CompactRIO™ programmable automation controller is a modular system; out of its modules we used the analogue-to-digital converter (NI 9201). The proportional solenoid valve was controlled with the help of the analog output module (NI 9472). The communication between the CompactRIO™ and the computer was ensured by an Ethernet connection. The circuit diagram of the pneumatic positioning system is presented on Figure 2.

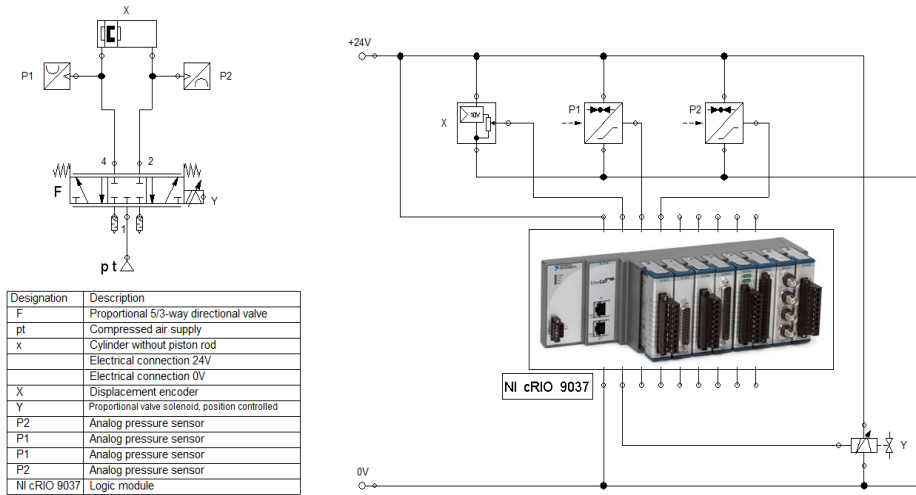


Figure 2. The pneumatic and electric circuit diagram

#### 4. Mathematical model of pneumatic linear drive system

The mathematical model of pneumatic linear drive system contains the model of the used cylinder and the proportional valve. To create mathematical model of double-acting pneumatic cylinder three main mathematical formulas have to be declared: the descriptive equation of the flow mass rate flowing through an orifice, the force equation and a vessel filling equation. During the deduction, the conservation laws (energy and mass), the ideal gas law and Newton 2nd law of motion were used. Some simplification were applied, as we consider the flowing gas as ideal gas, and neglecting the effect of the temperature change.

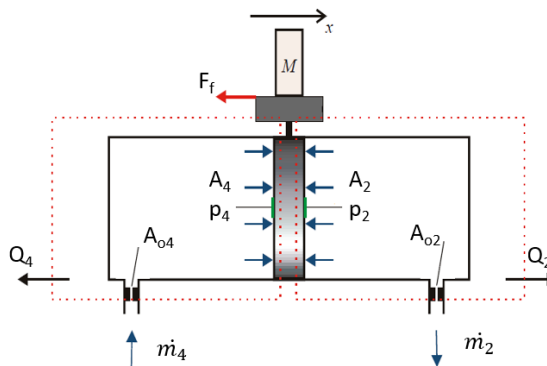


Figure 3. Outline of the cylinder

The mass flow rate through an orifice due to the pressure difference is:

$$\dot{m} = A_0 \cdot p_u \cdot \sqrt{\frac{2 \cdot \kappa}{(\kappa - 1) \cdot R \cdot T} \cdot \left( \left( \frac{p_d}{p_u} \right)^{\frac{2}{\kappa}} - \left( \frac{p_d}{p_u} \right)^{\frac{\kappa+1}{\kappa}} \right)} \quad (1)$$

The mass flow rate in function of  $p_d/p_u$  has a maximum value at  $\frac{p_d}{p_u} = \left( \frac{2}{\kappa + 1} \right)^{\frac{\kappa}{\kappa+1}} = 0.528$ , so this pressure ratio is called critical pressure ratio.

Below the critical pressure ratio the velocity of flow is maximal, and this velocity is the speed of the sound at exhausting temperature. Above the critical pressure ratio the velocity of flow is lower than the speed of sound, the value of it depends on the actual pressure ratio.

The force equation of the cylinder:

$$m \cdot \ddot{x} = A_4 \cdot p_4 - A_2 \cdot p_2 - F_f \cdot F_l \quad (2)$$

The container filling equation:

$$R \cdot T \cdot \dot{m} = V \cdot \dot{p} + \dot{V} \cdot p \quad (3)$$

In the Eq. 2, the friction force is defined with the use of Stribeck friction as follows:

$$F_f = \begin{cases} F_{str} & v \geq 0,001 m/s \\ \min(F_{br}, |\sum F_i|) \cdot \text{sign} F_i & v < 0,001 m/s \end{cases} \quad (4)$$

where  $F_i = p_4 \cdot A_4 - p_2 \cdot A_2 - F_l$ , and Stribeck friction is:

$$F_{Str} = (F_C + (F_{br} - F_C) \cdot \exp(-c_v \cdot |v|)) \cdot \text{sign}(v) + f \cdot v \quad (5)$$

The proportional directional control valve is the element that makes contact through pneumatics and electronic control. The opened cross-section of the valve is proportional with the input control signal, which is the setpoint (input) voltage (or current) signal ( $U_v$ ) of the actuating electromagnet. Considering the physical construction of 5/3 proportional valve it can be stated that the inlet and the outlet mass flow rates of the valve can be interpreted by the application of four orifices, which are the followings: two orifices ( $A_{1_4}$  and  $A_{1_2}$ ) between the supply port (1) and working ports (4, 2) and two orifices ( $A_{4_5}$  and  $A_{2_3}$ ) between the working

ports (4, 2) and the exhaust ports (5, 3). The mass flow through these orifices can be determined with use of Equation 1 and the proportional valve flow rate ( $q$  [%]) – setpoint voltage ( $U$  [V]) characteristics (Sárközi, Földi, 2016).

### 5. Applied control method: cascade controller

Cascade controller is one of the most popular structures for process control as it is a special architecture for dealing with disturbances. It is widespread in electric drives, as with the use of it not only position control can be achieved, but also speed and force (or angular speed and moment) control can be implemented. The cascade control structure is such a method where the control loop contains at least one another control loop within itself. The outer control loop supplies the setpoint to the inner loop, the control tasks should be shared between the embedded control loops (Gerhartz, 2001).

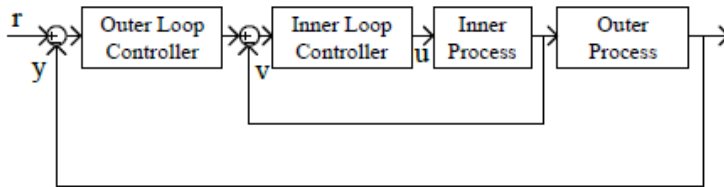


Figure 4. General block diagram of cascade control algorithm (Gerhartz, 2001)

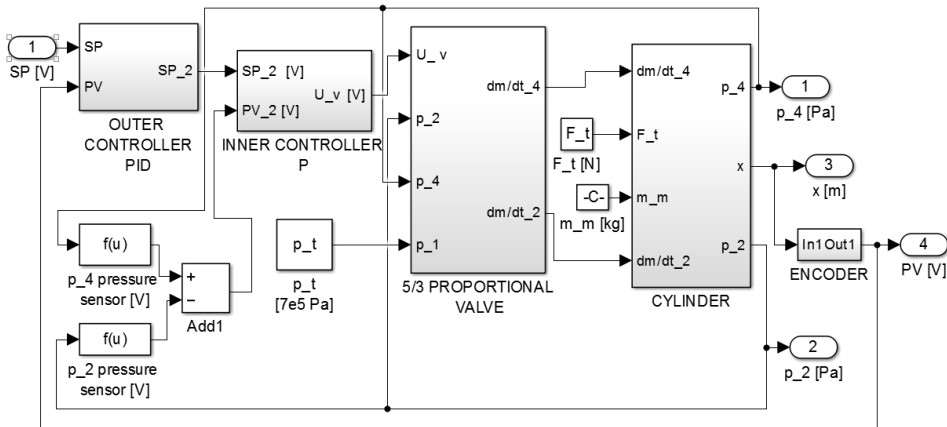


Figure 5. Block diagram of the applied PID-P cascade controller with the pneumatic system

In our work a cascade control algorithm with two loops was applied. The outer loop was a PID controller with the desired position as set point and the present position as feedback signal, the inner loop was a proportional (P) controller. The inner loop's set point was the outer loops output, and the

feedback signal of the inner loop was the pressure difference of the cylinder chambers. So as the two surfaces of the cylinder are the same, the inner loop itself executed a force control.

The controller needs tuning for the operation. Proper tuning of the controller is an optimization task, the result of it basically determinates the performance of the positioning. In case of cascade controller the primary controller and inner controller(s) should be tuned together, because they influences each other. As the tuning of such controller is rather complex, the selected tuning method is optimizing the control parameters by genetic algorithm combined with a gradient fminsearch method. Both algorithms perform large number of settings, so the optimization was implemented on the identified system model by MATLAB r2015 software Optimization Toolbox Genetic Algorithm Solver and fminsearch solver.

These solvers need a criterion for the optimization. The applied one is the Integral of Time multiply by Absolute Error (*ITAE*) criterion (Equation 6), as it takes into consideration the control error (*e*) - which is the difference between the set point (in case of positioning this is the target position) and the present value (the present position)- and the elapsed time (*t*).

$$ITAE = \int_0^{\infty} t|e(t)|dt \quad (6)$$

The positioning task was the following during the optimization: from start position (0 mm) the piston should move to 360 mm. The simulation time was 5 s. From 20 running results of the optimization process, the best 10 controller settings were chosen and evaluated.

## 6. Results

Evaluating the optimized positioning result of servopneumatic system with PID-P cascade control algorithm the positioning result was considered in 0→360 mm positioning task with constant load. During the evaluation the achieved accuracy as steady state error, the settling time and the overshoot were the main viewpoints.

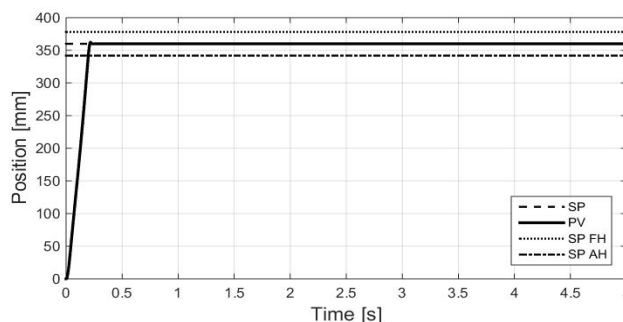


Figure 6. Positioning result

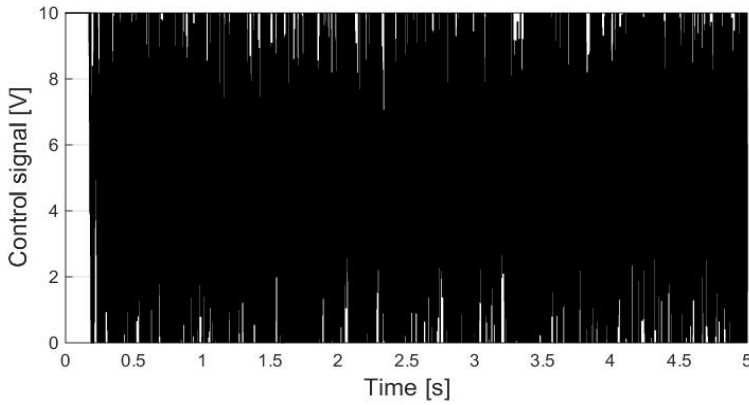


Figure 7. Control signal during the positioning

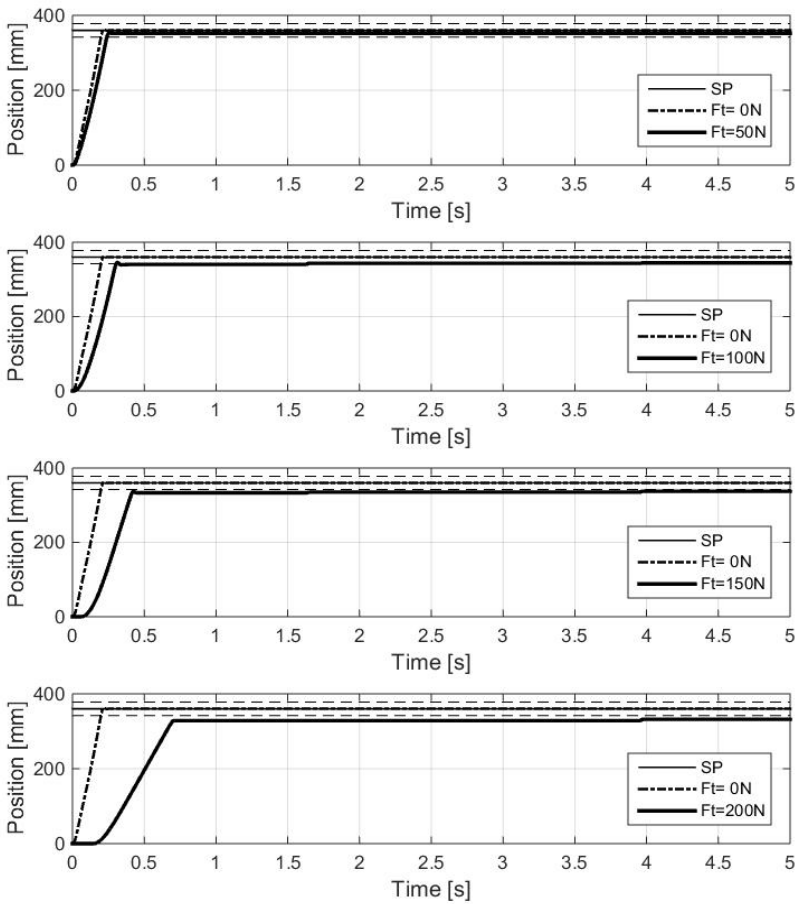


Figure 8. The effect of the load change on the positioning with PID-P cascade control algorithm

Based on the characteristics it can be declared that PID-P cascade algorithm operates appropriate in position control tasks, if the load is constant. The average steady state error of the 10 best tuned cascade controllers was  $0.01 \pm 0.001$  mm, which is within the expected 0.02 mm accuracy limit. The average overshoot was  $1.05 \pm 2$  mm, the average settling time was  $0.2 \pm 0.001$  s.

The effect of the external force load change was examined as well. In this case different outer forces were applied in the model from 0 N to 200 N in 50 N steps (Fig. 8.). The positioning task was the same: from 0 mm initial position to 360 mm position.

The examined servopneumatic system was not able to respond properly to the external force load change, as the absolute steady state error exceeded 5 mm in all 10 settings even at 50 N external force, and the error just increased as the load force increased.

## Summary

In this paper a cascade-structured controller was designed and applied in a servopneumatic system for position controlling purposes. The cascade controller contained a PID outer loop and a P inner loop with pressure difference feedback. The cascade controller was tuned by genetic algorithm combined with a gradient optimization process, the objective function of the optimization was an ITAE criterion. The evaluation took place on the best 10 optimized controller settings.

The PID-P controller worked proper in the optimized position control task, as the average absolute steady state error was  $0.01 \pm 0.001$  mm, which is within the expected 0.02 mm error limit. In contrast the PID-P cascade controller was not able to handle the external force load change at the expected level, as even just with 50 N external load the steady state error far exceeded the 0.02 mm error with more than 5 mm value.

## Nomenclature

$U_v$	- control signal (voltage)
$A_o$	- area of an orifice
$A_2$ or $A_4$	- surface of the piston (2 or 4 side)
$p_2$ or $p_4$	-pressure in cylinder chamber
$M$	- mass, moved by the cylinder
$x$	- displacement
$\dot{m}$	- mass flow rate
$V$	- volume
$w$	- velocity
$p_u$	- upstream pressure
$p_d$	- downstream pressure
$\rho$	- density

$\kappa$	- heat capacity ratio
R	- universal gas constant
T	- temperature
$F_f$	- friction force
$F_{Str}$	- Stribeck friction
$F_c$	- Coulomb friction
$F_{br}$	- Breakaway friction (static friction)
$c_v$	- coefficient
v	- relative velocity of the surfaces
f	- viscous friction coefficient
$F_l$	- external load force
E	- error
t	- time
PID	- Proportional-Integral- Derivative controller

## References

- [1] Czmerk, A. (2015). Pneumatikus rendszerek dimanikájának és beállási pontosságának a javítása. *PhD Thesis*. BME Budapest
- [2] FESTO. (2015). Proportional directional control valves MPYE. *Product catalog*
- [3] Gerhartz J.- Scholz, D. (2001) *Closed-Loop Pneumatics*, Copyright by Festo Didactic GmbH & Co., Denckendorf
- [4] Hamiti, K; Voda-Besançon, A.; Roux-Buisson H. (1996): Position control of a pneumatic actuator under the influence of stiction, *Control Engineering Practice*, Vol. 4. pp. 1079-1088
- [5] Sárközi E.- Földi L. (2016) The effect of the leakages on the behavior of 5/3 pneumatic proportional directional control valve, 11th International Conference of the Carpathian Euro-Region Specialists in Industrial Systems (CEurSIS 2016) 2-4 June, BAIA MARE, ROMANIA
- [6] Messina, A., A., G. N., & Gentile, A. (2005). Experimenting and modelling the dynamics of pneumatic actuators controlled by the pulse width modulation (PWM) technique. *Mechatronics*, Vol. 15. pp. 859–881.
- [7] Metwally M., E.-A. A. (2013). Effect of spool side chambers on dynamic response of contactless electro-operated pneumatic directional control valve, *Computres & Fluids*, Vol. 86. pp. 125-132.
- [8] Rahmat, M. F. (2011). Review on modeling and controller design in pneumatic actuator control system. Vol. 4., Nr. 4.
- [9] Takashi Miyajima, T. F. (2007). Development of a digital control system for high-performance pneumatic servo valve. *Precision Engineering*, Vol. 31. pp. 156-161.
- [10] Xiang, F., & W. J. (2004). Block-oriented approximate feedback linearization for control of pneumatic actuator system. *Control Engineering Practice*, pp. 387–399.

- [11] Yi-Chang Tsai, A.-C. H. (2008). Multiple-surface sliding controller design for pneumatic servo systems. *Mechatronics*, Vol. 18. pp. 506–512.
- [12] Laskawski M., Wcislik M. (2016) Sampling Rate Impact on the Tuning of PID Controller Parameters, *International Journal of Electronics and Telecommunicators*, 2016, Vol. 62, No. 1, PP. 43–48

# Analysis and optimization of gas meters

Costel Ieremie BREBAN, Nicolae Stelian UNGUREANU  
Technical University of Cluj-Napoca, North University Center of Baia Mare

## Abstract

This paper presents the current situation of gas meters in Romania, analyzing types of gas meters and also proposing new methods of optimization for those equipments, as finally to be able to achieve and optimize readings of gas meters with an increased safety against gas theft.

## Keywords

gas meter , analyse , optimize

## 1. Introduction

In industry, quality assurance and control products require continuous measurements carried out on raw materials, materials and components from suppliers or made by workers and quality controllers After each performance benchmarks after installation and on finished products.

In some manufacturing processes with high mechanization and automation, measuring instruments have a vital role, like the role of the nervous system in the body.

In the operation of complex products, to control while maintaining their performance, to ensure the security and safety installations, periodic measurements are made or repaired.

Tracking the consumption of raw materials, energy and fuel consumption and saving measures of requiring the use of measuring instruments. Trade to the population, commercial transactions between companies and the management of stocks can not be achieved only by means of measurements increasingly complex.

For the reasons stated above, measuring instruments are included as a category of products of particular importance to the national economy, whose manufacture, import, use, inspection and repair is regulated by law.

## 2. Types of natural gas gauges

According to the rules of measurement can divide the measuring systems in:

- a) The gas meters membrane (deformable walls)
- b) The measurement system of rotary piston meters or turbine

- c) The ultrasonic measuring meter
- d) The measuring orifice

**a) The gas meters membrane (deformable walls)**

These measurement systems are composed of gas-walled deformable converters volume mechanical or electronic converted into automatic mode the volume of gas measured under the working volume of gas at standard conditions and are used to measure the gas supplied to domestic consumers.

The maximum errors allowed to metrological control for these types of meters are:

Table 1. Maximum errors allowed

Flow	Initial verification	Check in service
$Q_{min} \leq Q < Q_{max}$	$\pm 3\%$	- 6% up to + 3%
$0,1 Q_{max} \leq Q \leq Q_{max}$	$\pm 1,5\%$	$\pm 3\%$

**Working principle:**

Four measuring chambers are separated by means of synthetic membranes. Rooms are filled and emptied periodically, and the movement membrane is transferred via a gear to the crankshaft. This move drawers admission control gas. Through a system of gears, the motion is transmitted by a magnetic coupling to a mechanical meter. Facility according to temperature compensation volume is provided mechanically by a bimetal.

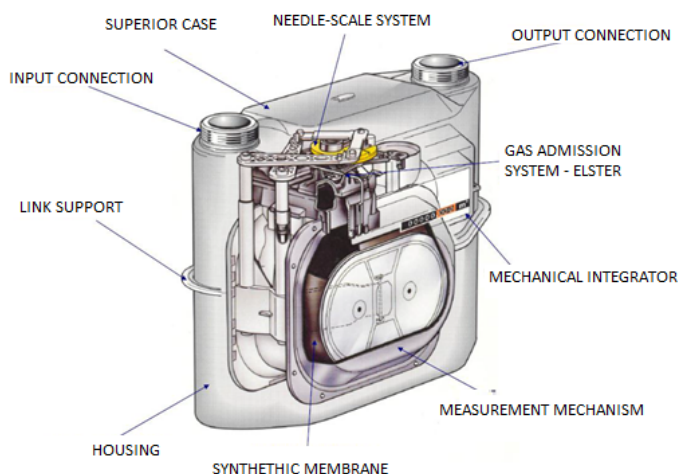


Figure 1. Volumetric gas meter

**b) The measurement system of rotary piston meters or turbine**

Rotary gas meters are characterized by a high measuring range and compact dimensions. Due to their measuring principle they do not require straight pipe sections at the entrance or exit. Rotary meters have to be lubricated with oil. For easy access and to inspect the oil level, oil cameras front and rear are connected to allow maintenance to be done only from the front.

The maximum errors allowed to metrological control for these types of meters are:

Table 2. Maximum errors allowed

Flow	Initial verification	Check in service
$Q_{min} \leq Q < Q_{transit}$	$\pm 2\%$	$\pm 2,5\%$
$Q_{transit} \leq Q \leq Q_{max}$	$\pm 1\%$	$\pm 2,5\%$

Working principle:

Rotary piston gas meter is the measuring volume of the highest precision. Body with an entry and an exit there are two rotary pistons rotating in the opposite direction of their movement is synchronized timing wheels.

Rotary meters are volumetric gas meters for gaseous media and operate according to the principle of positive displacement. These devices measure the gas volume under operating conditions. In order to transform this volume under standard conditions, the Electronic meters are equipped with correcting gas volume available with different characteristics. The actual measuring cell consists of two 8-shaped rotary pistons, which creates together with the housing 4 chambers / revolution, which are periodically filled and emptied. The number of revolutions is proportional to the throughput volume of the measurement chamber. The rotational movement is transmitted to a mechanical, where this volume.

With the gas flow carrying the pistons rotate and the outlet side of the gas amount, which is defined by the volume of the metering chamber.

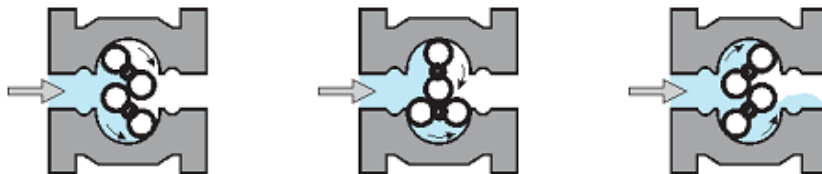


Figure 2. Rotary piston gas meter

**c) The ultrasonic measuring meter**

Ultrasonic gas meters are electronic measuring devices without moving mechanical parts. They are characterized by immediate response to changes in

flow and no pressure loss. Ultrasonic meters are therefore particularly suitable for regulating the process and to measure a wide range of combustible and non-combustible gases.

The advantages of this technology include:

- Precision: can be calibrated to  $<0.1\%$ ;
- Typical Rangeability  $> 50: 1$
- Volumes measured bidirectionally with comparable performance
- Tolerance wet gas: important for production applications
- Non intrusive: minimal pressure drop
- Low maintenance: no moving parts means low maintenance
- Fault tolerance: counters remain relatively accurate even if the sensors fail
- Full diagnosis: data to determine the status of the meter.

The most important however is the ability to diagnose meter. Other primary measuring devices, such as turbine meters ahead offers little if still functions correctly after a period of time.

Ultrasonic meters enables electronic diagnostic that can help validate proper operation involved and thus reduce internal inspection required by other devices. The internal diagnostics can also be used to identify whether other parts of the measuring station as well as measuring the temperature and gas composition also functions properly.

Gas meters installed an ultrasonic measuring principle transit time.

Working principle:

The figure below shows the simple geometry of two transducer, A and B, at an angle  $\phi$  with respect to the axis of the straight cylindrical pipe.

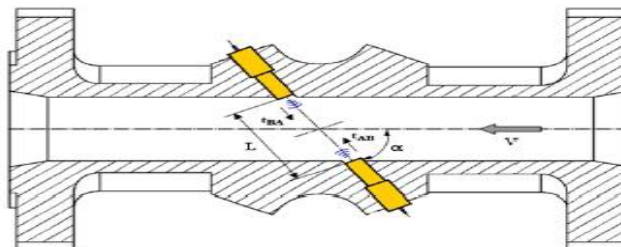


Figure 3. Ultrasonic measuring meter – cut

#### d) The measuring orifice

Systems for measuring the quantities of gas to the orifice are built on the principle of measurement of the flow orifice of the diaphragm. The measuring orifice is made up of the following components:

Upstream and downstream pipe sections;

Primary

1) orifice type:

- the pressure tap aperture angle;
- outlet pressure diaphragm flange;
- outlet pressure diaphragm  $D$  and  $D / 2$ ;

Diaphragms can be mounted in port aperture devices.

## 2) pressure tap

Secondary (transducers), which are:

- Static pressure transducers;
- differential pressure transducers;
- temperature sensors;
- multivariable transmitter;
- thermal resistance;
- the density sensor;
- chromatography line;

Tertiary element (calculated by flow rate);

Auxiliary elements which are impulse pipes for taking gas parameters;

Measurement uncertainty these systems the volume of natural gas must be within  $\pm 1.5\%$ .

Secondary elements of the measurement system, the static pressure transducers, respectively, the differential temperature, or multivariable density should not exceed a maximum error of  $\pm 0.1\%$ .

Measuring the tertiary element of the system, ie the flow computer (including input converters) will be the calculation of the maximum permissible error of  $\pm 0.2\%$  correct amount.

Working principle:

The measurement of fluid flow in the pipe with orifice element (diaphragm, nozzle, etc.) are based on the change in potential energy of the fluid from leaking through a cross-section of an artificial tapered pipe mounted as shown below.

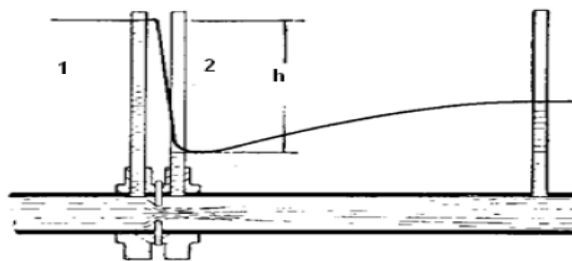


Figure 4. Orifice system measuring - cut

This causes a reduction in the passage section, with a consequent increase in the speed of flow in the section of the diaphragm. The second manometer tubes 1 and 2 combined make up a differential pressure gauge that measures the fluid pressure difference before and after the diaphragm. This pressure difference is

proportional to the velocity of the gas and hence, as was seen, can be used to determine flow.

### 3. Optimisation of gas meters

I will investigate and create theories, maybe some practical models regarding:

- a) Prevent locking the integrator of the gas meter.
- b) HOW : Identification of an alloy non-sensitive to temperature fluctuation.
- c) Leak in the meter case.
- d) HOW : Finding a new method of bonding the meter case.
- e) Tear of the membrane.
- f) HOW: Identification another compatible and resistant material.
- g) Intentional locking of the integrator mechanism.
- h) HOW: Creating a new type of housing for the integrator.
- i) Prevent intentional turn.  
HOW: Automatic lock in case of turn.

### Conclusion

In the field of energy, especially in the field of gas distribution in Romania, there is a need for improvement both of the consuming equipment (gas meters) and the meter reading mode and methods, in such a way that the distributor and the consumer have part of a real calculation of consumption.

### References

- [1] Alan S.Morris, Reza Langari ,(2012), Measurement and Instrumentation, London
- [2] Edoli Enrico,Fiorenzani Stefano,Vargiolu Tiziano,(2016), Optimization Methods for Gas and Power Markets Theory and Cases, Macmillan Published Limited,UK.
- [3] Milea, A.,(1985),The Metrologist's book, București,RO
- [4] Neagu, I., Constantin, Mariana, Ciocîrlea-Vasilescu, A., (2007), Measurements and metrology legislation, , Prosper& Printech, București.
- [5] Pustisek Andrej, Karasz Michael, (2017), Natural Gas- A commercial Perspective,Springer International Publishing AG,Switzerland
- [6] Smil Vaclav, (2015),Natural Gas,Fuel for the 21th Century,John Wiley and Sons Ltd., United Kingdom
- [7] Stoica Augustin ,(2011), Course support-Measuring and control devices.

# Model based optimization in smart livestock farming - an introduction

Viktor ERDÉLYI, László JÁNOSI

Institute for Mechanical Engineering Technology, Szent István University,  
Páter K. u. 1., Gödöllő, H-2100, Hungary,

## Abstract

This paper introduces the possible applications of the digital twin and digital shadow concept in pig farm optimization. These well-known two terms from Industry 4.0 show big potential to optimize production in a higher level than ever.

This article is about creating digital twin and digital shadow of a modern pig fattener. These models are based on the literature, and are identified on the data shared in these. However, these models can't be used on real systems before identifying them on the actual circumstances.

At the current state, the digital twin is suitable for describing the growth of pig's weight, daily weight gain and feed consumption of the pig. On the other hand, the digital shadow is only capable of modelling the heat-household of the barn. With these there is possibility to optimize certain factors of production (eg. nutrition, or cycle time), but further development is ongoing.

## Keywords

Industry 4.0, Agriculture, Smart livestock farming, Digital Twin, Digital Shadow

## 1. Introduction

Nowadays, the concept of Industry 4.0 is becoming more and more known. One of I4.0 core elements is modelling, known as *digital twin*, and *digital shadow*. These two are the digital equivalent of not only the production, but the product itself as well. The use of this concept in another areas of agriculture and engineering (Blahunka et al. 2017, Szabó et al. 2017) production system, such as a pig fattener speaks for itself (Dieter, 2015, Günther et al. 2017.).

This paper shows the so far achieved results of the ongoing research. In the smart livestock farming environment, the Digital Twin would be the digital model of the livestock with all the data from it, and the Digital Shadow is the computer counterpart of the production system itself. These, in the industry can be used to achieve predictive maintenance and predictive control which are advantageously affect the production parameters. So to examine its potential in

the smart livestock farming, we have to make computer models both of the pigs, the pig fattening process and its assets.

## 2. Materials and methods

As a first step in the research work, a general model of a pig farm will be designed. The model is based on the measured data found in the literature (Fenyvesi et al., 2004.) The parameter identification is based on the same data, however to use the models as an aid to design a pig fattener farm, or use it to control an existing one, further identification is needed based on other farms using the same technologies. These models are intended as commonly usable wireframes. Figure 1 illustrates the structure of the currently used farms where typical time-based control is used. Figure 2, conversely, illustrates a solution where control is effected through continuous feedback. Figure 1 illustrates the structure of the currently used farms where typical time-based control is used.

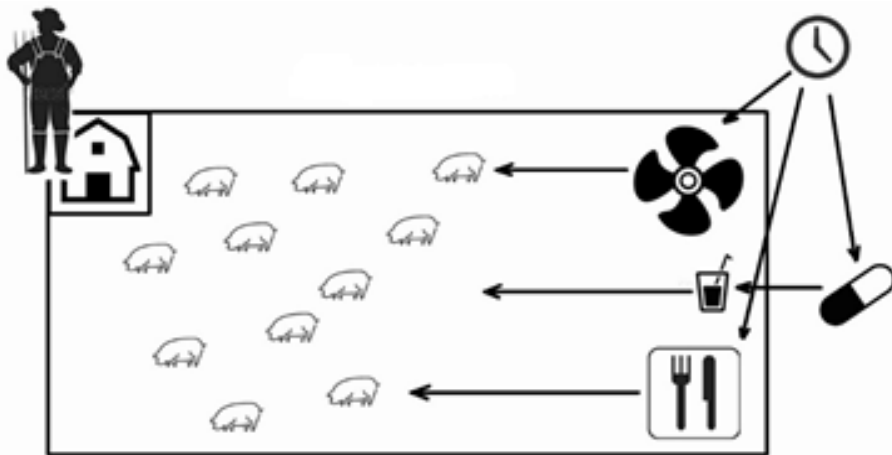


Figure 1. A graphical sketch of the current pig farm model

The model is based on a pig farm of this kind. In these fatters, there are only few fully automated systems using closed control loop. The main feedback is the swineherd himself. Therefore, interestingly it is fairly complicated to model this current solution, it would be much easier, if there were no uncertain factors in control like humans. So in the first steps only the modeling of singular subsystems take place, then these will be interlocked with some uncertainty, based on measured data.

Of course, the best solution would be a feedback coupled system, like on Figure 2, where control is effected through continuous feedback. Fortunately, if the sub models are available, this model will be much easier to build.

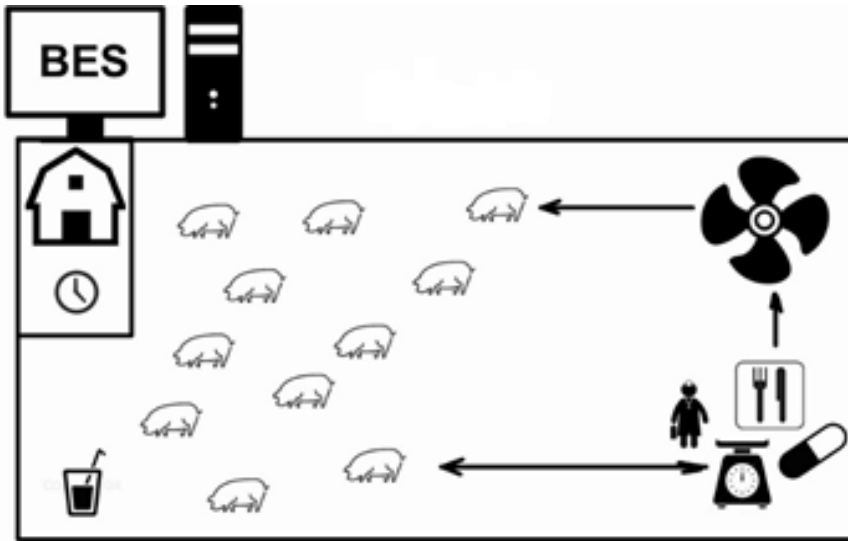


Figure 2. Schematic of a future pigfarm, where the production controlled by a Breeding Execution System in a closed loop

### 3. Digital twin

Because of the uncertain nature of the product aka the pig, there is a need to implement probability factors to simulate the deviations to average based on normal distribution. On Figure 3. the sketch of the porker model is to be seen.

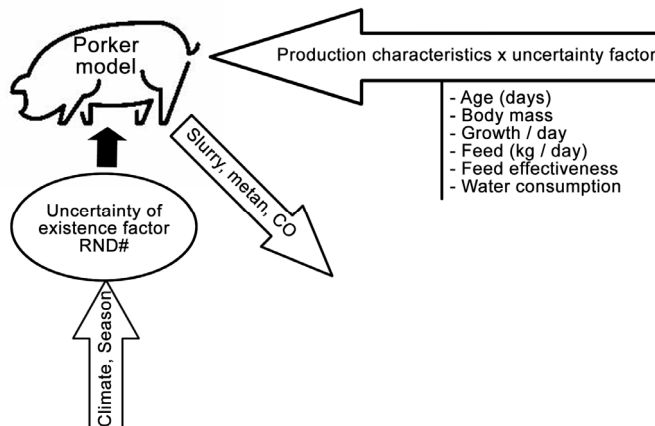


Figure 3. Simplified graphical sketch of porker model

The Second Degree Polynomial based on the weight gain data is the following equation:

$$\frac{dm}{dt} = a_m t^2 + b_m t + c_m \quad (1)$$

The MATLAB *polyfit()* method results the following correlation coefficient:  $R^2=0,99698$ .

The effect of *feeding* is described in the following equation, in which I assumed the simplest case, that only  $c_m$  is concerned, and only linearly (intuition). The equation so prescribed

$$g(t, m) = a_g t^2 + b_g t + c_g m + d_g \quad (2)$$

Parameter identification is done with the data found in literature.

$$\int_0^{t \max} (g_m - g(t, m))^2 dt \Rightarrow \min. \quad (3)$$

The *fminsearch()* method gave us the correlation coefficient of  $R^2=0,99677$ .

Formula (4) serves to determine parameter  $C_m$  in formula (1), which is assumed to be a linear relationship.

$$c_m(t) = a_c g(t, m) + b_c \quad (4)$$

The relation (5) shows the substitution of equation (4) in formula (1).

$$\frac{dm}{dt} = a_m t^2 + b_m t + a_c g(t, m) + b_c \quad (5)$$

Equation (6) used to determine the coefficients of the so-modified (1) equation so it can be written that,

$$\int_0^{t \max} (m_m - m_c(t))^2 dt \Rightarrow \min. \quad (6)$$

The re-running of *fminsearch()* algorithm, shows us that the correlation is improved, numerically to  $R^2=0,99787$ .

*Italics font* expressions indicate the feedback points.

Figure 4. illustrates the solution of these models in Matlab Simulink environment.

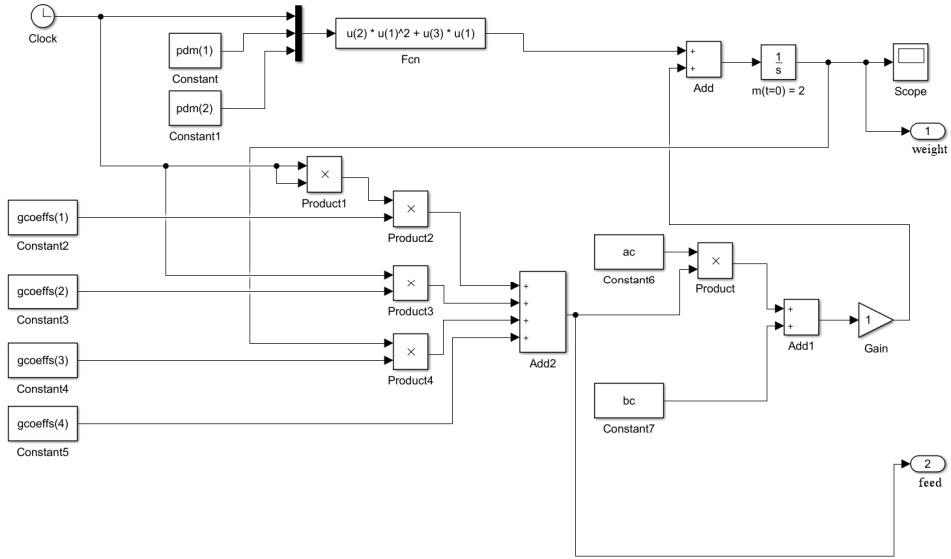


Figure 4. Solution of the porker model in Simulink environment

### Energy balance of pork

$$cm \frac{dT}{dt} = \eta m_t H(m) - kA(T - T_k) \quad (7)$$

where:

- c - specific heat of pig, J/kg°C
- m - mass of pig, kg
- T - temperature of pig, °C
- t - time, s
- η - nutrient heat utilization efficiency, -
- mt - mass of feed, kg
- H - nutrient energy content, kJ/kg
- k - heat transfer factor, W/m<sup>2</sup>
- A - heat transfer surface of pork, m<sup>2</sup>
- T<sub>k</sub> - ambient temperature, °C

According to the correlation (8), the energy content of the feed is dependent on the weight of the pig (ruling, 2003):

$$H(m) = \begin{cases} 14, & \text{if } m < 40 \\ 13,6 & \text{if } 40 \leq m < 70, \frac{MJ}{kg} \\ 13,4 & \text{else} \end{cases} \quad (8)$$

Based on the known density and mass of the pig the volume on an equivalent mass and density sphere could be calculated:

$$V = \frac{m}{\rho} = \frac{4 \cdot r^3 \cdot \pi}{3}, \quad (9)$$

from which the sphere radius is expressed as follows:

$$r = \sqrt[3]{\frac{3m}{4\pi\rho}} \quad (10)$$

where:

- V - volume of the sphere, m<sup>3</sup>
- r - radius of the sphere, m
- m - mass of the pig, kg
- $\rho$  - density of the pig, kg/m<sup>3</sup>

Thus, the surface of the spherical swine model can be expressed as follows:

$$A = 4r^2\pi \quad (11)$$

where:

- A - surface of the sphere, m<sup>2</sup>
- r - radius of the sphere, m

Parameters used at calculations:

- k = 4 W/m<sup>2</sup>
- $\eta$  = 10<sup>-6</sup>
- c = 260 J/kg°C
- T<sub>k</sub> = 30 °C
- T(t = 0) = 39.3 °C

#### 4. Digital shadow

In the following only one component of the barnmodel will be presented, which is the heat balance of the barn.

The first step of the stable modeling procedure is the introduction of the pig as a heat generator (Figures 6-7), ventilation as a cooling (if cooler than inside) and convection heat transfer of the stall.

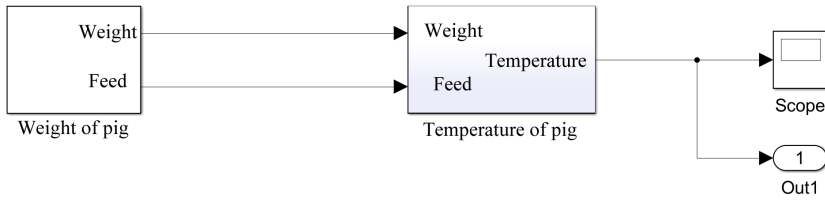


Figure 5. Temperature of porker

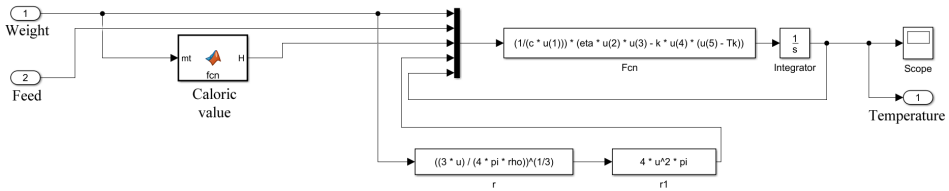


Figure 6. Energy balance of a porker

The mathematical description of the simplified model is the follows:

$$c_l m_{lb} \frac{dT_i}{dt} = \sum k_m A_m (T_m - T_i) - (k_i A_i (T_i - T_k) + c_l m_{k_l} (T_i - T_k)). \quad (12)$$

To make the above equation solvable to matlab, the equation has to be rearranged, so it expresses the temperature change in time.

$$\frac{dT_i}{dt} = \frac{\sum k_m A_m (T_m - T_i) - (k_i A_i (T_i - T_k) + c_l m_{k_l} (T_i - T_k))}{c_l m_{lb}} \quad (13)$$

where:

- $c_l$  - specific heat of air, J/kg°C
- $m_{lb}$  - mass of air inside of barn, kg
- $k_m$  - heat transfer coefficient of pork, W/m<sup>2</sup>
- $A_m$  - surface of the sphere model of pig, m<sup>2</sup>
- $T_m$  - temperature of porker, °C
- $T_i$  - inside temperature, °C
- $K_i$  - heat transfer factor of the barn wall, W/m<sup>2</sup>
- $A_i$  - the surface of the stable wall, m<sup>2</sup>
- $T_k$  - outside temperature, °C
- $m_{kl}$  - mass of exhaust air (negative pressure ventilation), kg

On Figure 7. is four porker-model are shown embedded to the barn-model, which uses fixed geometry, and physical parameters.

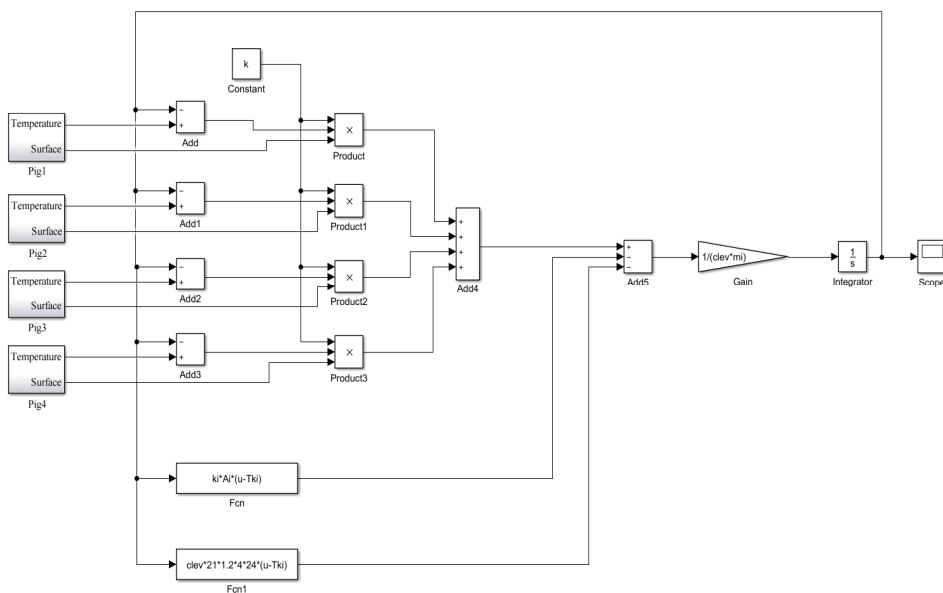


Figure 7. four porker model in the barn model

## Summary

The build of an existing pig fattener farm – model is now ongoing. This model – after identification and validation- will be used to consider the possibilities of the use of an Industry 4.0 grade closed loop control system. Can it be used without a modification, and if the answer is no, then how should I modify the architecture to gain the output parameters.

In my further work, I will search such solutions, where the subsequent sub-processes of livestock farming are interconnected in a larger master system. That can be stated if the consecutive sub-systems are codified, and they can be connected to each other (compatible information contents), then the operation can be optimized in a larger system, and will work more efficiently.

## References

- [1] Codex Pabularis Hungaricus (2004.)
- [2] Dieter, W. (2015.) Industrie 4.0 – die Zukunft der digitalen Fabrik, VVD-2015 Verarbeitungsmaschinen und Verpackungstechnik, Radebeul
- [3] Fenyvesi, L., Mátyás, L., Pazsiczki, I. (2004.) Technologies of pig husbandry, Hungarian Institute of Agricultural Engineering, pp. 10-11., Gödöllő, ISBN 963-611-426-9

- [4] Günter, S., Matthias, B., Jan, R., Martin, B. (2016.) Der Digitale Schatten in der Auftragsabwicklung, ZWF Zeitschrift für wirtschaftlichen Fabrikbetrieb: Vol. 111, No. 1-2, pp. 48-51.
- [5] Blahunka Z. Bártfai Z. Faust D. Kátai L. SzabóI.: Terrain surface monitoring with IMU equipped mobile robot. 7<sup>th</sup> International Conference on Biosystems Engineering 2017, Tartu, Estonia
- [6] Szabó, I., Hushki, M., Bártfai Z., Kátai L. 2017. Operator's behaviour measuring methodology inside off-road vehicle cabin, Operator's focusing scheme. Agronomy Research, 15. <https://doi.org/10.15159/AR.17.033>

# **Synergy of the triad: human, machine and environment in Design of Technologies and Products**

Radu-Iacob COTEȚIU, Adriana COTEȚIU

Technical University of Cluj-Napoca, North University Center of Baia Mare

## **Abstract**

The intergration of human-life with life of machines and ecology in the economical and psicho-social life rises new challenges in the design of technologies and products. This integration is present in every moment and in all aspects of relation between human, machine and environment each of them being forced to adapt to each-other. Therefore, the rational design of high reliability machines and eco-design constitutes a major preoccupation, especially for those learning to design. The realization of these demands supposes some tendencies. The eco-design must take into account a set of principles that can be group in specific areas.

## **Keywords**

ecotechsystems, ecodesign, industrial ecology

## **1 Introduction**

The intergration of human-life with life of machines and ecology in the economical and psicho-social life rises new challenges in the design of technologies and products. This integration is present in every moment and in all aspects of relation between human, machine and environment each of them being forced to adapt to each-other. Therefore, the rational design of high reliability machines and eco-design constitutes a major preoccupation. That activity must ensure quantity, quality, ecological aspects and economic efficiency at the same time demands which can be materialized if each part of machine in optimally designed.

## **2. Eco-Systems to Ecotech-Systems in the Constructive and Technological Design**

Kelly [5] observes that “by pushing industrial processes toward the organic model, bionic engineers create a *spectrum of ecosystem types*:

- At one extreme are pure, natural ecosystems like an alpine meadow or a mangrove swamp. These systems can selfishly be thought to produce

biomass, oxygen, foodstuffs, and thousands of fancy organic chemicals, a few of which we harvest.

- At the other extreme are pure, raw industrial systems, which synthesize compounds not found in nature, or not found in such large volumes.
- In between are a spectrum of hybrid ecosystems such as marshland sewage treatment plants (which use microbes to digest waste) or wineries (which use living yeast to make vintage brews), and soon, bioengineered processes that will use gene-spliced organisms to produce silk or vitamins or glues.

Both *genetic engineering* and *industrial ecology* promise the third category of *bionic systems - part biology, part machine*.

Industry will inevitably adopt biological ways:

- *Take less material to do the same better.* All manufacture goods now consume less material and give better performance. Manufacturers will have inspiration natural biological processes for their technical and technological solutions.
- *Today and in future the complexity of products and technologies will touch the biological complexity.* Artificial simple and complex systems will be deliberately infused with organic principles.
- *Nature will not move, so it must be accommodated.* Nature – which is larger than us and our contraptions – sets the underlying pace for industrial progress, so the artificial will have to conform to the natural in the long term.
- *The natural world itself – genes and life forms – can be engineered* just like industrial systems. This trend narrows the gap between the two spheres of natural and artificial/industrial ecosystems, making it easier for industry to finance and appreciate the biological.

The researchers focused on claiming that "natural evolution is a computational process of adaptation to an ever changing environment"; parallel problem solving from nature, treating nature as a supermodel. Also there are many efforts which were focused on copying different human systems as a model for learning. For every rapid step our society takes toward the manufactured, it is taking an equally quick step toward the biological. The newest products in our living room, office or garage will be based on ideas from these pioneering visions.

The short overview of evolution of the world can be summarized as follows: The nature invents human hunter and gatherers (raw biology); the hunter-gatherers invent agriculture (domestication of the nature); the farmers invent the industrialisation (domestication of the machine); the industrialists generated the currently emerging postindustrial era. The flavor of the next epoch is neo-biological rather than bionic (name given to concerns about devices and mechanisms in living systems, to find models for technical sciences). In the blending of the *made* and *born*, the organic is a dominant trait, while the mechanic is recessive and finally bio-logic always wins.

### **3. Optimization methods of the design activity**

The fundamentals of machine manufacturing design studies the general principles, the improvements of optimization methods of the design activity, the documentation methods as well as the principles used in adopting the shape of the parts, assemblies and subassemblies, in order to reduce weight, to increase rigidity, considering, at the same time the influence of stress concentrators, the type of loading, the forming technology of the semi-finished product and not at the last the manufacturing technology and evaluation of their impact on environment regarding Life Cycle Assessment.

The machine building by its implication in the entire economic activities has great importance. Therefore, the rational design of high reliability machines and eco-design constitutes a major preoccupation, especially for those learning to design. That activity must ensure quantity, quality, ecological aspects and economic efficiency at the same time demands which can be materialized if each part of machine is optimally designed.

Competitive surroundings and environment force manufacturing enterprises to produce in smaller series, with shorter lead time and with decreasing costs. Flexibility is one of the keys to solve the current state of production. Computer Aided Process Planning aids in creation of process plans for manufacturing and increases the flexibility of manufacturing.

For the machines design, the practical and theoretical experience accumulated until now, set into evidence the following principal demands: high functionality, high reliability specific to their destination; execution and utilization as efficient as possible from economical viewpoint. The realization of these demands supposes the following tendencies:

a. Increase of the quantitative and qualitative complexity degree of the machine (great number of components in diverse systems: mechanical, hydraulically, electrical etc.);

b. Provision of certain functional parameters (forces, pressures, speed, temperature), which to allow the weight, dimensions and energy losses decreasing;

c. The use of the most updated calculating methods, with the consideration of the actual operating conditions through the scientific research of actual behavior of components, estimating on probabilistic bases the complex notion of reliability;

d. The use of the new materials with higher strength and working characteristics (stainless steel, alloys of titanium, glass fiber reinforced plastic, sintered materials etc.);

e. The process improvement and their better organization, the introduction of high accuracy and productivity modern procedures, providing increased interchangeability conditions and higher quality of the machine elements, by dimensional precision, low roughness, higher surface's hardness, etc.;

f. The standardization and the typification of the components, subassemblies and assemblies, the constructional and functional diversity of the assemblies or

machine are realized by combining mass-produced typical components. Thus, all these are achieved by economical methods and not by their general diversification,

g. The utilization optimizing by suitable automated installations or by controlling the functional characteristics parameters, the wear degree etc., with suitable control devices;

h. The esthetic and actual design.

#### **4. Principles for eco-designers in the context of synergy of human, machines and environment**

The eco-design must take into account a set of principles that can be group in specific areas reference as follows:

Products:

- design Life cycles not only Products;
- increase Product life-time;
- design Services not only design Products;
- make your Product recyclable

Materials:

- use a minimum of Material
- use recycled Materials
- natural Materials are not always better;
- eco-Selection of Materials

Energy:

- do not underestimated Energy consumption;
- design for Low Energy Use or increase energy efficiency
- design for ‘Zero’ Energy Use

Design & Technology:

- design for Remanufacture/Design for Reuse
- design for Disassembly/Design for Recycling
- design for Extended Durability
- eco-Selection of Processes/Design for Cleaner Manufacturing
- design for Upgradeability/Modular Design
- design for Service/Leasing not for Ownership
- design for Low Consumption
- design for Minimum Pollution during Use
- design for Minimum Mass

Distribution/Sales

- design for Efficient Distribution

Disposal:

- design for Safe Disposal/Design for Degradability

#### **Conclusion**

The tendencies previously mentioned impress first a creative character to the design: the variety of combinations can be very great, securing the product high

competitive with relatively low costs. In the same time, the component typification and their mass-production allow to reduce the costs of the design and processing and to obtain considerable economy through calculation and technological improvement. The attention given to the rational design of the machine elements is also needed for the proper training of future designer.

Parallel to these aspects, on the last period the designers must take in account the ecological aspects in their activity. So, eco-design is a new preoccupation of all designers which complete the complex frame of restrictions and demands.

The researches made today in this field demonstrate that the design can be considered as a science, which applies the research results in industrial practice, having precise economic and ecologic purposes.

## References

- [1] Cotețiu, R., Kuric, I., Novak-Marcincin, J., Ungureanu, N. (2005) *New Trends in Mechanical Design and Technologies*. Editura Risoprint, Cluj-Napoca.
- [2] Cotetiu, R. , (2006) *Eco-Design Aspects of Product and Technologies in Development of Mechanical Engineering as a Tool for Enterprise Logistics Progress*. Poznan University of Technology, Institute of Mechanical Technology, Poznan- Poland, 2006, ISBN 83-89873-28-1, pg. 159-177.
- [3] Cotetiu, R., Eberst, O., Alexandrescu, M., Cotetiu, A., Ungureanu, N. (2008). *Technical Development Program with Friendly Materials Annals of DAAAM for 2008 & Proceedings of the 19th International DAAAM Symposium*, ISBN 978-3-901509-68-1, ISSN 1726-9679, Editor B. Katalinic, Published by DAAAM International, Vienna, Austria, pp. 0317-0318. [http://www.daaam.com/Thomson\\_Scientific\\_2008\\_01\\_14.pdf](http://www.daaam.com/Thomson_Scientific_2008_01_14.pdf)
- [4] Hardin, Tibbs (1991) "*Industrial Ecology*." Arthur D. Little
- [5] Kevin, Kelly (1995) *Out of Control. The New Biology of Machines, Social Systems, and the Economic World*, Perseus Books Group.
- [6] Legutko, St. et all (2006) *Development of Mechanical Engineering as a Tool for the Enterprise Logistics Progress*, Science Report. Editura ZPW M-DRUK Janusz Muszynski, Wagrowiec. Poznan, Poland

# 3D metal printing technologies and materials

Tamas PATAKI, Attila KÁRI-HORVÁTH,  
LÁSZLÓ ZSIDAI

Institute for Mechanical Engineering Technology, Szent István University, Páter K. u. 1.,  
Gödöllő, H-2100, Hungary,

## Abstract

The 3D printing is a very dynamically growing area in the industries. Nowadays the main aim in this area is the reserch of the prinable materials. Since about 2000 the 3D printing has become more and more popular. The first material was the polimer, what everybody used for 3D printing. It was easy to melt, and to form everything what we need. These parts were very weak, they were unusable for any part. Nowadays are we trying to create components with stronger materials that do not break easily. These materials are the metals. In this article we would like to introduce the 3D metal printing methodes, and show some materials what can be able to change the polimer in this part of the industry.

## Keywords

3D printing, metal printing, technology, material

## 1. Introduction

In the last few years, metal 3D printing has become increasingly popular. And rightly so: each material offers a unique combination of practical and aesthetic properties to suit a variety of products, be it prototypes, miniatures, jewelry, functional parts or even kitchenware.

The reason metal 3D printing is so hot is that parts will be serially 3D printed for mass adoption. In fact, some 3D printed parts are already just as good, if not better, than those manufactured by traditional methods.

In traditional manufacturing, making metal and plastic objects can be a wasteful process. Lot's of chunky parts and a lot of surplus material are used. When aircraft makers manufacture metal parts, up to 90% of the material is being cut away. 3D printing metal parts uses less energy and reduces waste to a minimum. Especially, as the finished 3D printed product can be up to 60% lighter compared to the machined part. The aviation industry alone saves billions of dollars through this weight reduction, mainly on fuel. [1-3]

So, what do you have to know about metal 3D printing?

## 2. Metal printing technologies

### *Metal 3D printing at „home”*

What can you do if you want to 3D print metal at home? As extremely high temperatures are needed for metal 3D printing, you cannot use a regular FDM 3D printer for it.

Simply put: There's no way you'll gonna 3D print pure metal at home this decade. And you probably won't have a dedicated metal 3D printer standing in your home until 2020. But in some years, as nanotechnology evolves, we might to see a substantial growth in new applications. Like conductive 3D printable silver that can be ink jetted using a system very similar to the 2D graphic printer, you have at home. Even mixing different materials, like plastics and metals into the same object, is going to be possible.[2]

Even if you can't 3D print metal objects at home, you can still resort to plastic filament with added metal powders. ColorFabb, ProtoPasta or TreeD Filaments offer interesting composite metal-PLA filaments. These are filaments that contain a significant percentage of metal powders but provide enough plastic to be printed at low temperature (200 to 300 degree Celsius) with just about any 3D printer. At the same time, they contain enough metal to look, feel and even weight of a metallic object. The iron-based filaments even form rust in certain conditions.

But you can go even further. Usually, metal 3D printer filament has 50 percent metal powder added. Dutch 3D printer filament company Formfutura claims they have ramped the ratio up to 85 percent metal powder and 15 percent PLA. The metal 3D printer filaments are called MetalFil Ancient Bronze and Metalfil Classic Copper. You can even print it at “moderate” temperatures of 190 to 200 degree Celsius [4].



Figure 1. Metal filaments for home use

These are the key facts of metal 3D printer filament for home use:

- Unique metallic finish and appearance

- Ideal for jewelry, statues, home hardware, or artifact replicas
- High durability
- Low flexibility, depends on structural design
- Not soluble
- Not considered food safe
- General print temperature range is 195°C – 220°C
- Very little shrinkage during cooling
- Heated bed not required
- Printing difficulty is high, requires fine-tuning of nozzle temperature, flow rate, and post-processing



Figure 2. The technology of the method and the part

### *Industrial metal 3D printing*

But what if you want better results or even full metal 3D prints? Should you buy a metal 3D printer for your business? We wouldn't advise it unless you want to 3D print metal every day. The price for a pro metal printer is high: a professional metal 3D printer from EOS or Stratasys will set your business back from \$100.000 to \$500.000. Also, the costs will rise as you need someone to operate and maintain the machine and also to finalize the print (i.e. polishing).

Simply put: Right now, there is no affordable metal 3D printer.[3]

Unless you want to start a 3D printing metal business and you need a professional part 3D printed in metal, you should better use a 3D printing service to suit your needs. 3D printing services like Shapeways, Sculpteo, and iMaterialise offer direct metal 3D printed parts [11].

Currently, their offer consists of these 3D printing metal materials:

- aluminum / aluminium
- steel
- brass
- copper
- bronze
- sterling silver
- gold
- platinum
- titanium
- If you're a goldsmith, you can also order wax models for casting special metals.

Speaking of wax models: They offer most 3D printed metals (including gold and silver) through a lost wax casting process. Not everything is 3D printed at their factories directly. They generally turn to other services that are specialized in metal 3D printing to carry out the order. But the number of “metal 3D printing services” is growing rapidly all over the world. Also, the metal 3D printers get more common at 3D printing services [7].

The reason big companies like it so much is that it can be used to build fully automated factories which can produce “topologically optimized” parts. This means it’s now possible to perfectly distribute the material in a component in order to make it thicker only where it needs to withstand more stresses, thus drastically reducing the weight without sacrificing structural integrity. However, this is not the only technology out there. Some are significantly more affordable and even accessible to any user [5-6].

Please be aware that 3D printing metal needs special CAD Design. Shapeways offers dedicated 3D printing metal guidelines that’s worth a look. For even more advanced information, take a look at Statasys’ information on metal 3D printers and the nuances of metal 3D printing.

### *Metal 3D Printing for Engineers and 3D Designers*

The current available metal printing technology are in four categories [8-10].

#### *1. Powder bed fusion (PBF)*

This technology has two types. The difference is between the two technologies is the concentrated energy beam.

##### *a) SLM - selective laser melting*

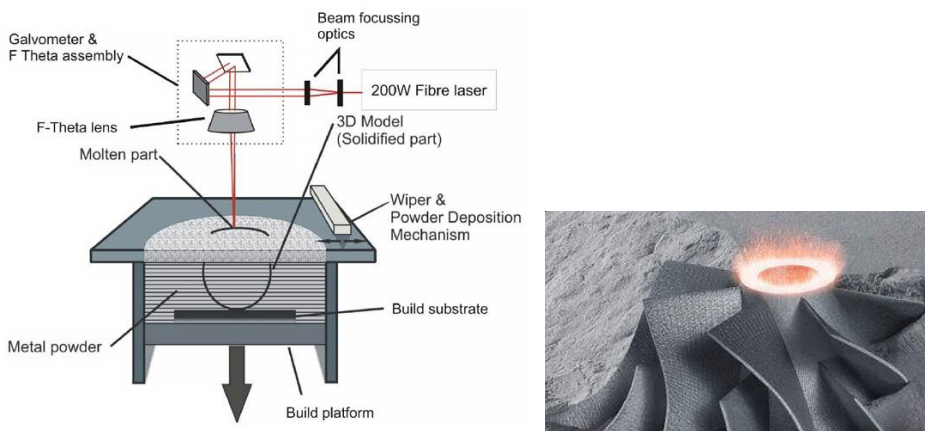


Figure 3. SLM technology [12]

##### *b) EBM – electron beam melting*

Compare to conventional casting, rapid melting and cooling of thin layers of metal occurs, where a more uniform microstructure is expected. Chemical composition is more uniform than casting resulting in better mechanical property.

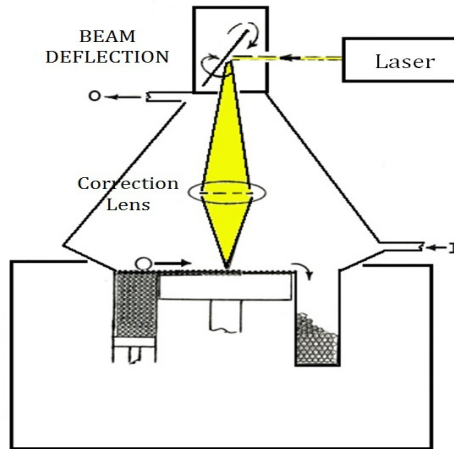


Figure 4. EBM technology [12]

*Limitations:*

- planing of support structure
- complex post process (removal of excess powder (Tapping), relieve of stress (Funranan cycles or Hipping), removal of support structure (manuually, risk of warpage), surface finishing)
- anisotropic mechanical behaviour
- operation environemnt (insert gas (0.1% oxygen) or vaccum)

2. *Binder jetting*

Known as the process where metal powder is “glued” up, can be used for high production volume due to low cost. support structure is not required in this process.

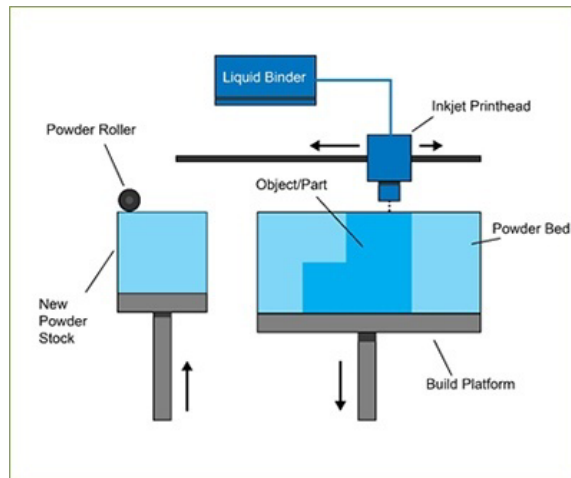


Figure 5. Binder jetting technology [12]

*Limitations:* limited mechanical property

### 3. Directed Energy Deposition (DOD)

Can feed either powder or wire of metals. material is only feeded at the selective area thus low material waste. suitable of part repair. Different types of metals can be mixed in the process. Also good for space application at zero gravity. efficiency at 80% approx.

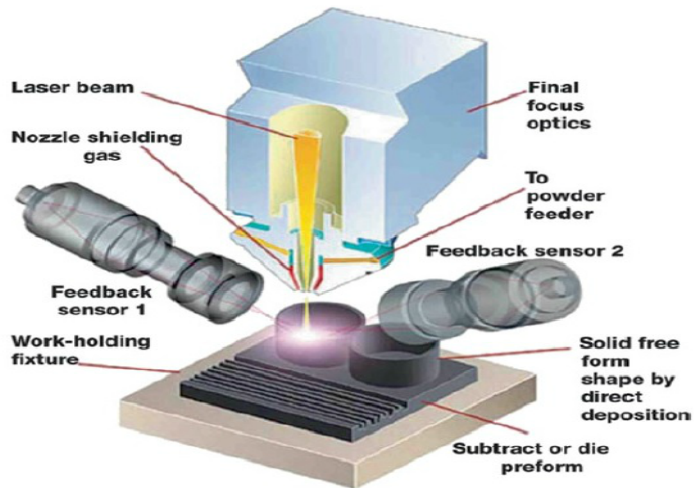


Figure 6. DOD technology [12]

#### Limitations:

- can not produce complex structure
- high surface roughness
- slow build time
- high residual stress, susceptible to cracking

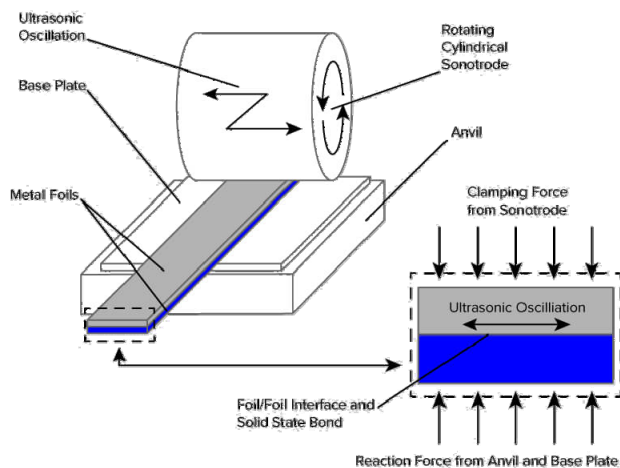


Figure 7. Sheet lamination [13]

#### 4. Sheet lamination

excellent surface finish with low heat input. Bond different materials is common. Low residual stress due to low heat process.

##### *Limitations:*

- Material wastage is high
- no overhang structure can be made by sheet lamination, no supports
- 85% strong as bulk material, genenerally worse in z direction

#### 5. Metal Deposition

You might think that the only 3D printing process “missing” from metal 3D printing is fused filament deposition but that is not entirely true. Of course, you cannot really fuse metal filament on your desktop and make something with that. However, the very large industrial metal manufacturers can. And do. There are two ways to go about “depositing metal”.

One is called DED (Directed Energy Deposition) or Laser Cladding. It uses a laser beam to fuse metal powder as it is slowly released and deposited to form the layers of an object by an industrial robotic arm.

This is usually done inside a closed chamber, however, a recent MX3D project implemented a similar approach to 3D print a real size bridge. The other is called EBAM (Electron Beam Additive Manufacturing), a type of soldering process, where a very powerful electron beam is used to fuse a 3 mm thick titanium wire and the molten metal is shaped into very large metal structures. Unless you work for the US Defense department you are unlikely to run into this technology, though.

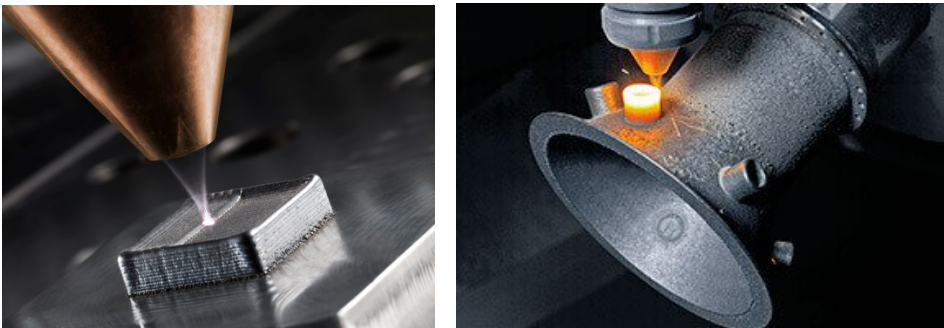


Figure 8. Additive manufacturing [14-15]

## 4. The metals what we can use for 3D printing [13]

### 1. Titanium

Pure titanium (Ti64 or TiAl4V) is one of the most commonly used metals for 3D printing and it is certainly one of the most versatile, as it is both strong and light. It is used both in powder bed fusion and binder jetting

processes, mainly in the medical industry (to make personalized prosthetics) and the aerospace/automotive/tooling industries (to make parts and prototypes). The only catch? It is highly reactive, which means it can easily explode when it is in powder form. That is why it needs to be 3D printed in a vacuum or in an argon gas atmosphere.



## 2. Stainless Steel

Stainless Steel is one of the most affordable metals in 3D printing. At the same time, it is very strong and can be used in a large variety of industrial and even artistic/design applications. This type of steel alloy, which also contains cobalt and nickel is particularly hard to break while at the same time it has very high elastic properties. It is used almost exclusively for industrial applications.



## 3. Inconel

Inconel is a superalloy produced by a company called Special Metals Corporation, that registered the name. It is composed primarily of nickel and chrome and it has a

high-temperature resistance. This is why it is used mainly for applications in the oil, chemical and aerospace industries (for airplane black boxes)



#### 4. Aluminum

Because of its lightness and versatility, Aluminum is now a very popular metal for 3D printing applications. It is used primarily as different Aluminum based alloys.



#### 5. Cobalt Chrome

This metal alloy has a very high specific strength (which is its strength divided by its density, which basically indicates the force required per unit area at failure). It is most commonly used to produce turbines, dental implants, and orthopedic implants: all areas where metal 3D printing is becoming the preferred manufacturing method.



## 6. Copper and Bronze

Apart from some exceptions, copper and bronze are mostly used in lost wax casting processes and not so much in powder bed fusion processes. That is because they are not ideal for industrial applications and are more commonly used in arts and crafts. colorFabb offers both metals as a base for its special metal filaments.



## 7. Iron

Iron – even magnetic iron – is also mostly 3D printed as an additive to PLA based filaments such as the ones produced by ProtoPasta and TreeD.



## 8. Gold, Silver and Other Precious Metals

Most powder bed fusion companies can 3D print with precious metals such as gold, silver and platinum. The challenge here, along with maintaining the materials aesthetic properties, is to make sure that the precious powder management is optimized. Precious metals are 3D printed both for jewelry, medical and electronics applications.



## Conclusion

At that moment in the world thousands of the researchers try to use many types of the material for 3D printing. It is the most easy way to produce a product. It is predicted by some additive manufacturing advocates that this technological development will change the nature of commerce, because end users will be able to do much of their own manufacturing rather than engaging in trade to buy products from other people and corporations. 3D printers capable of outputting in colour and multiple materials already exist and will continue to improve to a point where functional (electronic) products will be able to be output. With effects on energy use, waste reduction, customization, product availability, medicine, art, construction and sciences, 3D printing will change the manufacturing world as we know it.

## References

- [1] Robert Bogue, (2013) 3D printing: the dawn of a new era in manufacturing?, *Assembly Automation*, Vol. 33 Issue: 4, pp.307-311, <https://doi.org/10.1108/AA-06-2013-055>
- [2] Symes M D, Kitson P J, Yan J, et al. Integrated 3D-printed reactionware for chemical synthesis and analysis. *Nat Chem*, 2012, 4: 349–354
- [3] Dewidar M. M, Lim J-K, Dalgarno K. W: A Comparison between Direct and Indirect Laser Sintering of Metals, *Journal of Materials Science and Technology*, 24/2 (2008) 227-232
- [4] Ma M, Wang Z, Gao M, Zeng X: Layer thickness dependence of performance in highpower selective laser melting of 1Cr18Ni9Ti stainless steel, *Journal of Materials Processing Technology* 215 (2015) 142-150
- [5] Santos E. C, Shiomi M, Osakada K, Laoui T: Rapid manufacturing of metal components by laser forming, *Internal Journal of Machine Tools & Manufacture* 46 (2006) 1459-1468

- [6] Wang Y: Mechanical properties and microstructure of laser sintered and starch consolidated iron-based powders, Dissertation, Karlstadt University, Karlstadt, 2008
- [7] Shellabear M, Nyrhilä O: DMLS – Development history and state of the art, LANE 2004 Conference, Erlangen, Germany, Sept. 21-24, 2004
- [8] Terry Wohlers report, Additive manufacturing and 3D printing state of the industry, 2013
- [9] EOS GmbH: EOSINT M Technology for Direct Metal Laser-Sintering (DMLS), Application Notes, Design Rules for DMLS, EOS Whitepaper, [www.eos.info](http://www.eos.info), 2007, 110
- [10] Kleszczynski S, Jacobsmühlen J, Sehrt J. T, Witt G: Error Detection in Laser Beam Melting Systems by High Resolution Imaging, Proceedings of the Twenty Third Annual International Solid Freeform Fabrication Symposium, 2012
- [11] Hatos I, Zsoldos I: Checking the geometry of parts made by DMLS, Factory Automation (2012) 42-45
- [12] Anatol Locker 2017, About Metal 3D Printing
- [13] <https://3dprinting.com/what-is-3d-printing/>
- [14] <https://pinshape.com/blog/3d-printing-metal/>
- [15] <https://all3dp.com/app/uploads/2015/12/3e-5-3d-bauteil.jpg>